Western Michigan University
ScholarWorks at WMU

Master's Theses | Graduate College

4-2014

Analytical Performance Evaluation of Thermoelectric Modules Using Effective Material Properties

Sean Lwe Leslie Weera
Western Michigan University, seanweera@gmail.com

Follow this and additional works at: http://scholarworks.wmich.edu/masters_theses

 Part of the Electro-Mechanical Systems Commons, and the Heat Transfer, Combustion Commons

Recommended Citation
Weera, Sean Lwe Leslie, "Analytical Performance Evaluation of Thermoelectric Modules Using Effective Material Properties" (2014). *Master's Theses*. 483.
http://scholarworks.wmich.edu/masters_theses/483

This Masters Thesis-Open Access is brought to you for free and open access by the Graduate College at ScholarWorks at WMU. It has been accepted for inclusion in Master's Theses by an authorized administrator of ScholarWorks at WMU. For more information, please contact maira.bundza@wmich.edu.

ANALYTICAL PERFORMANCE EVALUATION OF THERMOELECTRIC MODULES USING EFFECTIVE MATERIAL PROPERTIES

Sean Lwe Leslie Weera

A thesis submitted to the Graduate College in partial
fulfillment of the requirements for the degree of
Master of Science in Engineering (Mechanical)
Mechanical and Aeronautical Engineering
Western Michigan University
April 2014

Thesis Committee:

HoSung Lee, Ph.D., Chair
Christopher Cho, Ph.D.
Muralidhar Ghantasala, Ph.D.

ANALYTICAL PERFORMANCE EVALUATION OF THERMOELECTRIC MODULES USING EFFECTIVE MATERIAL PROPERTIES

Sean Lwe Leslie Weera, M.S.E.

Western Michigan University, 2014

Designers often face the predicament of non-standardized forms of performance data provided by thermoelectric module manufacturers. Other than experimental means the only method to evaluate the performance of a product would be through analytical modeling using material properties that are usually undisclosed and unknown. This work studies the theoretical approach of obtaining such material properties using the maximum operating parameters reported by the manufacturers. These values are then analytically employed to evaluate the performances of these thermoelectric modules. Experimental means are also devised and carried out on these test samples to validate the integrity of the results. Three-way comparisons between the analytical, experimental and manufacturer-provided results indicate acceptable agreement.

Copyright by
Sean Lwe Leslie Weera
2014

ACKNOWLEDGEMENTS

First and foremost I would like to thank my advisor, Dr. HoSung Lee, for sparking my interest and continuously inspiring me with his constant drive to further his knowledge and proficiency in the field of thermoelectricity. The concept, idea and motivation of this work would not have been possible without his teaching and advice. I would also like to extend my gratitude to the members of the committee, Dr. Christopher Cho and Dr. Muralidhar Ghantasala for their guidance and feedback towards the improvement of this work.

I would also like to especially thank two faculty members at the university; Mr. Glenn Hall and Mr. Peter Thannhauser whom have lent their knowledge, time and expertise to me while designing the experimental setup. More importantly, my gratitude is greatly extended to my colleague, Alaa Attar. All the hours of brainstorming and late nights in the laboratory have materialized through the success of this work.

I would also like to thank my family and friends whom have constantly lent their time and support to me. And finally, last but not least, I would like to thank Cathy for her support and understanding throughout the endeavor of this work.

Sean Lwe Leslie Weera

TABLE OF CONTENTS

Table of contents - continued

Table of contents - continued

LIST OF TABLES

LIST OF FIGURES

List of Figures - continued

List of Figures - continued

List of Figures - continued

CHAPTER I

INTRODUCTION AND BACKGROUND

The thermoelectric phenomenon deals with the conversion of thermal energy into electrical energy and vice-versa. When operating as an energy-generating device the thermoelectric device is termed a thermoelectric generator (TEG). The source of thermal energy manifests itself as a temperature difference across the TEG. When operating in a cooling or heating mode the thermoelectric device is termed a thermoelectric cooler (TEC). Similarly, the thermoelectric device produces heating or cooling that takes the form a heat flux which then induces a temperature difference across the TEC. Thermoelectric devices are solid-state mechanisms that are capable of producing these three effects without any intermediary fluids or processes. They have no moving parts, reducing their susceptibility to mechanical failure while allowing for prolong periods of operation with minimal maintenance. Additionally, this allows quiet cooling operations compared to conventional compressor-based refrigeration systems and produce no pollutants or environmentally detrimental byproducts. These criteria make thermoelectric devices highly attractive for a multitude of applications.

For power generation applications thermoelectric devices are used in automobiles as exhaust gas waste heat recovery devices where thermal energy is scavenged along the exhaust line of a vehicle and converted into useful electricity [1]. Space exploration

robotic rovers utilize TEGs to convert heat energy released from the decay of radioisotopes to electricity [2]. Solar thermoelectric generators capture incoming sunlight and convert solar thermal energy into electricity using thermoelectric principles [3] [4].

On the other hand, thermoelectric devices are widely implemented for heating, ventilation and air-conditioning (HVAC) purposes in vehicles. These take the form of thermoelectric air-conditioners and climate controlled seats that may potentially replace conventional compressor-based air-conditioning systems in automobiles [5]. Due to their high manufacturability and ability to be miniaturized thermoelectric devices are suitable candidates for controlling temperature sensitive equipment such as surgical tools and fiber-optic lasers in telecommunication applications [6]. These TECs can also be embedded into microprocessors to achieve precise temperature control as well as hot spot mitigation when physical space around the microprocessor is limited [7].

Thermoelectric Phenomenon

Governing Effects

The discovery of the thermoelectricity began in 1821 when a German physicist, by the name of Thomas Johann Seebeck, discovered that an electromotive potential (or electrical voltage) was produced in a circuit of two dissimilar metals when one of the junctions of circuit was heated or at a higher temperature than the other junction (refer to Figure 1) [8]. The proportionality of the electrical potential to temperature difference was

governed by the Seebeck coefficient, which is an inherent property of the circuit of two dissimilar metals. The relationship between voltage and temperature difference is

$$V = \alpha \Delta T \tag{1.1}$$

where V is the voltage across the junctions of the circuit, α is the Seebeck coefficient and ΔT is the temperature difference across the junctions of the circuit. In Figure 1 the temperature difference across the circuit is expressed as $\Delta T = T_h - T_c$, where T_h and T_c are the hot and cold junctions, respectively. I represents the direction of current in the circuit that is generated due to a potential difference.

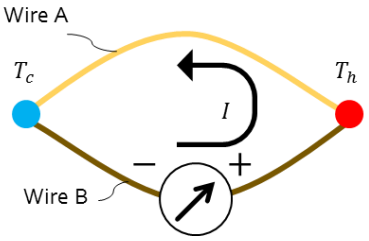

Figure 1. Seebeck Effect in a Circuit of Two Dissimilar Metals

Later on in 1834 the reverse of the Seebeck effect was discovered by a French physicist, Jean Peltier, whereby heat would be absorbed and liberated at opposite ends in the same circuit of dissimilar metals when current (or a voltage potential) was present [9]. The direction of current would determine the direction of heating or cooling. The proportionality of the rate of heat transfer $Q_{Peltier}$ to amount of current I in the circuit was governed by the Peltier coefficient π. This is expressed as

$$Q_{Peltier} = \pi I \tag{1.2}$$

Figure 2 illustrates the Peltier effect where the direction of heat transfer into the circuit indicates heat absorbed and direction of heat transfer out of the circuit indicates heat liberated. This also dictates the sign convention of the Peltier coefficient π making it positive for heat absorbed (entering the circuit) and negative for heat liberated (leaving the circuit). The Peltier effect is reversible between heat and electricity, meaning that the effects either of producing heat transfer from electricity or producing electricity from heat transfer are interchangeable without a loss of energy.

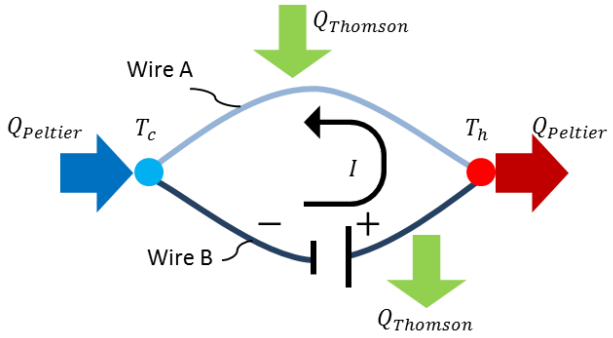

Figure 2. Peltier and Thomson Effect in a Circuit of Two Dissimilar Metals

Finally, in 1851, English physicist William Thomson (later known as Lord Kelvin) discovered that a current carrying conductor with a temperature gradient, such as a wire with current passing through it, would either absorb or liberate heat depending on the material of the conductor and the direction of the current (refer to Figure 2) [10].

$$Q_{Thomson} = \tau I \Delta T \tag{1.3}$$

Equation (1.3) governs the proportionality of Thomson heat $Q_{Thomson}$ to both current I and temperature difference $\Delta T = T_h - T_c$ (see Figure 2) using the Thomson

coefficient τ. Similar to the Peltier effect the sign convention of τ is positive for heat absorbed (Wire A) and negative for heat liberated (Wire B).

These three effects cumulatively give rise to the thermoelectric phenomenon as a whole. These effects are not exclusive to thermoelectric materials alone but are present in all metals and semi-metals. Only in select combinations of dissimilar semi-metals (thermoelectric materials) are their effects most observable and practical from an application standpoint.

Figure of Merit and Thermoelectric Materials

The figure of merit Z is a metric used to gauge the performance of a certain thermoelectric material and is given as

$$Z = \frac{\alpha^2}{\rho k} \tag{1.4}$$

where α is the Seebeck coefficient (given in units of $V\ K^{-1}$), ρ is the electrical resistivity (given in units of Ω m) and k is the thermal conductivity (given in units of $\mathrm{W\ m^{-1}\ K^{-1}}$). A higher figure of merit indicates a better performance in heating, cooling or power generation applications.

These three material properties themselves are functionally dependent on temperature. Thus, it is convenient to represent the figure of merit in a dimensionless form (termed the dimensionless figure of merit $Z\bar{T}$) by multiplying equation (1.4) with

the average operating temperature $\bar{T}$ of the material and is given as $\bar{T} = 1/2(T_h + T_c)$. The components of the dimensionless figure of merit (α, ρ and k) are also evaluated at $\bar{T}$.

Upon studying equation (1.4) there are mainly two means to increasing the value of Z. These approaches are usually achieved using nanofabrication to control these parameters [11]. One method would be to increase the power factor ($PF = \alpha^2/\rho$). However, this entails difficulty in most thermoelectric materials as the Seebeck coefficient and electrical resistivity are usually proportionally related to each other; increasing one would cause the other to increase as well, causing insignificant change to the power factor [12].

The other method would be to decrease the thermal conductivity of the material. The thermal conductivity is a summation of the electronic k_e and lattice k_l thermal conductivities of a material ($k = k_e + k_l$). The electronic thermal conductivity and electrical resistivity of a material are related together by the Wiedemann-Franz law. The law states that the product of electronic thermal conductivity k_e and electrical resistivity ρ are proportional to temperature T. This proportionality is governed by the Lorenz number L_z, a constant [12]. The relationship between these parameters is expressed as

$$\frac{k_e \rho}{T} = L_z = 2.44 \times 10^{-8}\ \mathrm{W\,\Omega\,K^{-2}} \tag{1.5}$$

Since all three components of the Wiedemann-Franz law in equation (1.5) must adhere to the Lorenz number decreasing k_e would cause ρ to increase for any temperature. Decreasing k while increasing ρ in equation (1.4) nullifies the increase of Z.

Thus, the only free parameter left to manipulate is the lattice thermal conductivity which is reduced by manipulating the phonon scattering of the material, achieved through nanofabrication of thermoelectric materials such as quantum wires, dots and wells [12].

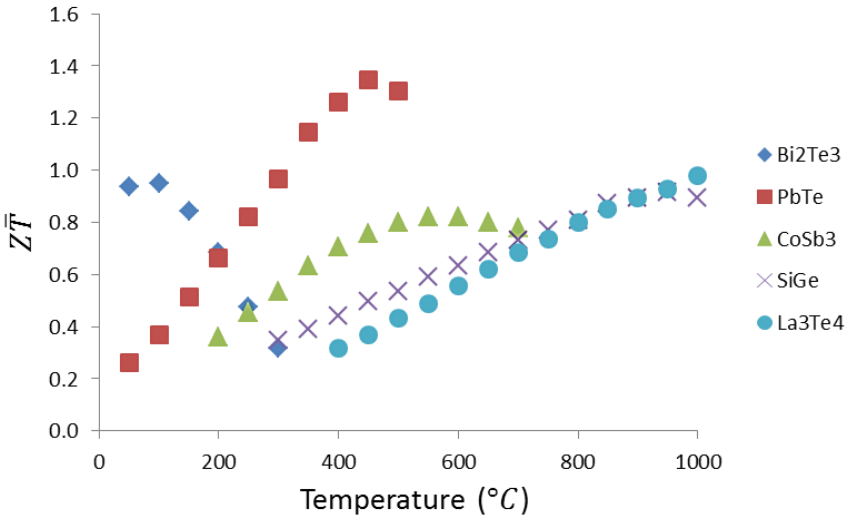

Figure 3. Dimensionless Figure of Merit of Common Thermoelectric Materials [13]

Figure 3 shows the $Z\bar{T}$ values of commonly used thermoelectric materials as a function of operating temperature. Bismuth telluride (Bi_2Te_3) has the highest $Z\bar{T}$ value for low to room temperature applications, making it the best candidate for a majority of cooling applications as well as low grade waste heat recovery. The present $Z\bar{T}$ value of bismuth telluride is usually around 1.0 or slightly less. Nanotechnology such as quantum wells and wires have enabled higher $Z\bar{T}$ values of almost up to 1.4 [14]. Exhaust gas waste heat recovery applications that have higher operating temperatures usually utilize lead telluride (PbTe) materials that can have higher $Z\bar{T}$ values compared to bismuth

telluride. Extremely high temperature applications (exceeding 500°C) would utilize silicon germanium (SiGe) materials or equivalently lanthanum telluride (La_3Te_4).

Thermoelectric Ideal Equations

General Governing Equations

The equations presented in this section are in vector form to represent generalized three-dimensional cases. Considering a non-uniformly heated thermoelectric material that has isotropic material properties, the continuity equation for a constant current flux $\vec{J}$ is given as

$$\vec{\nabla} \cdot \vec{J} = 0 \tag{1.6}$$

where $\vec{\nabla}$ is the differential operator with respect to length. The electric potential (or electric field $\vec{E}$ in this case) has contributions from both Ohm's Law and the Seebeck effect, which is obtained by differentiating equation (1.1) with respect to length. The electric field is given as

$$\vec{E} = \vec{J}\rho + \alpha\vec{\nabla}T \tag{1.7}$$

The heat flow density vector $\vec{q}$ is expressed as

$$\vec{q} = \alpha T\vec{J} - k\vec{\nabla}T \tag{1.8}$$

where T is the temperature of the heat flux boundary. The $\alpha T\vec{J}$ term is the Peltier heat contribution while the $k\vec{\nabla}T$ term gives heat transfer from Fourier's Law of conduction. The general heat diffusion equation as a function of time is given by

$$-\vec{\nabla} \cdot \vec{q} + \dot{q} = \rho_m c_p \frac{\partial T}{\partial t} \tag{1.9}$$

where $\dot{q}$ is the heat generated per unit volume, ρ_m is the mass density of the material, c_p is the specific heat capacity and $\frac{\partial T}{\partial t}$ is the rate of change of temperature with respect to time. Only considering steady state conditions causes the time dependent term $\frac{\partial T}{\partial t}$ to become zero. Equation (1.9), after rearranging, reduces to

$$\dot{q} = \vec{\nabla} \cdot \vec{q} \tag{1.10}$$

The relationship between the rate of thermal energy generated and electrical power is expressed as

$$\dot{q} = \vec{E} \cdot \vec{J} = J^2 \rho + \vec{J} \cdot \alpha \vec{\nabla} T \tag{1.11}$$

Equations (1.8) and (1.11) can be substituted into equation (1.10) to obtain

$$\vec{\nabla} \cdot \left(k \vec{\nabla} T\right) + J^2 \rho - T \frac{d\alpha}{dT} \vec{J} \cdot \vec{\nabla} T = 0 \tag{1.12}$$

where $T \frac{d\alpha}{dT} = \tau$ and is known as the Thomson coefficient from before. The $J^2 \rho$ term is a form of Joule heating that occurs in all current carrying materials due to the interaction between electrical current and resistance. Studies by [15] and [16] indicate that exact solutions that include the integral of the Thomson coefficient as a function of temperature show almost exact agreements with exact solutions that neglect the Thomson coefficient $\left(T \frac{d\alpha}{dT} = 0\right)$. As such, this study will also assume that the Thomson coefficient is negligible and that the Seebeck coefficient is independent of temperature.

Thermoelectric Couple Equations

Expanding on the concept of a circuit of two dissimilar metals a thermoelectric couple is nothing more than thermoelectric elements connected to each other and to either a load resistance (in the case of a power producing TEG) or a power source (in the case of a power consuming TEC). Each element, interchangeably termed as a thermoelectric leg or a pellet, is either positively (denoted as p-types) or negatively (denoted as n-types) doped to modulate its thermoelectric properties. Together two elements form a thermoelectric couple and is used as the basis to formulate the governing equations of thermoelectric devices.

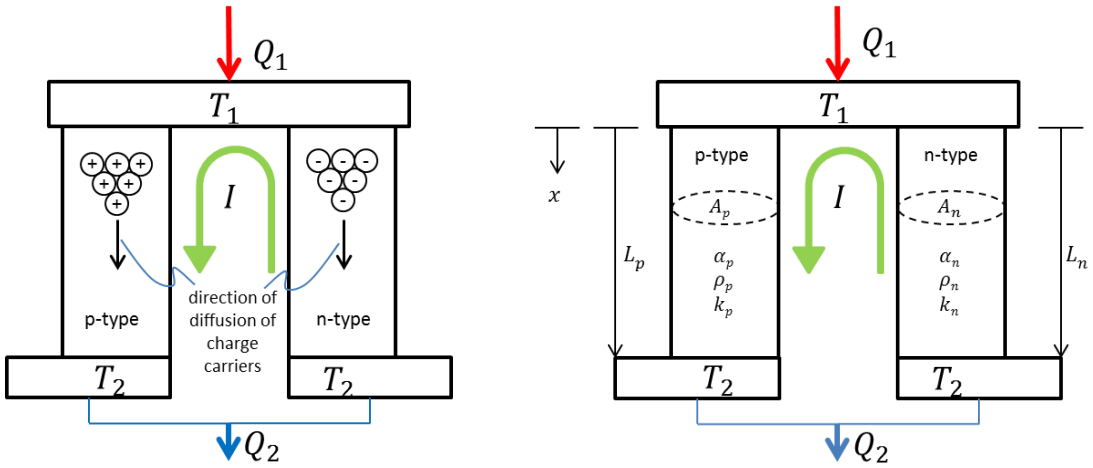

(a) (b)

Figure 4. Longitudinal Cross-section of a Thermoelectric Couple

The thermoelectric elements are doped to allow their charge carriers to be more easily perturbed and freed. In the case of power generation a source of perturbation, such as heat, forms free electrons and holes that move in opposite directions. The movement of

these charge carriers dictates the direction of current within the thermoelectric couple with holes move in the direction of the current and electrons in the opposite. In contrast, when an electrical current is supplied the holes adhere to the direction of the current while the electrons travel in the opposite direction. This is illustrated in Figure 4 (a). The free electrons carry thermal energy with them while traveling and this enables heat transfer to occur.

A thermoelectric couple that consists of one p-type and one n-type element with all its constituent material properties (α, ρ and k) and geometric information (longitudinal length L and lateral cross-sectional area A) is represented in Figure 4 (b). Subscripts p and n refer to p- and n-type materials, respectively. Both elements experience the same junction temperatures T_1 and T_2 at opposite ends where uniform heat fluxes occur and both elements are subjected to the same magnitude of current I. Q_1 and Q_2 are the heat transfer rates that occur at junctions with temperatures T_1 and T_2, respectively. The direction of x is nothing more than a coordinate system for reference.

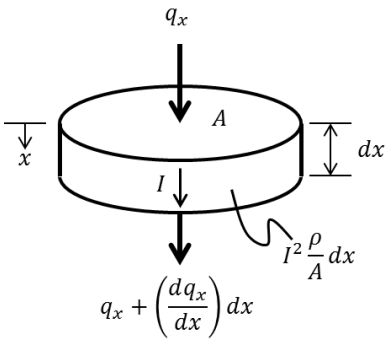

Figure 5. Differential Element of a Thermoelectric Element

Consider a differential element of one of the thermoelectric legs with cross-sectional area A and differential length dx as shown in Figure 5. A uniform current I that passes through the differential element with electrical resistivity ρ will evoke Joule heating effects. It is now assumed that Joule heating is the only source of internal energy generated within the differential element. Adopting the sign convention that heat flow into element is positive, considering only one-dimension and rearranging equation (1.10), the heat balance on the differential element now becomes

$$q_x - \left(q_x + \frac{dq_x}{dx}\right) dx + \frac{I^2 \rho}{A} dx = 0 \tag{1.13}$$

where q_x is the heat flow. Equation (1.8), multiplied by the area normal to the direction of heat flux A in this 1-D case, yields

$$q_x = \alpha T(x) I - kA \frac{dT}{dx} \tag{1.14}$$

where $I = J_x A$ and the temperature T is a function of position x. At $x = 0$ in equation (1.14) becomes

$$q_{x=0} = \alpha T_1 I - kA \frac{dT}{dx}\Big|_{x=0} \tag{1.15}$$

Differentiating equation (1.15) with respect to x gives

$$\frac{dq_x}{dx} = -kA \frac{d}{dx}\left(\frac{dT}{dx}\right) \tag{1.16}$$

Substituting equation (1.16) into equation (1.13) and rearranging yields

$$kA\frac{d}{dx}\left(\frac{dT}{dx}\right) = -\frac{I^2\rho}{A} \tag{1.17}$$

Integrating equation (1.17) once gives

$$kA\int d\left(\frac{dT}{dx}\right) = -\frac{I^2\rho}{A}\int dx \rightarrow \frac{dT}{dx} = -\frac{I^2\rho}{kA^2}x + C_1 \tag{1.18}$$

where C_1 is a constant of indefinite integration. Integrating equation (1.18) again from $x = 0$ to $x = L$ with the boundary conditions $T(x = 0) = T_1$ and $T(x = L) = T_2$ leads to

$$\int_{T_1}^{T_2} dT = -\frac{I^2\rho}{kA^2}\int_0^L x + \int_0^L x\, C_1 \rightarrow (T_2 - T_1) = -\frac{I^2\rho}{2kA^2}L^2 + C_1 L \tag{1.19}$$

Equation (1.19) can be rearranged to obtain the constant of integration C_1as

$$C_1 = \frac{(T_2 - T_1)}{L} + \frac{I^2\rho}{2kA^2}L \tag{1.20}$$

Substituting equation (1.20) into (1.18) at $x = 0$ yields

$$\left.\frac{dT}{dx}\right|_{x=0} = \frac{(T_2 - T_1)}{L} + \frac{I^2\rho}{2kA^2}L \tag{1.21}$$

By similar fashion evaluation equation (1.18) at $x = L$ yields

$$\left.\frac{dT}{dx}\right|_{x=L} = \frac{(T_2 - T_1)}{L} - \frac{I^2\rho}{2kA^2}L \tag{1.22}$$

Substituting equation (1.21) into (1.14) yields

$$q_{x=0} = \alpha T_1 I - \frac{1}{2}I^2\frac{\rho L}{A} + \frac{kA}{L}(T_1 - T_2) \tag{1.23}$$

For their respective elements (p- and n-type) equation (1.23) becomes

$$q_{p,x=0} = \alpha_p T_1 I - \frac{1}{2} I^2 \frac{\rho_p L_p}{A_p} + \frac{k_p A_p}{L_p}(T_1 - T_2) \tag{1.24}$$

$$q_{n,x=0} = -\alpha_n T_1 I - \frac{1}{2} I^2 \frac{\rho_n L_n}{A_n} + \frac{k_n A_n}{L_n}(T_1 - T_2) \tag{1.25}$$

The Seebeck coefficient for the n-type element is negative because it is negatively doped and carries a preceding negative sign in order to validate the thermoelectric equations. By similar fashion the heat transfer equations at $x = L$ for the p- and n-type, with $T(x = L) = T_2$ and equation (1.22), are found to be

$$q_{p,x=L} = \alpha_p T_2 I + \frac{1}{2} I^2 \frac{\rho_p L_p}{A_p} + \frac{k_p A_p}{L_p}(T_1 - T_2) \tag{1.26}$$

$$q_{n,x=0} = -\alpha_n T_2 I + \frac{1}{2} I^2 \frac{\rho_n L_n}{A_n} + \frac{k_n A_n}{L_n}(T_1 - T_2) \tag{1.27}$$

From Figure 4 (b), realizing that $Q_1 = q_{p,x=0} + q_{n,x=0}$ and $Q_2 = q_{p,x=L} + q_{n,x=L}$, the respective heat transfer rates at junctions of the thermoelectric couple are

$$Q_1 = (\alpha_p - \alpha_n) T_1 I - \frac{1}{2} I^2 \left(\frac{\rho_p L_p}{A_p} + \frac{\rho_n L_n}{A_n} \right) + \left(\frac{k_p A_p}{L_p} + \frac{k_n A_n}{L_n} \right)(T_1 - T_2) \tag{1.28}$$

$$Q_2 = (\alpha_p - \alpha_n) T_2 I + \frac{1}{2} I^2 \left(\frac{\rho_p L_p}{A_p} + \frac{\rho_n L_n}{A_n} \right) + \left(\frac{k_p A_p}{L_p} + \frac{k_n A_n}{L_n} \right)(T_1 - T_2) \tag{1.29}$$

The material properties of the p- and n-type elements can be related together using the following equations

$$\alpha = \alpha_p - \alpha_n \tag{1.30}$$

$$R = \frac{\rho_p L_p}{A_p} + \frac{\rho_n L_n}{A_n} \tag{1.31}$$

$$K = \frac{k_p A_p}{L_p} + \frac{k_n A_n}{L_n} \tag{1.32}$$

where R and K are the total electrical resistance and thermal conductance of the couple, respectively. Using equations (1.30) to (1.32), equations (1.28) and (1.29) can be simplified to become

$$Q_1 = \alpha T_1 I - \frac{1}{2} I^2 R + K(T_1 - T_2) \tag{1.33}$$

$$Q_2 = \alpha T_2 I + \frac{1}{2} I^2 R + K(T_1 - T_2) \tag{1.34}$$

Equations (1.33) and (1.34) are known henceforth in this study as the Ideal Equations. Excluding the preceding signs, the first term in equations (1.33) and (1.34) $\alpha T I$ is known as the Peltier/Seebeck effect and is reversible. This is the driving force of thermopower; the stronger the Peltier/Seebeck effect, the greater the effect of heating, cooling or power generation. The second term $\frac{1}{2} I^2 R$ in the above two equations is the Joule heating term which comes from the interaction between electrical current and resistance and works against the primary objective to cool or generate power. It however, aids devices aimed at heating. The last term $K(T_1 - T_2)$ is the thermal conduction term which occurs due to a temperature difference in any material and also works against the cooling power of TECs. Both the Joule heating and conduction terms are irreversible.

Thermoelectric Modules

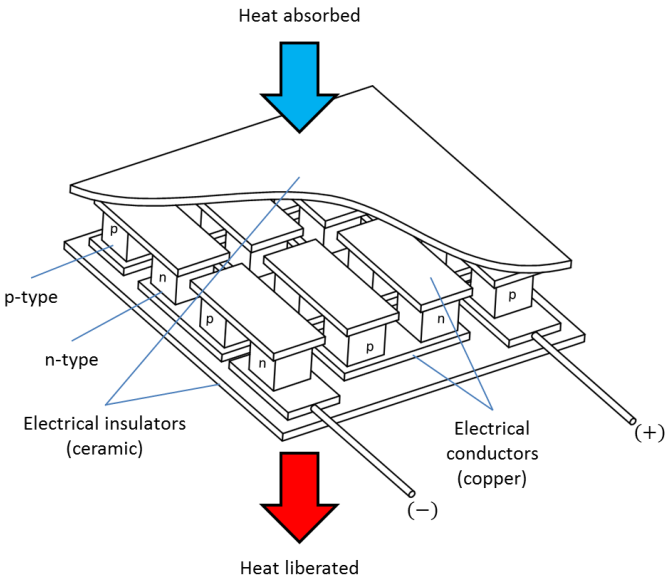

Figure 6. Cutaway of a TEC Module

The basic building block of a thermoelectric couple is one p-type and one n-type thermoelectric element. These thermoelectric couples subsequently become the basis in forming a thermoelectric module. Figure 6 illustrates a typical thermoelectric module which consists of several thermoelectric couples connected to each other by electrical conductors and sandwiched between two ceramic plates. The electrical conductors are arranged so that the thermoelectric couples are electrically in series with each other. The ceramic plates act as an insulator to prevent the conductors and couples from shorting while allowing the couples to be thermally in parallel – the top of every couple is subjected to the same constant temperature T_c while the bottom of every couple is at another constant temperature T_h in the case of a TEC (refer to Figure 7).

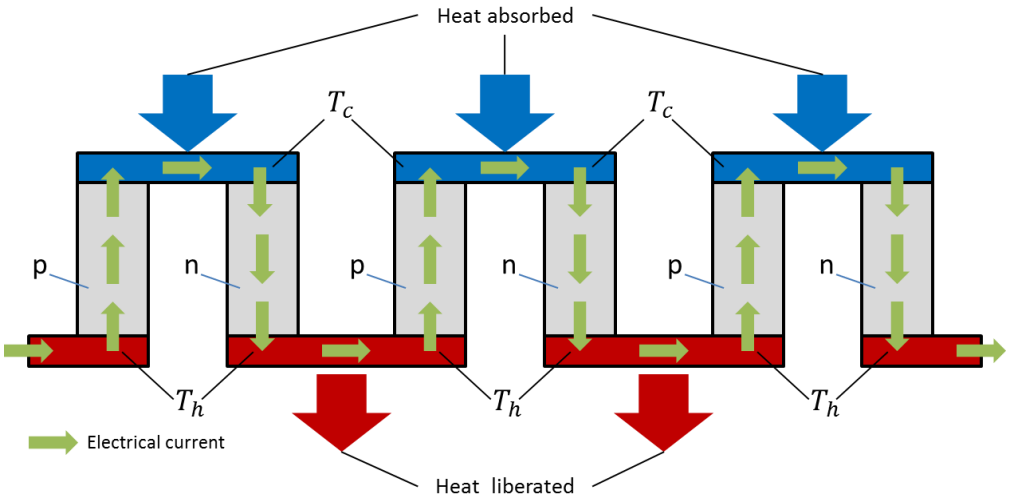

Figure 7. Electrical and Thermal Connectivity of TEC Couples within a Module

Thermoelectric Generators (TEGs) Ideal Equations

A TEG functions to convert thermal energy or a temperature difference across the thermoelectric device directly into useful electricity. The output power is connected to a power consuming device that has an electrical load associated with it (refer to Figure 8). Using respective hot and cold junction temperatures, T_h and T_c, in lieu of temperatures T_1 and T_2, respectively, equations (1.33) and (1.34) become

$$Q_h = \alpha T_h I - \frac{1}{2} I^2 R + K(T_h - T_c) \tag{1.35}$$

$$Q_c = \alpha T_c I + \frac{1}{2} I^2 R + K(T_h - T_c) \tag{1.36}$$

where Q_h and Q_c are the heat transfer rates at the hot and cold junctions of the TEG, respectively.

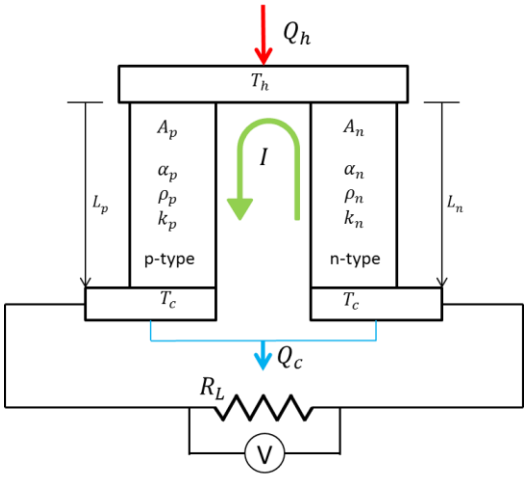

Figure 8. A TEG Attached to a Load Resistance

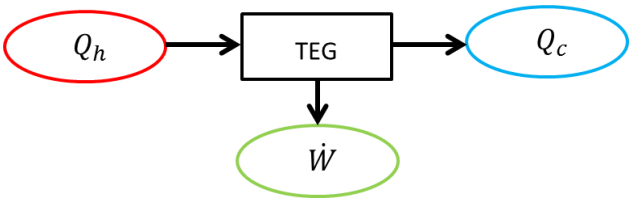

Figure 9. Energy Balance for a TEG

Visualizing the TEG as analogous to a heat engine the first law of thermodynamics states that that the sum of all energies entering and exiting an isolated system must be accounted for. The sign convention adopted here is: positive for heat flow or energy into the system and negative for heat flow or energy out of the system, as shown in Figure 9. The direct correlation between heat transfer rates and electrical output is

$$\dot{W} = Q_h - Q_c \tag{1.37}$$

$$\dot{W} = \alpha I(T_h - T_c) - I^2R \tag{1.38}$$

Similarly, instead of using the internal resistance of the thermoelectric couple R, the output power $\dot{W}$ can be computed in terms of the load resistance R_L (refer to Figure 8) with

$$\dot{W} = I^2 R_L = IV \tag{1.39}$$

where V is the voltage across the load resistor. Alternatively, V can computed from contributions by Ohm's Law and the Seebeck voltage through the following equation

$$V = IR_L = \frac{\dot{W}}{I} = \alpha(T_h - T_c) - IR \tag{1.40}$$

Thus, the current in the circuit is equal to

$$I = \frac{\alpha(T_h - T_c)}{R_L + R} \tag{1.41}$$

The thermal efficiency of the TEG η is the ratio of output power to input power (heat transfer rate into the system) and is given as

$$\eta = \frac{\dot{W}}{Q_h} = \frac{I^2 R_L}{\alpha T_h I - \frac{1}{2} I^2 R + K(T_h - T_c)} \tag{1.42}$$

The ratio of resistances R_L/R is an important parameter in design. Using the definition of the figure of merit, from equation (1.4), and current, from equation (1.41), equation (1.42) can be rearranged in terms of the resistance ratio R_L/R to become

$$\eta = \frac{\frac{R_L}{R}\left(1 - \frac{T_c}{T_h}\right)}{\left(1 + \frac{R_L}{R}\right) - \frac{1}{2}\left(1 - \frac{T_c}{T_h}\right) + \frac{1}{2Z\bar{T}}\left(1 + \frac{R_L}{R}\right)^2 \left(1 + \frac{T_c}{T_h}\right)} \tag{1.43}$$

There are two modes of maximum parameter operation for a TEG: maximum power output or maximum conversion efficiency. The variable parameter in both these cases is R_L/R. These modes can be set by the user according to the demand or objective of the application by setting the appropriate R_L/R value. In the case of maximum power output the output power $\dot{W}$ in equation (1.38) is differentiated with respect to R_L/R and set to zero. This gives

$$\frac{d\dot{W}}{d\left(\frac{R_L}{R}\right)} = 0 \rightarrow \frac{R_L}{R} = 1 \tag{1.44}$$

The resultant current I_{mp}, power output $\dot{W}_{max}$ and efficiency η_{mp} at maximum power, respectively, are

$$I_{mp} = \frac{\alpha(T_h - T_c)}{2R} \tag{1.45}$$

$$\dot{W}_{max} = \frac{\alpha^2(T_h - T_c)^2}{4R} \tag{1.46}$$

$$\eta_{mp} = \frac{1 - \left(\frac{T_c}{T_h}\right)}{2 - \frac{1}{2}\left(1 - \frac{T_c}{T_h}\right) + 4\frac{\frac{T_c}{T_h}}{ZT_c}} \tag{1.47}$$

The other mode of maximum parameter operation is when a TEG operates at maximum conversion efficiency. The thermal efficiency η is differentiated with respect to the ratio of resistances R_L/R and set to zero, yielding

$$\frac{d\eta_{th}}{d\left(\frac{R_L}{R}\right)} = 0 \rightarrow \frac{R_L}{R} = \sqrt{1 + Z\bar{T}} \tag{1.48}$$

where $\bar{T}$ is the average junction temperatures and is equal to

$$\bar{T} = \frac{T_h + T_c}{2} = \frac{1}{2}\left[1 + \left(\frac{T_c}{T_h}\right)^{-1}\right] \tag{1.49}$$

The resultant current I_{mc}, power output $\dot{W}_{mc}$ and efficiency η_{max} at maximum conversion efficiency, respectively, are

$$I_{mc} = \frac{\alpha(T_h - T_c)}{R\left(\sqrt{1 + Z\bar{T}} + 1\right)} \tag{1.50}$$

$$\dot{W}_{mc} = \frac{\alpha^2(T_h - T_c)^2\sqrt{1 + Z\bar{T}}}{\sqrt{1 + Z\bar{T}} + 1} \tag{1.51}$$

$$\eta_{max} = \left(1 - \frac{T_c}{T_h}\right)\frac{\sqrt{1 + Z\bar{T}} - 1}{\sqrt{1 + Z\bar{T}} + \frac{T_c}{T_h}} \tag{1.52}$$

The maximum performance parameters can now be defined by normalizing the power output $\dot{W}$, the current I and voltage V with their respective single point maximum values of maximum power $\dot{W}_{max}$, maximum current I_{max} and maximum voltage V_{max}. Using equations (1.39) and (1.41) and dividing by (1.46) ratio of output power to maximum output power is

$$\frac{\dot{W}}{\dot{W}_{max}} = \frac{\left[\frac{\alpha(T_h - T_c)^2}{R_L + R}\right]^2 R_L}{\frac{\alpha^2(T_h - T_c)^2}{4R}} = \frac{4\frac{R_L}{R}}{\left(\frac{R_L}{R} + 1\right)^2} \tag{1.53}$$

The maximum current I_{max} occurs when the load resistance $R_L$in equation (1.39) is set to zero – a short-circuit scenario. Thus, the maximum current is

$$I_{max} = I_{sc} = \frac{\alpha(T_h - T_c)}{R} \tag{1.54}$$

Equation (1.39) and (1.54) give

$$\frac{I}{I_{max}} = \frac{\frac{\alpha(T_h - T_c)}{R_L + R}}{\frac{\alpha(T_h - T_c)}{R}} = \frac{1}{\frac{R_L}{R} + 1} \tag{1.55}$$

The maximum voltage V_{max} occurs at an open circuit scenario. Referring to Figure 10 both load and internal resistances will be in a serial circuit configuration, making the sum of resistances in the circuit $\sum R = R_L + R$. Using Ohm's Law and from equation (1.40)

$$V_{max} = V_{oc} = I(R_L + R) = \alpha(T_h - T_c) \tag{1.56}$$

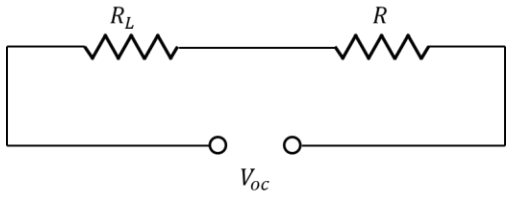

Figure 10. TEG Open Circuit Diagram

Alternatively, equation (1.40) can be viewed as Ohm's Law voltage working against the Seebeck voltage, whereby the maximum occurs when the Ohm's Law voltage becomes zero (since $R \neq 0, I = 0$). This leads to an open-circuit.

Dividing equation (1.40) by (1.56) the ratio of voltage to maximum voltage is

$$\frac{V}{V_{max}} = \frac{IR_L}{I(R_L + R)} = \frac{\frac{R_L}{R}}{\frac{R_L}{R} + 1} \tag{1.57}$$

Dividing equation (1.43) by (1.52) gives the normalized efficiency and can be algebraically manipulated in terms of ZT_c to obtain

$$\frac{\eta}{\eta_{max}} = \frac{\frac{R_L}{R}\left[\sqrt{1 + \frac{ZT_c}{2}\left(1 + \left(\frac{T_c}{T_h}\right)^{-1}\right)} + \frac{T_c}{T_h}\right]}{\left[\left(\frac{R_L}{R} + 1\right) - \frac{1}{2}\left(1 - \frac{T_c}{T_h}\right) + \frac{\left(\frac{R_L}{R} + 1\right)^2 \frac{T_c}{T_h}}{ZT_c}\right]\left[\sqrt{1 + \frac{ZT_c}{2}\left(1 + \left(\frac{T_c}{T_h}\right)^{-1}\right)} - 1\right]} \tag{1.58}$$

The cold junction temperature T_c is usually the basis for TEGs because it depicts the constraint to the amount of cooling a TEG system is subjected to – the performance of a TEG module is ultimately limited by how cool the cold side is maintained during operation. These four normalized parameters can be plotted as functions of the resistance ratio R_L/R at specific junction temperature ratios T_c/T_h and dimensionless figure of merit (evaluated at the cold junction temperature) ZT_c values. The resistance ratio is a variable parameter that can be controlled while the junction temperature ratio and dimensionless figure of merit represent operating parameters and material constraints, respectively. The junction temperatures are indicative of the environmental or mechanical constraints such as the temperature of the hot and cold reservoir and heat sink designs while the dimensionless figure of merit is bound to the type of thermoelectric material implemented.

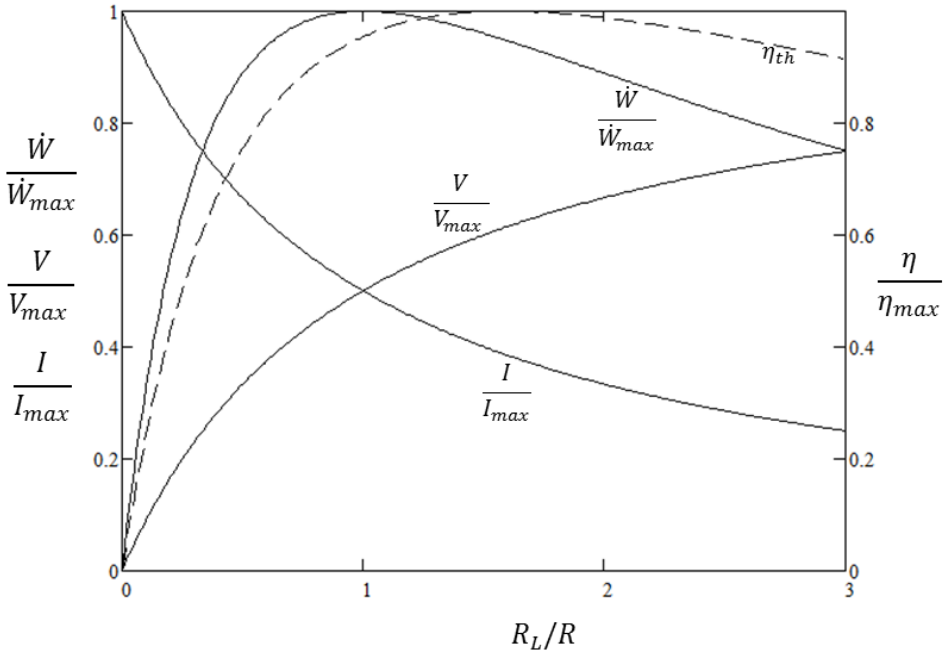

Figure 11. Generalized TEG Performance with $T_c/T_h = 0.5$ and $ZT_c = 1$

Figure 11 illustrates the generalized performance characteristic of a TEG with typical values of $T_c/T_h = 0.5$ and $Z\bar{T} = 1$. The parameters were analytically obtained using equations (1.53), (1.55), (1.57) and (1.58). The maximum power occurs when the load resistance is matched to the internal resistance ($R_L/R = 1$) as predicted. The plot of efficiency follows closely with the normalized power output but its maximum value occurs at $R_L/R = \sqrt{1 + Z\bar{T}}$, or specifically at 1.581 in this case. On the basis of T_c

$$Z\bar{T} = \frac{ZT_c}{2}\left(1 + \left(\frac{T_c}{T_h}\right)^{-1}\right) \tag{1.59}$$

Since a thermoelectric module is a combination of more than one thermoelectric elements some of the parameters for a thermoelectric module are simply equal to the

parameters of a single couple multiplied by the total number of couples within a module n. These modular parameters, denoted with an m subscript, are

$$\left(\dot{W}\right)_m = n\dot{W} \tag{1.60}$$

$$(Q_h)_m = nQ_h \tag{1.61}$$

$$(Q_c)_m = nQ_c \tag{1.62}$$

$$(R)_m = nR \tag{1.63}$$

$$(R_L)_m = nR_L \tag{1.64}$$

$$(V)_m = nV \tag{1.65}$$

$$(K)_m = nK \tag{1.66}$$

The current passing through a thermoelectric module $(I)_n$ and load resistance is consistent with the current that passes through a single couple I since all the couples are connected together electrically in series. The efficiency of a single couple within a module is also representative of the efficiency of the entire module because the couples are thermally in parallel; each couple absorbs and liberates the same amount of heat and produces the same amount of output power.

Thermoelectric Coolers (TECs) Ideal Equations

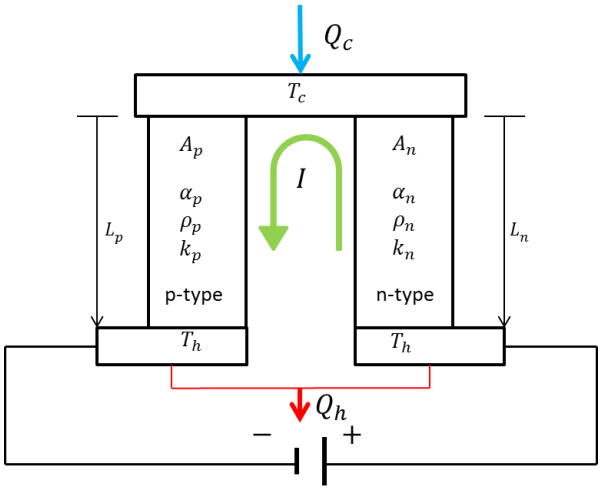

Figure 12. A TEC Attached to a Power Supply

Since the Peltier effect is reversible supplying current (or power) to a thermoelectric device will cause it to absorb and liberate heat depending on the direction of current. This effect becomes advantageous for mainly cooling and some heating applications. Using respective cold and hot junction temperatures, T_c and T_h, in lieu of temperatures T_1 and T_2, respectively, equations (1.33) and (1.34) become

$$Q_c = \alpha T_c I - \frac{1}{2} I^2 R - K(T_h - T_c) \tag{1.67}$$

$$Q_h = \alpha T_h I + \frac{1}{2} I^2 R - K(T_h - T_c) \tag{1.68}$$

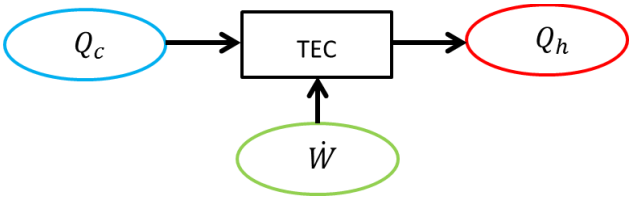

Figure 13. Energy Balance for a TEC

Similarly, the first law of thermodynamics can be applied to the system of TEC and power supply to obtain the power consumed by the TEC.

$$\dot{W} = Q_h - Q_c \tag{1.69}$$

$$\dot{W} = \alpha I(T_h - T_c) + I^2R \tag{1.70}$$

The power consumed by the TEC can be computed directly from the voltage V and current I of the power supply, yielding

$$\dot{W} = IV \tag{1.71}$$

The voltage V is

$$V = \frac{\dot{W}}{I} = \alpha(T_h - T_c) + IR \tag{1.72}$$

Compared to the voltage across the load resistance connected to a TEG in equation(1.40) the input voltage to a TEC is now the combination of both Seebeck and Ohm's Law voltages.

A metric of performance of cooling devices is the coefficient of performance COP which is the ratio of cooling (or heating) power to the input power.

$$COP = \frac{Q_c}{\dot{W}} = \frac{\alpha T_c I - \frac{1}{2} I^2 R + K(T_c - T_h)}{\alpha I (T_h - T_c) + I^2 R} \tag{1.73}$$

Similar to the maximum performance modes of a thermoelectric generator (TEG) the TEC has both modes of maximum cooling power and maximum COP. The variable parameter in this case is the current supplied I. Equation (1.67) is differentiated with respect to I and set to zero to obtain the current for maximum cooling power I_{mp}.

$$\frac{dQ_c}{dI} = 0 \rightarrow I_{mp} = \frac{\alpha T_c}{R} \tag{1.74}$$

For junction temperatures and using I_{mp} the maximum cooling power $Q_{c,mp}$ and corresponding voltage V_{mp} and coefficient of performance COP_{mp}, respectively, at those junction temperatures are

$$Q_{c,mp} = \frac{\alpha^2 T_c^2}{2R} + K(T_c - T_h) \tag{1.75}$$

$$V_{mp} = \alpha T_h \tag{1.76}$$

$$COP_{mp} = \frac{\frac{T_c^2}{2} + \frac{(T_c - T_h)}{Z}}{T_c(T_c + 1)} \tag{1.77}$$

The maximum COP can be obtained in a similar fashion, by differentiation equation (1.73) with respect to I and setting it equal to zero. The result is

$$\frac{dCOP}{dI} = 0 \rightarrow I_{mc} = \frac{\alpha(T_h - T_c)}{R\left[\sqrt{1 + Z\bar{T}} - 1\right]} \tag{1.78}$$

The subsequent cooling power $Q_{c,mc}$, voltage V_{mc} and maximum COP_{max}, respectively, are

$$Q_{c,mc} = \frac{\alpha^2 T_c (T_h - T_c)}{R\left[\sqrt{1+Z\bar{T}}-1\right]} - \frac{\alpha^2 (T_h - T_c)^2}{2R\left[\sqrt{1+Z\bar{T}}-1\right]} + K(T_c - T_h) \tag{1.79}$$

$$V_{mc} = \alpha(T_h - T_c)\left[1 + \frac{1}{\sqrt{1+Z\bar{T}}-1}\right] \tag{1.80}$$

$$COP_{max} = \frac{T_c}{T_h - T_c}\frac{\sqrt{1+Z\bar{T}} - \frac{T_h}{T_c}}{\sqrt{1+Z\bar{T}}+1} \tag{1.81}$$

The maximum input current will yield the maximum cooling power at particular junction temperatures. This leads the maximum current I_{max} to be

$$I_{max} = I_{mp} = \frac{\alpha T_c}{R} = \frac{\alpha(T_h - \Delta T_{max})}{R} \tag{1.82}$$

where ΔT_{max} is the maximum possible temperature difference across the junctions. The temperature difference is defined as

$$\Delta T = T_h - T_c \tag{1.83}$$

The maximum temperature difference occurs when the current is at its maximum value and the heat removed at the cold junction is equal to zero ($Q_c = 0$). Using equation (1.67) I and ΔT are set to I_{max} and ΔT_{max}, respectively, and solved to obtain

$$\Delta T_{max} = \frac{\alpha^2 T_c^2}{2KR} = \frac{1}{2} Z T_c^2 \tag{1.84}$$

Alternatively, using the definition of the figure of merit from equation (1.4) and rearranging gives $KR = \alpha^2/Z$. Substituting this into equation (1.84) the maximum temperature difference on the basis of T_h becomes

$$\Delta T_{max} = \left(T_h + \frac{1}{Z}\right) - \sqrt{\left(T_h + \frac{1}{Z}\right)^2 - T_h^2} \tag{1.85}$$

Equation (1.84) and (1.85) provide the definition of ΔT_{max} on the basis of T_c and T_h, respectively. The maximum cooling power $Q_{c,mp}$ at a given set of junction temperatures in equation (1.75) can be rewritten using equations (1.83) and (1.84) to become

$$Q_{c,mp} = K(\Delta T_{max} - \Delta T) \tag{1.86}$$

By simple observation, equation (1.86) yields the maximum possible cooling power for a particular material property and geometry (embedded in the $K = kA/L$ term) when $\Delta T = 0$. Thus, the maximum possible cooling power $Q_{c,max}$ occurs $\Delta T = 0$. This leads to

$$Q_{c,max} = K\Delta T_{max} \tag{1.87}$$

The difference between equations (1.86) and (1.87) is that $Q_{c,mp}$ is the maximum cooling power for a particular ΔT whereas $Q_{c,max}$ is the absolute maximum cooling power. Both equations depend on the maximum junction temperature difference ΔT_{max} that is determined by the constituent materials and junction operating temperature as seen in equations (1.84) and (1.85).

The maximum voltage can be computed using I_{max} and no heat load ($Q_c = 0$). Substituting equations (1.82) and (1.84) into equation (1.72) gives

$$V_{max} = \frac{\alpha^3 T_c^2}{2R} + \alpha T_c = \alpha(\Delta T_{max} + T_c) = \alpha T_h \tag{1.88}$$

Equation (1.88) can is shown in two forms, either in as a basis of T_c or T_h. Again, the above performance parameters can be normalized to obtained a generalized performance of a TEC. Using equations (1.74) and (1.84) into (1.64) and dividing by (1.75) the ratio of cooling power to maximum possible cooling power is

$$\frac{Q_c}{Q_{c,max}} = 2\left(\frac{I}{I_{max}}\right) - \left(\frac{I}{I_{max}}\right)^2 - \frac{\Delta T}{\Delta T_{max}} \tag{1.89}$$

Alternatively, on the basis of T_h, equation (1.89) can be rewritten as

$$\frac{Q_c}{Q_{c,max}} = \frac{2\left(\frac{\Delta T}{\Delta T_{max}}\frac{\Delta T_{max}}{T_h}\right)\frac{I}{I_{max}}}{1+\frac{\Delta T_{max}}{T_h}} - \frac{\left(1-\frac{\Delta T_{max}}{T_h}\right)\left(\frac{I}{I_{max}}\right)^2}{1+\frac{\Delta T_{max}}{T_h}} - \frac{2\frac{\Delta T}{\Delta T_{max}}\frac{\Delta T_{max}}{T_h}}{ZT_h\left[1-\left(\frac{\Delta T_{max}}{T_h}\right)^2\right]} \tag{1.90}$$

where

$$\frac{\Delta T_{max}}{T_h} = \left(1+\frac{1}{ZT_h}\right) - \sqrt{\left(1+\frac{1}{ZT_h}\right)^2 - 1} \tag{1.91}$$

Using equations (1.84) and (1.64) into equation (1.73) the COP can be rewritten as

$$COP = \frac{2\left(\frac{I}{I_{max}}\right) - \left(\frac{I}{I_{max}}\right)^2 - \frac{\Delta T}{\Delta T_{max}}}{\left(\frac{I}{I_{max}}\right)\left(\frac{\Delta T}{\Delta T_{max}}\right)ZT_c + 2\left(\frac{I}{I_{max}}\right)^2} \tag{1.92}$$

Equation (1.92) can also be rewritten in terms of T_h to become

$$COP = \frac{\left(1 - \frac{\Delta T}{\Delta T_{max}}\frac{\Delta T_{max}}{T_h}\right)\frac{I}{I_{max}} - \frac{1}{2}\left(1 - \frac{\Delta T_{max}}{T_h}\right)\left(\frac{I}{I_{max}}\right)^2 - \frac{\frac{\Delta T}{\Delta T_{max}}\frac{\Delta T_{max}}{T_h}}{ZT_h\left[1 - \frac{\Delta T_{max}}{T_h}\right]}}{\frac{\Delta T}{\Delta T_{max}}\frac{\Delta T_{max}}{T_h}\frac{I}{I_{max}} + \left(1 - \frac{\Delta T_{max}}{T_h}\right)\left(\frac{I}{I_{max}}\right)^2} \tag{1.93}$$

The normalized voltage can be obtained using equations (1.84) and (1.64) into (1.72) and dividing by (1.87). This leads to

$$\frac{V}{V_{max}} = \frac{\frac{\Delta T}{\Delta T_{max}}\frac{ZT_c}{2} + \frac{I}{I_{max}}}{\frac{ZT_c}{2} + 1} \tag{1.94}$$

Equation (1.94), rewritten in terms of T_h, becomes

$$\frac{V}{V_{max}} = \frac{\frac{\Delta T}{\Delta T_{max}}\frac{\Delta T_{max}}{T_h}}{\left(1 - \frac{\Delta T_{max}}{T_h}\right)\left(\sqrt{1 + Z\bar{T}} - 1\right)} \tag{1.95}$$

where

$$Z\bar{T} = ZT_h\left(1 - \frac{1}{2}\frac{\Delta T_{max}}{T_h}\frac{\Delta T}{\Delta T_{max}}\right) \tag{1.96}$$

The basis of T_h is usually used because it provides a limiting constraint as to what temperature the hot side of the TEC module is to be maintained at. The heat absorbed by the TEC on its cold side must be liberated at its hot side and the T_h basis stipulates the constraint of how the well the cooling of the hot side of the TEC should be to maintain the operating junction temperatures.

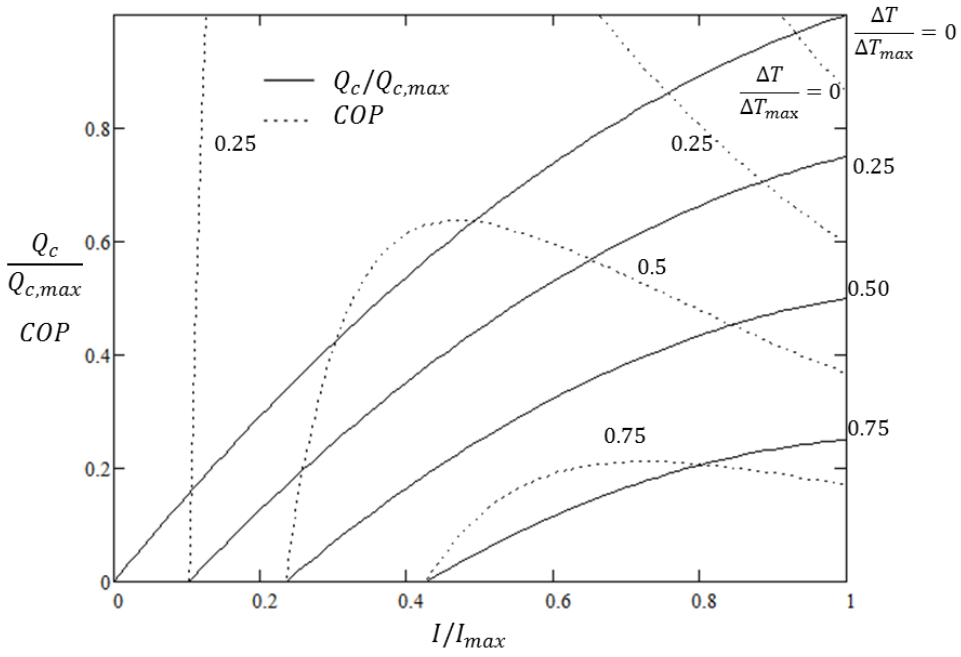

Figure 14. Generalized TEC Performance as a Function of Normalized Current of with $ZT_h = 1$

Figure 14 shows the generalized performance of a TEC for various temperature ratios as functions of the input current ratios. As predicted the increase of I/I_{max} increases the cooling power Q_c. Beyond the maximum input current ($I > I_{max}$) the cooling power begins to decrease. More importantly, the lower $\Delta T/\Delta T_{max}$, the higher the cooling power. This indicates that the higher the demand of temperature difference required for a specific application, the lower the cooling power obtained. As for the COP the maximum values at increasing $\Delta T/\Delta T_{max}$ occur at increasing I/I_{max}. Figure 15 illustrates a generalized performance of a TEC at various current ratios as functions of junction temperature ratio $\Delta T/\Delta T_{max}$. The parameters were analytically computed using equations (1.90), (1.93) and (1.95) on the basis of T_h.

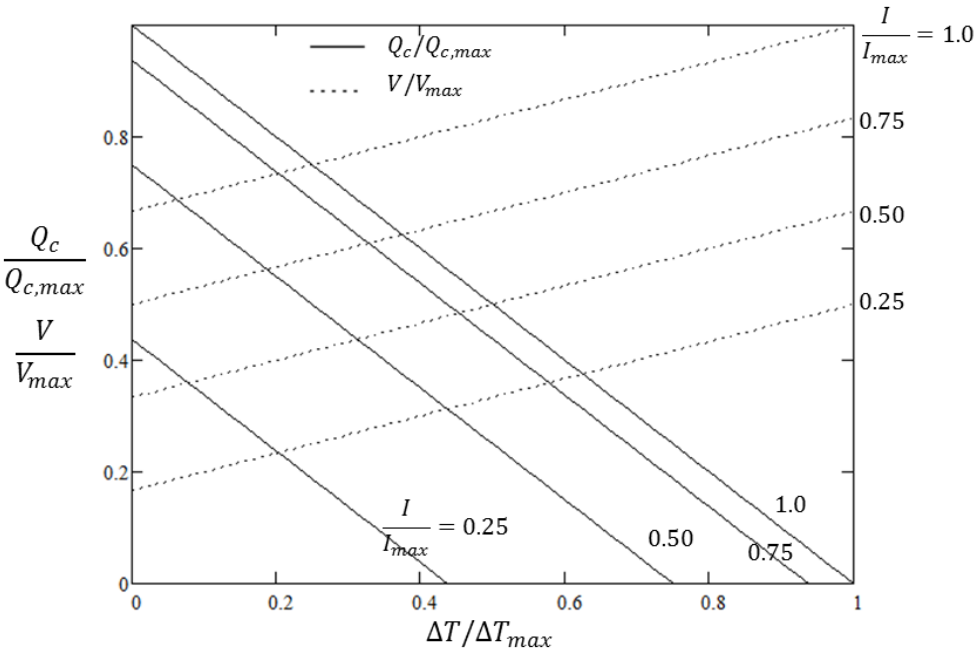

Figure 15. Generalized TEC Performance as a Function of Normalized Temperature with $ZT_h = 1$

Similar to TEGs the parameters of a TEC module are simply equal to the parameters of a single TEC couple multiplied by the total number of couples within a module n. These modular parameters, denoted with an m subscript, are

$$\left(\dot{W}\right)_m = n\dot{W} \tag{1.97}$$

$$(Q_c)_m = nQ_c \tag{1.98}$$

$$(Q_h)_m = nQ_h \tag{1.99}$$

$$(R)_m = nR \tag{1.100}$$

$$(V)_m = nV \tag{1.101}$$

$$(K)_m = nK \tag{1.102}$$

Again, the current from the power source passing through a thermoelectric module $(I)_n$ is consistent with the current that passes through a single couple I since all the couples are connected together electrically in series. The COP of a single couple within a module is also representative of the efficiency of the entire module because the couples are thermally in parallel; each couple absorbs and liberates the same amount of heat and produces the same amount of output power.

Assumptions of the Thermoelectric Ideal Equations

Due to the simplification of equations presented in the previous section it is of importance to highlight the assumptions that are embedded within these equations to avoid underestimation or overestimation of a thermoelectric module's performance. The first assumption is that the Thomson effect is negligible as described in the description for equation (1.12). It has been proven both analytically [15] and experimentally [16] that the Thomson effect has minimal effects on the performance of a thermoelectric module for both TEGs and TECs.

It is also assumed that the interfaces between the ceramic substrates that sandwich the thermoelectric elements as well as the electrical conductors that connect the couples together are perfect. In reality, due to imperfections during manufacturing and assembly, there are electrical contact resistances between the conductors and the junctions of each thermoelectric element and there are thermal resistances through the ceramic plates and electrical conductors. k_c in Figure 16 refers to the combined thermal conductivity of the ceramic plates and electrical conductors whereas ρ_c refers to the electrical resistivity of

the electrical conductors. Due to these contact resistances the junction temperature of the elements (indicated by $T_{c,1}$ and $T_{c,2}$) differ from the temperatures at the outer surfaces of the ceramic plates (indicated by T_1 and T_2). These contact resistances are difficult to measure and poor control during the manufacturing phase leads to detrimental module performances. The Ideal Equations assumes that these contact resistances are negligible.

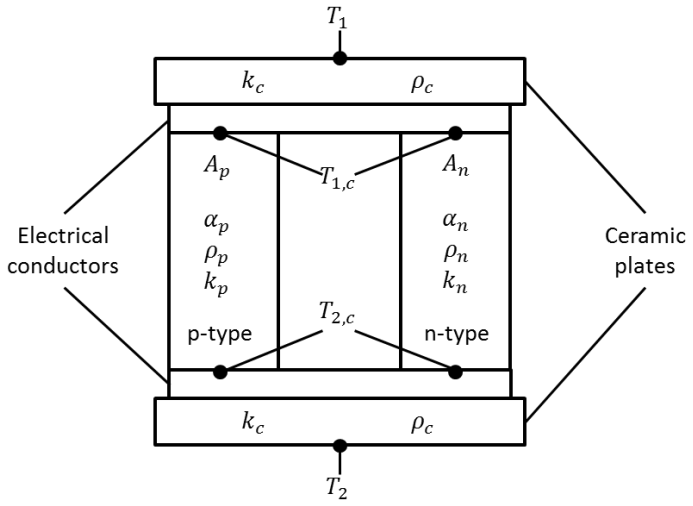

Figure 16. Configuration of Thermoelectric Couple Considering Contact Resistances

Other parasitic losses around the thermoelectric elements occur through convection and radiation during realistic operations. Most manufacturers insulate the outlying sides of the thermoelectric module to prevent convective losses. However, convection and radiation losses occur between the air gaps of the two ceramic plates, regions unoccupied by thermoelectric elements. The fill factor is the ratio of surface area occupied by thermoelectric elements to the total surface area of a module and is given as

$$FF = \frac{nA}{A_{TE}} \times 100\% \tag{1.103}$$

where A_{TE} is the total lateral surface area of a thermoelectric module. The smaller the fill factor the larger the potential losses through convection and radiation within a module. In most cases these parasitic losses are assumed to negligible, including in this study.

Another assumption employed within the Ideal Equations is the temperature independence of material properties. As aforementioned, the dimensionless figure of merit for various thermoelectric materials (refer to Figure 3) is dependent on the average operating temperature. According to equation (1.4) the figure of merit is composed of the Seebeck effect α, electrical resistivity ρ and thermal conductivity k which are evaluated at the average operating temperature. In actuality, these material properties vary according operating temperature, thus yielding the dependence of the $Z\bar{T}$ on $\bar{T}$ as seen in Figure 3. However, for the purposes and simplification of this study, the material properties were assumed to be independent of temperature and the results in CHAPTER IV have shown favorable agreement.

CHAPTER II

OBJECTIVE AND LITERATURE REVIEW

Problem Statement and Objective

With the ubiquity of thermoelectric devices being implemented in a gamut of applications the mass production and commercialization of thermoelectric modules have become widespread in today's thermal control and alternative energy industry. Such ramifications have caused manufacturers to produce a vast range thermoelectric products; from inexpensive thermoelectric modules for low-end, small scale applications to high performance and costly forms [17]. Designers aiming to incorporate thermoelectricity into their systems are faced with a challenging task of selecting the right type of thermoelectric module that would meet either their heating, cooling or power generation requirements.

As such, manufacturers are inclined to provide as much information as possible to their consumers. This information takes the form of performance curves or upper (or lower) operating limits. Manufacturers provide such information readily on their company or vendor websites. These websites tend to include either electronic formats of the documented performances or integrated online software that aids the customer in selecting a particular thermoelectric module to meet his or her criteria. Searching between products within the domain of one company tends to be straightforward but

predicaments arise when these performance charts are not standardized between different manufacturers. Designers would often find comparing products difficult in such cases. This is further exacerbated when manufacturers provide such performances in differing forms from one another. An example would be two TEC manufacturers providing performance information regarding their products. One would provide a graph of cooling power against current for a particular junction temperature difference while the other provides temperature difference against current for a particular cooling power. Although manufacturers provide as much information as possible regarding their products the commonality between each is limited.

The only surefire method of evaluating the actual performances of these thermoelectric modules would be to obtain them through purchase from the manufacturer and experimentally test them. Such methods are laborious, costly and time consuming to the consumer. Furthermore, not all consumers may have access to testing such modules in controlled environments. A viable alternative is to analytically determine the performance of these modules using the simplified or Ideal Equations presented in CHAPTER I. However, upon further inspection, these equations are not employable in the absence of module property information (the Seebeck coefficient α, electrical resistace R and thermal conductance K). This information is usually not available from the manufacture due to several reasons. Manufacturers that only assemble thermoelectric modules and package them for sale tend to obtain the thermoelectric elements from bulk vendors or an outside source. They are usually not provided with material property information by their suppliers or choose not to provide them to their customers (due to

material property testing inabilities or cost factors). In other cases these material properties may be deemed as proprietary information and not available to even customers. Thus, manufacturers provide alternative forms of performance information in non-standardized forms.

Despite the variations in representing information the maximum performance parameters are usually always provided by the manufacturer. In the case of the TEGs the maximum parameters are the maximum current I_{max}, the maximum voltage V_{max}, the maximum output power $\dot{W}_{max}$ and the corresponding efficiency at the maximum output power η_{mp}. On the other hand, for TECs they are the maximum temperature difference between the junctions of the module ΔT_{max}, the maximum current I_{max}, the maximum voltage V_{max} and the maximum cooling power (heat absorbed at the cold junction) $Q_{c,max}$.

A theory on using limited information to predict the performance of thermoelectric modules has been developed by Lee et al. [18]. The maximum performance parameters are used as components in the Ideal Equations in CHAPTER I to compute the material properties of a thermoelectric module. These computed material properties, known here within as the effective material properties, are substituted back into the Ideal Equations to analytically determine the performance of that particular thermoelectric module. One of the goals of this study was to experimentally validate this theory of effective material properties from the maximum performance parameters by comparing the experimental performance results with the analytical prediction and

against the performance data provided by the manufacturers. A test stand that could accommodate both TEG and TEC testing was constructed and a semi-automated testing algorithm designed and implemented. Thermoelectric modules were obtained from several thermoelectric manufacturers along with their respective performance curves and maximum performance parameters.

Thus, the objectives of the study can be summarized as

- To provide an analytical approach for designers to predict the performances of thermoelectric modules solely based on maximum parameters provided by the manufacturers.
- To experimentally validate the integrity of the provided commercial data and serve as a true basis of comparison against the analytical predictions.

Study of Previous Work

Evaluating the performance of a thermoelectric module has been a topic of constant study. Both analytical and experimental approaches appear in the literature with a varying degree of accuracy when compared to the actual manufacturer's performance data. Similarities were found in analytical and experimental techniques and methodologies between various research groups and publications allowing for categorization and classification. Here, four main groups are presented: basic performance evaluation, module property evaluation, the Harman method and performance based on maximum parameters.

Basic Performance Evaluation

Researchers tend to favor simpler methods of performance evaluation as these can easily be conveyed and reproduced by thermoelectric consumers or system designers. Experimental studies usually evaluate the integrity of a manufacturer's product by comparing experimental results with the results provided by the manufacturer. The studies presented in this section are not concerned with the thermoelectric material properties of a module but rather focus on the experimental methods to recreate the performance curves presented by the manufactures. These tests are conducted under various operating conditions as the actual testing conducted by the respective manufacturers is unknown. A prime example would be whether the testing of the product occurred in a vacuum environment or not. A vacuum environment would enable accurate heat transfer measurements at the cost of inaccurately representing a realistic operating scenario.

D'Angelo and Hogan designed a continuous long-term (1 month) test procedure to determine the performance of a TEG module manufactured by Tellurex [19]. Their test stand included a vacuum enclosure and a constant heat source, provided by a nickel-chromium wire, on the hot junction of the module. Their resultant performance curve of was in good agreement with the data provided by Tellurex. This study is indicative of the requirement of an evacuated environment to minimize convective losses around the test apparatus that would otherwise affect results.

Vazquez et al. designed a test bench to measure the performance of commercial TEG modules [20]. Their design revolved around sandwiching their test subject between a main block and an aluminum water cooled block. The main block would be the source of heat and was insulated to prevent as much losses to the environment as possible. They performed two modes of operation with the first being variation of the hot junction temperature while the cold junction temperature was maintained. The second mode of operation was to maintain the cold junction while the input power to the main block was varied. Their results agreed with the data provided by the manufacturer (Hi-Z) and they attributed their discrepancies to heat losses. They however, did not account for these losses in their calculations.

Rauscher et al. conducted testing on the efficiency of TEG modules [21] [22]. The test sample was sandwiched between a heater and cooling block. Since the efficiency is the ratio of output power to input heat transfer rate, as indicated by equation (1.42), two primary measurements are required. The output power was easily measured using electronic loads that provided variable load resistance. As for the input heat transfer rate, instead of conducting a more difficult heat transfer measurement, the measurement was purely electrical. The input electrical power to the heater block was computed as the heat transfer rate into the TEG sample. The losses from the heater block were eliminated using the principle of a guard heater. An outer heater was used to encase the primary heater and manipulated using proportional integral derivative (PID) controllers so that the temperature of the outer heater was at the same temperature of the primary heater. When both objects were at thermal equilibrium no heat loss would take place between the

primary heater and the environment. All the heat emitted from the primary heater was then absorbed by the TEG only. The results however, were not compared to commercial data.

The similar method of using guard heaters was employed by Anatychuk and Havrylyuk [23]. Their setup included a heat meter between the cold side of the sample and the cold heat sink. In their experiments they realized that the power output of the heater at the hot junction could be correlated to the heat flow through the heat meter at the opposite end. Thus, they calibrated the heat meter readings to the input power into the heater for quicker evaluations. This method however, was cumbersome because a lot of parasitic losses had to either be accounted for or prevented.

Takazawa et al. also computed efficiency measurements on TEGs with large temperature differences up to 500 K [24]. Similar to Anatychuk and Havrylyuk [23] the heat transfer rate on the hot junction was measured directly from the power input into the heater while the heat transfer rate at the cold junction was measured from the heat calibration of a copper block. The temperature gradient of the block was initially measured with its thermal conductivity accurately known. The copper block was constantly maintained at 300 K during the experiments. The test apparatus were placed within a vacuum ($< 10^{-3}$ Pa) enclosure to improve performance by reducing the thermal conductivity of air. Although radiation shielding was employed not all radiation losses were prevented at extreme temperatures.

Sandoz-Rosado and Stevens developed a test stand to characterize the performance of TEG modules [25]. They highlighted that the heat transfer rates were the most difficult measurements to accurately conduct. They analytically predicted the performance of TEG modules with known intrinsic material properties. These module properties were provided by Melcor and Hi-Z. Their analytical model accounted for parasitic losses that occurred in the unoccupied regions between the ceramic plates. Comparing their analytical and experimental results with the performance provided by the manufacturers it was concluded that the initially provided material properties were inaccurate.

Chen and Gwillaim conducted an experimental study on the heat transfer rate and efficiency of thermoelectric cooling systems [26]. Their analytical approach utilized the basic thermoelectric equations (similar to those presented by the Ideal Equations for thermoelectric coolers with the aforementioned assumptions). As for the thermoelectric material properties they considered two approaches: one using temperature dependent properties and the other independent of temperature. The material properties were provided by the manufacturer as empirical correlations of temperature. Alongside these values Chen and Gwillaim also evaluated material properties (using the same empirical correlations) at the average operating temperature. Their results showed their either approach had a discrepancy of less than 10% when evaluating the optimum current required for maximum COP of the system at particular junction temperatures and cooling rate required.

Module Property Evaluation

The performance of a thermoelectric module can be analytically evaluated when its material properties are known. Unfortunately, as aforementioned, these properties are generally unavailable to the consumer. Researchers have developed methods to determine these properties through a series of tests at steady state conditions that revolve around the Ideal Equations presented in CHAPTER I.

Huang et al. developed an automated means of determining a TEC module's properties [27]. They focused on designing a vacuum test chamber to minimize as much parasitic heat losses through convection to emulate the same type of high-performance testing by the module manufacturers. The test subject was sandwiched between a heater block and a cooling jacket to emulate two constant junction temperatures that were measured using thermocouples. By measuring the voltage and junction temperatures at open circuit conditions ($I = 0$) equation (1.72) was employed to determine the Seebeck coefficient α. The heater block was insulated and set to dissipate a particular amount of power. In this assumption no heat was lost from the heater block to the surroundings and all heat dissipated by it was absorbed by the thermoelectric module at steady state conditions. By knowing the power supplied to the heater block at such conditions and assuming minimal electrical loss the heat absorbed Q_c was determined. By knowing the value of Q_c and junction temperatures at open circuit conditions equation (1.67) was used to determine the thermal conductance K of the module. Once α and K were known the electrical resistance of the module R was determined using the equation (1.67) again but

at a known value of I. Repeating these measurements at various junction temperatures they found that the material properties were slight functions of the operating temperature. Their analytical prediction of the performance curves agreed well with the data provided by the manufacturer although they did not fit perfectly. They attribute this discrepancy to the fact that they employed the simplified Ideal Equations but the assumptions did not hold true. As such, they finally developed an empirical correlation to replace equation (1.67), with the limitation being that the correlation was only valid for that particular module itself, and not even the same model due to potential manufacturing variability.

This methodology of computing the Seebeck coefficient α and electrical resistance R of a module demonstrated by Huang et al. [27] is widely applied. This was also demonstrated by Leephakpreeda [28]. The only variation was that the thermal conductance K was computed from the heat dissipation of a copper plate across the TEC module during an open circuit operation. The value of Q_c in equation (1.67) at $I = 0$ was determined from the heat capacitance of a copper block over a period of time, assuming perfect thermal contact between the TEC module and the copper block.

Kraftmakher conducted a series of simple experiments with a thermoelectric module to operate as a heater, cooler and power generator [29]. A heater block and an ice bath were used to generate the necessary temperatures, loads and heating sources to the module. While operating in the mode of power generation the heat transfer rate at the hot junction was accurately computed by setting and maintaining the cold junction at $0\,°C$ using the ice bath and adjusting the heater at the hot junction until the temperatures were

equal to the ambient temperature. In such as case, no heat from the heater is lost to the environment and is absorbed entirely by the module. When operating as a cooler the hot junction was maintained at ambient temperature while the heater on the cold junction was set so that the temperature would difference across the module would be nullified ($T_h = T_c$). With such conditions, using equations (1.2) and (1.67) and knowing that T_c is equal to the ambient temperature as well as I and R (from separate testing), the Peltier coefficient was computed.

Faraji and Akbarzadeh designed a compact test stand to evaluate the performance of TEG modules [30]. The heat source was provided by a heater block while the temperature at the cold junction of the module was maintained using a water cooling loop. The heat was removed from the recirculating fluid using TECs to further minimize space. The Seebeck coefficient was computed by measuring the open circuit voltage of the module at known junction temperatures and employing equation (1.72). The thermal conductance was measured as an effective property that included the ceramic and electrical contacts as well as all the interfaces within the module at open circuit operation using equation (1.67). Since a TEG operates in the mode of maximum power output when the load resistance is matched with the internal resistance of the module the internal resistance of the tested module was computed through a sweep of variable resistances while maintaining the junction temperatures. A parabolic output of power as a function of load resistance was obtained. The load resistance value at which the maximum power output was achieved was determined to be the internal resistance of the module. The cold side heat transfer rate was additionally computed using an enthalpy flow equation. Their

performance curve results from experiments matched closely to the data provided by the manufacturer. They did not however, reemploy the calculated material properties to analytically predict the performance curves of the TEG. In their study they emphasized on the importance of exerting sufficient clamping force between the TEG and its interfaces; increasing the compressive force allowed for lower interface contact resistance and improved the power output up to a certain limit. This study of sufficient clamping force to reduce contact resistances was also supported by Montecucco et al. [31] (no module or material property evaluation) and by Hi-Z [32].

Hsu et al. conducted studies that focused on finding the thermopower of a module, namely by determining what they termed as "effective Seebeck coefficient" [33]. Their results on the Seebeck coefficient showed about a 30% difference when compared to theoretical values provided by the manufacturers and they attribute these discrepancies to two effects. The first was the effect of increased thermal resistance between the junctions of the module at lower clamping forces. The second source of error was attributed to inaccurate temperature readings of thermocouples placed on the ceramic plates of the module during operation. These temperatures were inaccurate due to thermal contact resistances and thus, they constructed a detailed thermal resistance network to account for the temperature difference and accurately determine the exact temperatures of the junctions. They suggested that by employing the concept of the "effective Seebeck coefficient" (determined from experimental procedures) the analytical computations were more accurate as the contact resistance errors were embedded into a smaller Seebeck coefficient value.

Mitrani et al. devised a methodology of extracting the properties of a TEC module [34]. Their experimental setup was similar to that of Huang et al. [27] except the cold side was cooled by an auxiliary TEC with a heat sink attached. Between the sample module and auxiliary TEC an aluminum block with known thermal conductivity and heat capacitance was placed. This allowed for either transient or steady state computations of the heat transfer rate at the hot junction.

Tanji et al. introduced a new method of screwing to assemble the thermoelectric elements within a module [35]. This was done to reduce thermal shear stress that would occur in conventional solid-joint methods. Since the screws would induce additional contact resistances they compensated this by using liquid InGa and solid Zn paste at the interfaces. To measure the heat transfer rates the junctions of the modules they instead used heat flux measurements through a nickel block of known thermal conductivity. They did not evaluate the Seebeck coefficient or electrical resistance of the module but computed the thermal conductance which included the ceramic plates and electrical conductors within the module.

Muto et al. evaluated the material properties of a single TEG element under large temperature differences [36]. As such, the effects of radiation and Thomson heating were included in their analysis and the material properties were evaluated as functions of temperature. These material properties were further simplified to become “effective material properties” that were evaluated as integrals over the operating temperature.

The Harman Method

The Harman method is a simplistic but accurate method of measuring the dimensionless figure of merit $Z\bar{T}$ that is widely implemented in the field of thermoelectrics [37]. This method was first proposed by T.C. Harman in 1958 and the term was named after him. The technique is based on measuring the total voltage and the voltage that stemmed from the electrical resistance, IR in equation (1.72) when a current is passed through a sample. By subtracting the electrical resistance component the voltage from the Seebeck effect V_α would be known and the Seebeck coefficient can be computed based on equation (1.1). Without considering Joule heating and Thomson effects Harman showed that

$$Z\bar{T} = \frac{V_\alpha}{IR} \tag{2. 1}$$

Some precautions using this method include ensuring that the test sample is in an evacuated environment and adequate current supply that is small enough to induce a Peltier effect and cause a temperature difference across the sample but not enough to induce substantial Joule heating [38]. Since the figure of merit is a good gauge to a thermoelectric materials performance its value is meaningful to designers.

Lau studied the effects of various levels of vacuum on a test sample when the Harman method of determining $Z\bar{T}$ was applied [39]. Nusselt number correlations were provided to correct for convection losses during testing. However, the results did not account for all uncertainties in various pressure levels in vacuum enclosures.

Min and Rowe proposed a modification of the Harman method in determining $Z\bar{T}$ [40]. They showed that Harman's method was quicker but induced about 20% of uncertainty where else measuring $Z\bar{T}$ from the individual material (or module) properties was more accurate (about only 10% uncertainty). In their publication they showed that by measuring the short-circuit temperature difference ΔT_s and open circuit temperature difference ΔT_o one would be able to determine the dimensionless figure of merit as

$$Z\bar{T} = \frac{\Delta T_s}{\Delta T_o} + 1 \tag{2. 2}$$

The advantage of this method over Harman's original proposal is that this only requires steady state conditions and not adiabatic environments as prescribed by Harman. The Harman method is not imperative in this study but is nonetheless highlighted as being an importance in the area of performance evaluation of thermoelectric devices.

Performance Based on Maximum Parameters

The methods presented here in this section are discussed in great detail in CHAPTER III. The maximum operating parameters of most thermoelectric modules were documented by manufacturers during their respective testing stages. In the case of TEGs three out of the four maximum parameters (I_{max}, V_{max}, $\dot{W}_{max}$ and η_{mp} or η_{max}) are required to reformulate the equations so that the module properties (α, R and K) can be obtained. Of the three maximum parameters two of them, $\dot{W}_{max}$ and η_{mp} or η_{max}, are essential, leaving the options to either be V_{max} or I_{max}. As for TECs the similar trend of three out of four maximum parameters (ΔT_{max}, I_{max}, V_{max} and $Q_{c,max}$) are required.

Again, of these three two of them (ΔT_{max} and I_{max}) are essential resulting in either $Q_{c,max}$ or V_{max} being arbitrary choices. Three out of four of the maximum parameters are required because three equations are required to solve for three unknowns. When the geometric information (cross-sectional area A and length L) of the thermoelectric elements are known, ρ and k can be computed directly from the module properties. The computation of the Seebeck coefficient α is independent of the element geometry information but depends on the number of couples n.

Lineykin and Ben-Yakoov developed an analytical model to determine the module material properties of thermoelectric modules provided by Kryotherm and Hi-Z [41]. They utilized three maximum parameters (ΔT_{max}, I_{max} and V_{max}) to reversely compute the module properties (α, R and K). They employed computer software to analytically predict the performance curves and compared the results with data provided by the manufacturers. Their results indicated good agreement. Zhang conducted a similar study and approach in reconstructing the performance curves of TECs based on ΔT_{max}, I_{max} and V_{max} values provided by manufacturers [42]. They experimentally verified their analytical work and compared their performance curve results against previous studies for TEC cooling on microprocessors.

Luo [43] employed the same method used by Lineykin and Ben-Yakoov [41] by using the maximum parameters (ΔT_{max}, I_{max} and V_{max}) to determine the module properties and analytically predict the performance of the module. A second approach of using ΔT_{max}, I_{max} and $Q_{c,max}$ was used and both methods varied only about 5% in

predicting the module properties. Both methods were then compared to the one of four manufacturer's performance curve and showed an acceptable highest difference of 13%.

A step-by-step concept on selecting appropriate TEC products from various manufacturers from a consumer's perspective was introduced by Tan and Fok [17]. They discussed difficulties faced by consumers due to the non-standardization of information presented by manufacturers and propose a standard means of comparing the performance of modules from different companies. They described the method of using three maximum parameters, ΔT_{max}, I_{max} and V_{max}, to compute the module properties and predict performance curves. Their analytical results were supported by experimental data and both forms agreed with data from the manufacturer up to about two thirds of I_{max}. The discrepancy of performance curves beyond that point was suggested to be due to the inherent temperature dependence of the material properties.

Ahiska et al. proposed an alternative computer-controlled method to measure module properties [44]. This concept relied on the maximum parameters of a module but did not have to be provided from the manufacturer. Also, they instead used parameters I_{max}, V_{max} and E_{max} which were determined through a series of automated tests on a computer-controlled test bench. E refers to the electromotive force (e.m.f.) that would be produced from a module solely based on temperature differences, which is nothing more than the open circuit voltage that stems from the Seebeck coefficient and temperature gradient and E_{max} is the maximum e.m.f. that can be produced by that module at a particular temperature difference across its junctions. A computer controlled algorithm

was written such that the steady state temperatures at the junctions were determined for a particular current supply value at which the voltage and e.m.f. were computed. The system would then increase the supplied current by a user defined step and repeat the same measurements until the maximum temperature difference was achieved at which the values of I_{max}, V_{max} and E_{max} would be recorded. Using this data the performance curves were analytically predicted, experimentally validated and showed good agreement with the data from the manufacturers. The goal behind the automated testing was to implement such features into large scale testing and quality control during manufacturing of modules. These concepts were also repeated and supported by Ciylan and Yimaz [45] in their work.

Summary of Literature Review

A wide array of experimental methods and techniques have been developed to evaluate the performance of thermoelectric modules and devices. Some researchers did not disclose the name of the manufacturers whose products were tested on and some did not make any comparison to commercially available data. The four categories of literature reviewed are summarized from Table 1 to Table 4. Under the 'Results and Comparisons' column only entries with 'versus' (vs.) denote cross-comparison while other entries denote independent results.

Table 1. Summary of Basic Performance Literature Review

Author(s)	Module Type(s)	Results and Comparisons	Comments
D'Angelo and Hogan	TEG	Experimental vs. commercial (Tellurex)	Vacuum
Vazquez et al.	TEG	Experimental vs. commercial (Hi-Z)	Parasitic losses unaccounted
Rauscher et al.	TEG	Experimental	PID guard heater
Anatychuk and Havrylyuk	TEG	Experimental	PID guard heater
Takazawa et al.	TEG	Experimental	Vacuum with radiation shielding
Sandoz-Rosado and Stevens	TEG	Analytical vs. experimental vs. commercial (Melcor and Hi-Z)	Used intrinsic properties
Chen and Gwillaim	TEC	Experimental	Temperature dependent material properties
Montecucco et al.	TEG	Experimental	Evaluated parasitic losses

Table 2. Summary of Module Property Evaluation Literature Review

Author(s)	Module Type(s)	Results and Comparisons	Comments
Huang et al.	TEC	Analytical vs. commercial	Empirical analytical model
Leephakpreeda	TEC	Analytical vs. experimental	Heat capacitance method to determine thermal conductivity
Kraftmakher	TEG and TEC	Analytical and experimental	Temperature difference nullification
Faraji and Akbarzadeh	TEG	Analytical and experimental	Studied effect of various compressive forces
Mitrani et al.	TEC	Analytical and experimental	Temperature dependent module properties derived
Tanji et al.	TEG	Experimental	Computed module thermal conductance only
Muto et al.	TEG	Analytical and experimental	Analysis accounts of radiation and Thomson heating effects
Kraftmakher	TEG and TEC	Analytical and experimental	Temperature difference nullification

Table 3. Summary of The Harman Method Literature Review

Author(s)	Module Type(s)	Results and Comparisons	Comments
Lau	TEC and TEG	Experimental	Various Nusselt number correlations to account for convection losses
Min and Rowe	TEC and TEG	Analytical	Junction temperatures to compute $Z\bar{T}$

Table 4. Summary Performance Based on Maximum Parameters Literature Review

Author(s)	Module Type(s)	Results and Comparisons	Comments
Lineykin and Ben-Yakoov	TEC	Analytical vs. experimental vs. commercial (Kryotherm and Hi-Z)	Used ΔT_{max}, I_{max} and V_{max} from manufacturers
Zhang	TEC	Analytical vs. experimental vs. commercial	Used ΔT_{max}, I_{max} and V_{max} from manufacturers
Luo	TEC	Analytical	Used ΔT_{max}, I_{max}, V_{max} and ΔT_{max}, I_{max}, $Q_{c,max}$
Tan and Fok	TEC	Analytical vs. commercial	Used ΔT_{max}, I_{max} and V_{max} from manufacturers
Ahiska et al.	TEC	Analytical vs. experimental	Analytical model uses experimental I_{max}, V_{max} and E_{max}
Ciylan and Yimaz	TEC	Analytical vs. experimental vs. commercial (Melcor)	Analytical model uses experimental I_{max}, V_{max} and E_{max}

CHAPTER III

THERMOELECTRIC MODULE PERFORMANCE EVALUATION

Effective Material Properties from Maximum Performance Parameters

The Ideal Equations provided in CHAPTER I are simple enough for most thermoelectric users and designers to evaluate the performance of a particular module. In order to utilize these equations it is necessary that the module properties (α, R and K) and junction temperatures (T_h and T_c) be known in either case of a thermoelectric generator or cooler. The junction temperatures are usually the objective or constraint to which the module is operated within. However, as aforementioned in CHAPTER II, the material (or module) properties are usually not available commercially or provided to the consumer. The maximum performance parameters are usually provided to gauge the performance of a particular module, albeit being insufficient to completely characterize the performance of a thermoelectric module alone without transforming them into material properties.

In such cases, the maximum performance parameters, alongside the Ideal Equations, can be algebraically manipulated to obtain the module properties. This concept of reverse computation, for TECs, is heavily based off work done by Lee et al. [18] with adaptions made for the cases of TEGs. When geometric information is available the material properties of that particular module can be further computed. This geometric

information encompasses the number of couples n, the cross-sectional area of each element A and the length of each element L. The provided maximum performance parameters are usually experimentally determined by the manufacturer. Although the testing conditions are unknown the results of the experiment have the effects that were once assumed to be negligible (such as parasitic losses) are now included in them. These previously assumed effects included both thermal and electrical contact resistances, the Thomson effect and parasitic (convection and radiation) losses. In reality these effects are present and are usually not accounted for due to the added complexity in analytical modeling. However, since the results from the experiment reflect realistic scenarios the maximum performance parameters obtained from these experiments should therefore contain these effects. The module (or material) properties that are derived from these experimentally determined values would also include such effects. Thus, these properties are appropriately termed "effective material properties" in this study because they include realistic effects (Thomson effect and parasitic losses) during operation as well as manufacturing defects (such as contact resistances). By employing the effective material properties directly into the Ideal Equations the heating, cooling or power generation performances can be accurately determined without having to account for the assumptions.

Both TECs and TEGs have four maximum parameters each. It is shown in the following section that each case will have two essential and one arbitrary (total of three) maximum parameters required to determine the effective material properties. This is in accordance to algebraically solving for three unknowns (α, ρ and k) whereby three

equations are sufficient. It is important to note that the results from either combination of three out of four of the maximum parameters will yield no convergence. This is due to the contradiction of the formulation of the Ideal Equations and the real measurements. The combination choice is highlighted in each case of TEG or TEC and its importance to the consumer is illustrated in practical purposes in CHAPTER IV.

Effective Material Properties of TEGs

Since thermoelectric modules contain one or more thermoelectric couples the number of couples n is an important parameter to consider in the Ideal Equations. Using the definition of modular TEG parameters from equations (1.60) and (1.65) onto equations (1.46) and (1.56), respectively, the maximum modular power output and voltage are

$$(\dot{W})_{m,max} = \frac{n\alpha^2(T_h - T_c)^2}{4R} \tag{3.1}$$

$$(V)_{m,max} = n\alpha(T_h - T_c) \tag{3.2}$$

The maximum current I_{max} is independent of the number of couples and was defined in equation (1.54) to be

$$I_{max} = \frac{\alpha(T_h - T_c)}{R} \tag{1.54}$$

For similar p- and n-type materials in every identical couple of a module the modular resistance $(R)_n$ and thermal conductance $(K)_n$, given in equations (1.64) and (1.66), respectively, can be redefined as

$$(R)_m = nR = n\rho\left(\frac{L}{A}\right) \tag{3.3}$$

$$(K)_m = nK = nk\left(\frac{A}{L}\right) \tag{3.4}$$

There are now two means of obtaining the effective modular electrical resistance $(R)_n^*$ from the maximum power output in equation (3.1): either by using the maximum current or voltage. Using the maximum current and by observing and comparing equations (3.1) and (1.54) it is found that

$$(R)_m^* = \frac{4(\dot{W})_{m,max}}{(I_{max})^2} \tag{3.5}$$

Alternatively, by using the maximum voltage, equations (3.1) and (3.2) yield

$$(R)_m^* = \frac{\left((V)_{m,max}\right)^2}{4(\dot{W})_{m,max}} \tag{3.6}$$

If the geometric ratio (element cross-sectional area *A* to length *L*) is known and it is assumed that the module has identical couples with both p- and n-type elements having the same geometry the effective electrical resistivity ρ^* can be computed. For similar p- and n-type materials and using equation (3.3), equations (3.5) and (3.6) respectively yield

$$\rho^* = \frac{4\left(\frac{A}{L}\right)(\dot{W})_{m,max}}{n(I_{max})^2} \tag{3.7}$$

$$\rho^* = \frac{\left(\frac{A}{L}\right)\left((V)_{m,max}\right)^2}{4n(\dot{W})_{m,max}} \tag{3.8}$$

The effective Seebeck coefficient α^*, obtained using the maximum current from equations (1.54) and (3.7), is

$$\alpha^* = \frac{4\left(\dot{W}\right)_{m,max}}{nI_{max}(T_h - T_c)} \tag{3.9}$$

Using the maximum modular voltage from equation (3.2) the effective Seebeck coefficient can also be obtained as

$$\alpha^* = \frac{(V)_{m,max}}{n(T_h - T_c)} \tag{3.10}$$

The junction temperature difference $(T_h - T_c)$ used in equations (3.9) and (3.10) must be the temperatures at which the maximum parameters were obtained. Also, the effective Seebeck coefficient is independent of the geometry but depends on the number of couples n because the thermopower effect is multiplicative. If information about the number of couples is absent the modular effective Seebeck coefficient α_n^* is computed instead. Using the maximum current and maximum modular voltage, respectively, they are

$$\alpha_n^* = n\alpha^* = \frac{4\left(\dot{W}\right)_{m,max}}{I_{max}(T_h - T_c)} \tag{3.11}$$

$$\alpha_n^* = n\alpha^* = \frac{(V)_{m,max}}{n(T_h - T_c)} \tag{3.12}$$

The effective figure of merit Z^* can be obtained from the maximum conversion efficiency of a TEG given in equation (1.52). Using the definition of average junction temperature $\bar{T}$ from equation (1.49) and algebraic manipulation yields

$$Z^* = \frac{2}{T_c\left[1+\left(\frac{T_c}{T_h}\right)^{-1}\right]}\left[\left(\frac{1+\left(\frac{\eta_{max}}{\eta_c}\right)\left(\frac{T_c}{T_h}\right)}{1-\left(\frac{\eta_{max}}{\eta_c}\right)}\right)^2 - 1\right] \tag{3.13}$$

where $n_c = 1 - \frac{T_c}{T_h}$ is the Carnot efficiency. Equation (3.13) is a convenient normalized form that utilized the ratio of junction temperatures $\left(\frac{T_c}{T_h}\right)$, cold junction temperature T_c and ratio of maximum thermal efficiency to maximum possible (Carnot) efficiency $\left(\frac{\eta_{max}}{\eta_c}\right)$. This is also known as the second law efficiency. The cold junction temperature is usually the base temperature in a TEG system due to mechanical constraints. More often than not equation (3.13) may not be applicable since manufacturers may not provide the maximum conversion efficiency but instead give the efficiency at maximum power, defined in equation (1.47). After algebraic manipulation this yields

$$Z^* = \frac{\frac{4}{T_c}\left(\frac{T_c}{T_h}\right)}{\eta_c\left(\frac{1}{\eta_{mp}}+\frac{1}{2}\right)-2} \tag{3.14}$$

By using either equation (3.13) or (3.14) the effective modular thermal conductance $(K)_n^*$ can be obtained through the definition of the figure of merit from equation (1.4) as

$$(K)_m^* = \frac{{\alpha_m^*}^2}{(R)_m^* Z^*} \tag{3.15}$$

If information regarding the geometry of the element and total number of couples are available the effective thermal conductivity k^* from equation (3.15), using equation (3.4), is

$$k^* = \frac{(\alpha^*)^2}{\rho^* Z^*} \tag{3.16}$$

Thus, with all three effective material or modular properties the performance of TEG module can easily be computed by using these effective values into the Ideal Equations. It is also shown that the maximum power output and efficiency (either at maximum conversion or maximum power) are essential for determining the effective properties but an arbitrary choice can be made for either the maximum current or voltage. It should also be noted that the effective material properties are obtained for a couple. If the material properties for a single element, either the p- or n-type is desired, the obtained value should be divided by two. This again, assumes similar p- and n-type materials and geometry in each couple.

Effective Material Properties of TECs

The input current I into the TEC module is a highly important parameter. The maximum current I_{max} is the current that yields the maximum temperature difference ΔT_{max} at no load on the cold side (cooling power $Q_c = 0$). The maximum current, occurring at ΔT_{max}, was expressed as

$$I_{max} = \frac{\alpha T_c}{R} = \frac{\alpha(T_h - \Delta T_{max})}{R} \tag{1.82}$$

The maximum temperature difference was defined in equation (1.85) as

$$\Delta T_{max} = \left(T_h + \frac{1}{Z}\right) - \sqrt{\left(T_h + \frac{1}{Z}\right)^2 - T_h^2} \tag{1.85}$$

The maximum modular cooling power occurs when the temperature difference $\Delta T = 0$ and the maximum current I_{max} is supplied. Using this definition alongside equations (1.75) and (1.98) the maximum modular cooling power is expressed as

$$(Q_c)_{m,max} = n\left[\frac{\alpha^2(T_h - \Delta T_{max})^2}{2R}\right] \tag{3.17}$$

The maximum modular voltage $(V)_n$ is obtained from equations (1.88) and (1.101), yielding

$$(V)_m = n\alpha T_h \tag{3.18}$$

There are two means of obtaining the effective Seebeck coefficient α^*: using the maximum current or voltage. Using the maximum current from equation (1.82) and maximum cooling power from equation (3.17) gives

$$\alpha^* = \frac{2(Q_c)_{m,max}}{nI_{max}(T_h + \Delta T_{max})} \tag{3.19}$$

Alternatively, using the maximum voltage from equation (3.18) alone yields

$$\alpha^* = \frac{(V)_{m,max}}{nT_h} \tag{3.20}$$

The modular effective Seebeck coefficient α_m^* can be computed when the number of couples n is unknown. Equations (3.19) and (3.20) become

$$\alpha_m^* = n\alpha^* = \frac{2(Q_c)_{m,max}}{I_{max}(T_h + \Delta T_{max})} \tag{3.21}$$

$$\alpha_m^* = n\alpha^* = \frac{(V)_{m,max}}{T_h} \tag{3.22}$$

The maximum temperature difference from equation (1.85) can be algebraically rearranged to obtain the effective figure of merit such that

$$Z^* = \frac{2\Delta T_{max}}{(T_h - \Delta T_{max})^2} \tag{3.23}$$

The effective modular resistance $(R)_n^*$ can be obtained using from the maximum current in equation (1.82) and the computed effective modular Seebeck coefficient that yields

$$(R)_m^* = \frac{\alpha_n^*(T_h - \Delta T_{max})}{I_{max}} \tag{3.24}$$

If geometric information and the number of couples are known the effective electrical resistivity ρ^* can be computed from equations (3.24) and (3.3) as

$$\rho^* = \frac{\alpha^*(T_h - \Delta T_{max})\left(\frac{A}{L}\right)}{I_{max}} \tag{3.25}$$

Finally, the effective modular thermal conductance $(K)_n^*$ is computed from the figure of merit defined in equation (3.23) to become

$$(K)_m^* = \frac{{\alpha_n^*}^2}{(R)_n^* Z^*} \tag{3.26}$$

If information regarding the geometry of the element and total number of couples are available the effective thermal conductivity k^* from equation (3.26), using equation (3.4), is computed as

$$k^* = \frac{\alpha^*}{\rho^* Z^*} \tag{3.27}$$

The choice of α_n^* or α^* being computed from either the maximum modular cooling power or voltage is arbitrary. However, the maximum current is required in either case. The effective figure of merit can only be computed from the maximum temperature difference. Thus, the maximum current and temperature difference are required to compute the effective module or material properties alongside either the maximum cooling power or maximum voltage. If the material properties for a single element, either the p- or n-type is desired, the obtained value should be divided by two. This again, assumes similar p- and n-type materials and geometry in each couple.

Experimental Method

The experimental results served as a means to identify if the commercial data obtained for comparison against the analytical method of effective material properties were repeatable and indeed experimentally obtained in the laboratory settings of their respective manufacturers. The goal was not to obtain the maximum performance parameters stipulated by the manufacturers but to investigate how accurate the analytical predictions would be when using information solely from the manufacturer's data sheets. The experimental results were to also be another basis of comparison in addition to comparing the analytical results to data provided by the manufacturer.

Experimental Overview

When a thermoelectric module is operated as a generating device the key parameters that are controlled to vary performance output values are the junction temperatures and attached load resistance. Since all performances are evaluated at steady state conditions these temperatures must be constant to signify that the rate of heat transfer is at a net value and is unchanging with time. The hot side is usually equipped with a heat source that can take various forms. The most common practice is surface to surface solid heating using plate or flat heaters [19] [30]. Cartridge heaters or resistance wire are sometimes embedded into metallic blocks of high thermal conductivity (usually aluminum or copper) instead of using prefabricated heaters. These heaters are insulated at all surfaces other than the one in contact with the module. The heat source is powered by a stable source (such as a DC power source) to ensure continuous and constant power so that steady state conditions can be achieved.

Heat has to constantly be rejected at the cold side of the module otherwise both junctions of the module would eventually reach thermal equilibrium and there would be no power generation. Heat dissipation on the cold side is usually achieved using forced fluid convection cooling. This depends on the amount of heat dissipated by the module. Forced air convection using fans or air blowers and heat fin type heat sinks would be sufficient for smaller heat dissipation rates while liquid cooling using water through cooling jackets or heat exchangers are used when a larger amount of cooling is required. Liquids such as ethylene glycol mixtures are commonly used to achieve cooling water

temperatures below freezing. Constant flow rates of these cooling fluids are crucial to achieving and maintaining steady state conditions. Forced air convection flow rates can be easily varied or maintained at a constant value by manipulating the input power to the fans. Liquid cooling is primarily achieved through a secondary heat exchange processes where the absorbed heat from the intermediary fluid is dissipated to the ambient using a heat pumping or refrigeration process. Recirculating chillers or bath temperature controllers are employed to achieve such conditions. These devices are electronically configured and controlled either by using internal or external control systems that usually employ a form of proportional-integral-derivative (PID) control [20] [23] [30]. This ensures that the circulating fluid is maintained at a desired temperature. Variable speed or positive displacement pumps are used to supply flow of liquid. When using positive displacement pumps bypass lines with adjustable valves are used to control the fluid flow rate [27].

The load resistance value, attached to the TEG, can be manipulated by using electronic loads. Electronic loads are primarily used to test power supplies, fuel cells and power generating devices. The electronic load, when attached to a power producing device, draws either a constant amount of voltage or current. Alternatively, the device can simulate a constant resistance value with precise control over extended periods of testing.

The important parameters when testing TECs are the junction temperatures and input power to the device (current and voltage). DC voltage and current to the module is fed to the module via a power supply. TECs are primarily tested as cooling devices but

can have their direction of current simply reversed to obtain heating. The cold side of the module is supplied with a constant heat source, similar to the heat sources when testing TEGs. This simulates cooling a constant heat flux. Since a TEC operates on the thermodynamic principle of a heat pump the absorbed heat and input power must be liberated at its hot side. Again, this cooling of the TEC is achieved using the same aforementioned as testing for a TEG, usually using some form of forced fluid convection.

Experimental Setup

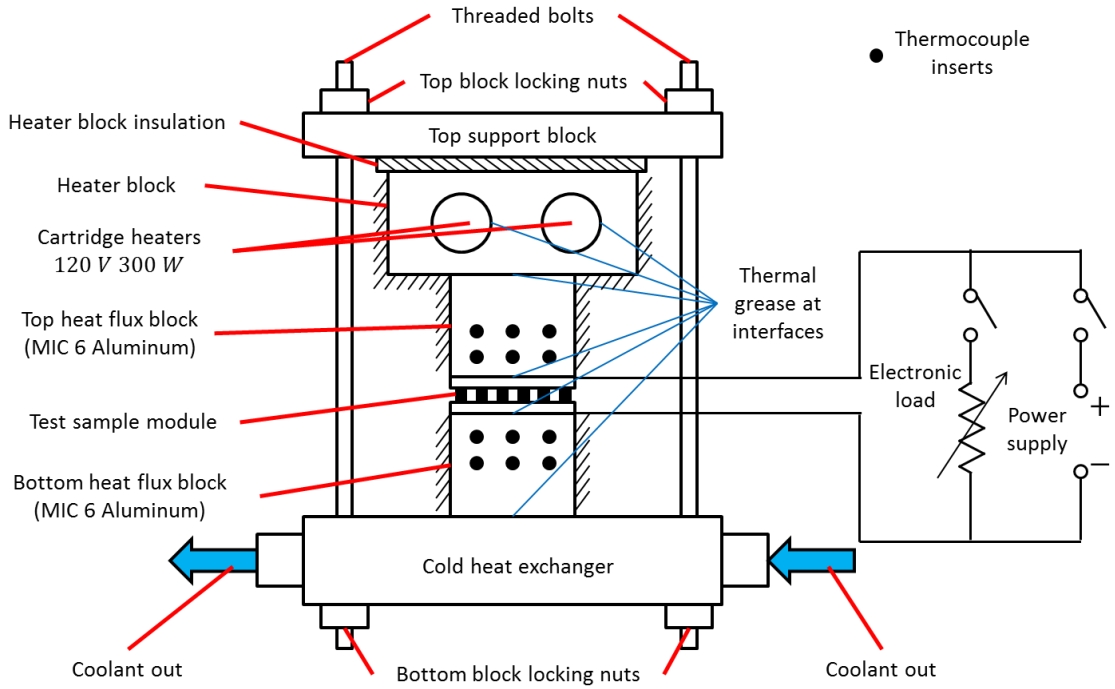

Figure 17. Schematic of Experimental Setup

The setup used in this study was designed to evaluate the performances of both TEG and TECs. The test stand accommodates commercial thermoelectric modules with

areas of up to 30×30 mm^2. Figure 17 shows the setup of the test stand connected to a switchable circuit that consists of an electronic load and a power supply while Figure 18 shows a photograph of the test stand with the side insulation pads removed.

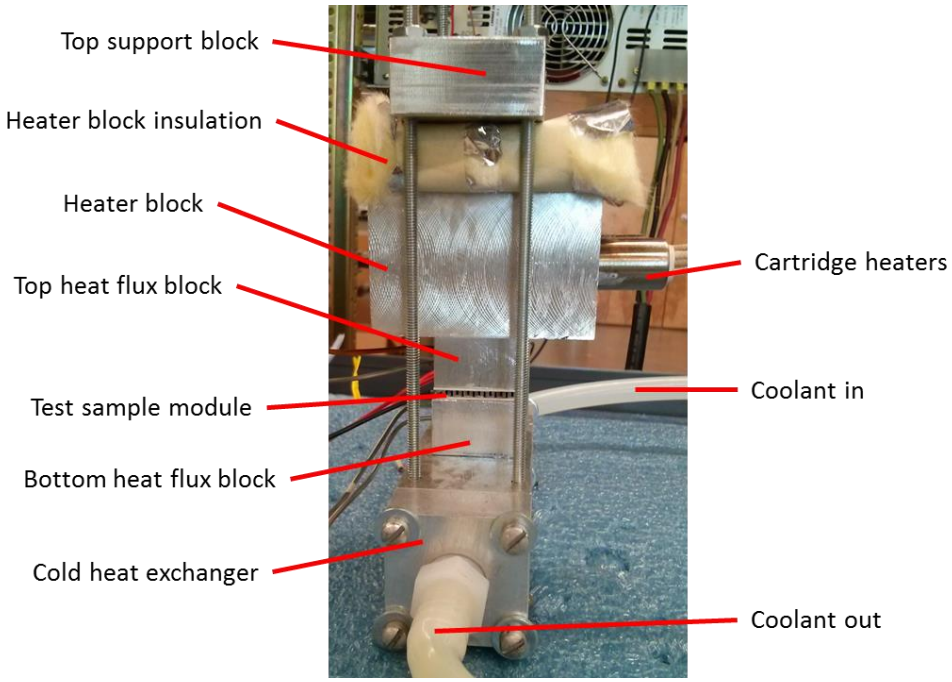

Figure 18. Photograph of Test Stand (without Side Insulation)

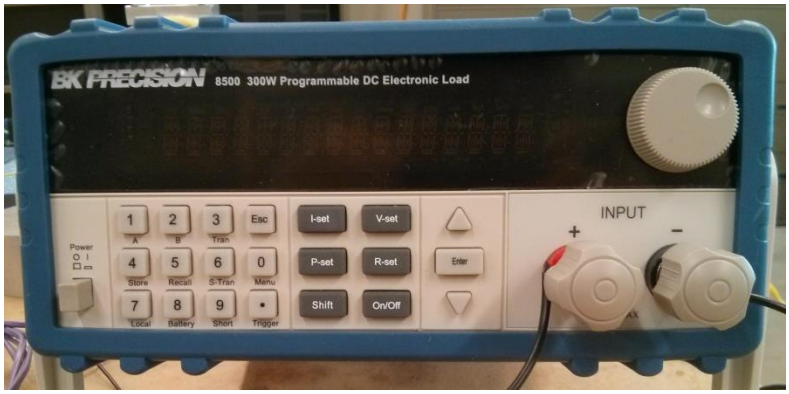

Figure 19. Test Stand Electronic Load

When testing TEGs the electronic load was used while the power supply was used when TECs were tested. The electronic load was a BK8500 Precision model (refer to Figure 19) that was capable of testing to 300 Wof power from a source. The unit can measure from 0 to 120 V of voltage and 0 to 30 A of current. The power supply to the TECs was a TCR 10 20S30D-2-D model (refer to Figure 20) that has an output of up to 20 V of DC voltage and 30 A of DC current (maximum of 600 W of power).

Figure 20. Test Stand Power Supplies

The heat was supplied by a heater block that consists of two cartridge heaters embedded within. The cylindrical cartridge heaters were manufactured by Omega Engineering, Inc. (part no. CSS-403300/120V) and are have dimensions of 5/ 8" (15.875 mm) in diameter and 3.5" (88.9 mm) in length. Each cartridge heater was rated to have up to 50 W/in^2 (0.078 W/mm^2) of power density, with a total of 300 W at a maximum voltage of 120 V. The resistance coils were embedded within a rust resistant sheath with a maximum temperature of 667°C, which was far beyond the

requirements of the experiments. Stainless steel sheaths were not required since the cartridge heaters would not be exposed to any ionized or corrosive fluids. The power supply connected to the cartridge heaters was a TDK-Lambda EMS80-60 model (refer to Figure 20) with an output of up to 80 V and 60 A of DC power for a maximum of about 5 kW of power.

Figure 21. Test Stand Recirculating Chiller

The heat dissipation of the module was achieved using a Thermo Scientific NESLAB RTE 7 recirculating chiller. The chiller consisted of a refrigeration system, circulating pump and a microprocessor temperature controller. The unit employed was capable of a temperature range between $-25°C$ and $150°C$. The pump had a capacity of

15 liters/min at 0°C. The operating fluid used was 50/50 glycerin/water with freezing and boiling temperatures of -22.8°C and 106°C, respectively. An internal 800 W heater was used alongside an embedded PID control to maintain the recirculating fluid at a desired working temperature (set point). The working fluid absorbed the heat liberated from the module via a one-pass, rectangular channel heat sink.

Both the heater and cold side heat sink sandwiched the test sample with respective heat flux blocks in between. These heat flux blocks were machined from MIC 6 aluminum alloy with an approximate thermal conductivity of $142\ \mathrm{W\,m^{-1}K^{-1}}$. Each block had a contact surface area of $30 \times 30\ \mathrm{mm^2}$ and height of 20 mm. There were six thermocouple inserts in each block with three slots on one horizontal level and another three on another horizontal level with a perpendicular distance of 5 mm between each row (center to center). These inserts were fitted with K-type thermocouples clad in standard stainless steel sheathing. Each insert had a diameter of 2 mm and a depth of 20 mm. The heat flux blocks were insulated at all surfaces other than those in contact with either the cold or hot sources and the module's surfaces using fiberglass held together by reflective tape.

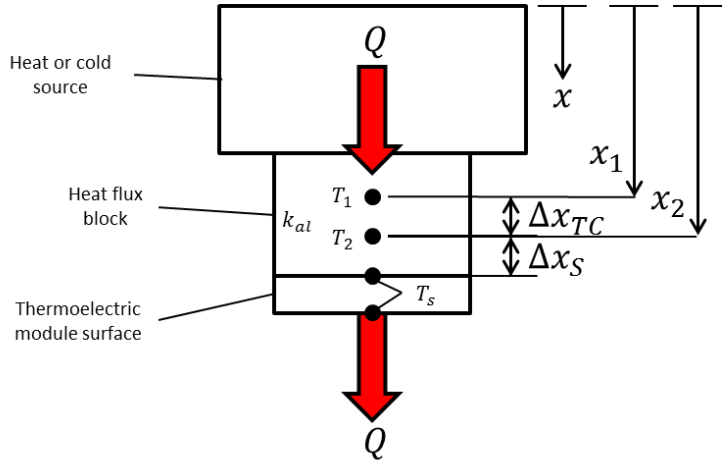

Figure 22. Temperature Extrapolation and Heat Flux Measurement

These heat flux blocks had two purposes. The first was to measure the heat flux that occurred at the particular junctions of the module and the second was to measure the junction temperature of the modules through a linear method of extrapolation. Consider the heat transfer diagram in Figure 22. With proper insulation and assuming perfect contact between interfaces as well as uniform heat fluxes from the cold or heat sources the heat transfer rates need only be considered one-dimensionally. For one-dimensional, steady state conductive heat transfer without any internal heat generation the governing equation for the heat flux block is given as

$$\frac{d^2T}{dx^2} = 0 \tag{3.28}$$

where T is the temperature as a function of distance x.The known boundary conditions (measured from thermocouples) are

$$T(x = x_1) = T_1 \tag{3.29}$$

$$T(x = x_2) = T_2 \tag{3.30}$$

Integrating equation (3.28) twice yields

$$T(x) = C_1 x + C_2 \tag{3.31}$$

where C_1 and C_2 are constants of integration. Applying the boundary conditions from equations (3.30) and (3.31) give a linear temperature profile within the heat flux block, that is

$$T(x) = \left(\frac{T_1 - T_2}{x_1 - x_2}\right) x + \left(T_1 - \frac{T_1 - T_2}{x_1 - x_2} x_1\right) \tag{3.32}$$

Since the temperature profile is linear x_1 can be set to the datum of 0 and $x_2 = x_1 + \Delta x_{TC} = \Delta x_{TC}$. This set up had $\Delta x_{TC} = \Delta x_S = 5$ mm. Equation (3.32) becomes

$$T(x) = \left(\frac{T_2 - T_1}{\Delta x_{TC}}\right) x + T_1 \tag{3.33}$$

Also, the surface temperature T_s at $x = \Delta x_{TC} + \Delta x_S$ can be obtained as

$$T_s = T(\Delta x_{TC} + \Delta x_S) = \left(\frac{T_2 - T_1}{\Delta x_{TC}}\right) \Delta x_s + T_2 \tag{3.34}$$

Furthermore, in accordance to the assumption of no contact resistances between the surfaces ceramic insulators and the actual junctions of the thermoelectric couples of the module, the extrapolated surface temperature T_s can be assumed to be the junction temperature of the module. This means of obtaining the junction temperature through extrapolation is equivalent to attaching an actual thermocouple probe between the ceramic surface and heat or cold source. The advantage of the method of direct measurement is a more precise temperature reading in the event of non-linearity

occurring in the temperature distribution of the heat flux block. The drawback of this method would be the induction of additional thermal contact resistances between the heat or cold source and the ceramic surface of the module unless extremely fine or flat thermocouples are used. Tape type thermocouples are generally more expensive than traditional cylindrical or wire types and may still induce unwanted thermal contact resistances between the interfaces.

The main goal of using the heat flux block was to facilitate the measurement of heat transfer rates at the junctions of the module without having to account for losses that occurred. Most previous research methods employed direct measurement of heat transfer rates from the heaters [23] or enthalpy equations for the cold side [30]. The power supplied to the heater was assumed to be the heat transfer rate absorbed by the module. Accounting for thermal losses was a tedious process and often the assumption of minimal losses with proper insulation was utilized. Based on the literature the most effective means of insulating the heat source was by using guard heaters around the main heater to ensure minimal to no temperature differences between them, thus eliminating as much conductive, convective and radiation losses. However, the amount of input power into the guard heaters would have to equal to, if not more, than the main heater, to ensure thermal equilibrium. This would entail a large consumption of input power.

The enthalpy method can be employed by knowing the temperature change of the cooling fluid between the outlet and inlet of the heat exchanger ΔT, the mass flow rate $\dot{m}$ and the heat capacitance of the fluid c_p evaluated at approximately the film (average)

temperature of the fluid. Equation (3.35) can then be used to compute the total heat transfer Q at the cold side at steady state conditions and assuming no thermal losses.

$$Q = \dot{m} c_p \Delta T \tag{3.35}$$

The heat meter used by [23] works based on this same principle. The use of this heat flux block was a much simpler approach as the losses need not be accounted for since the actual heat flux into and out of the module can be directly measured based on the existing thermocouple measurements. From Fourier's law of conduction and using equation (3.33), the heat flux is

$$q'' = \frac{Q}{A_{al}} = -k_{al} \frac{dT(x)}{dx} = -k_{al} \left(\frac{T_2 - T_1}{\Delta x_{TC}} \right) \tag{3.36}$$

where A_{al} is the cross-sectional area normal to the direction of heat flux and k_{al} is the thermal conductivity of the aluminum heat flux block. The heat transfer through either heat flux block is $Q = q'' A_{al}$. The setup had $k_{al} = 142\ W\ m^{-1}K^{-1}$ and $A_{al} = 30 \times 30\ \text{mm}^2$.

Preliminary tests of the cold and hot sources from the heater and chiller have shown uniform heat transfer throughout the heat flux block. This was indicated by the uniformity of temperature of any set of three thermocouples on one horizontal row; at steady state conditions they differed no more than ± 0.05°C. This further validates the assumption of one-dimensional heat transfer through the heat flux block.

To reduce thermal contact resistances between the interfaces highly conductive thermal paste/grease was applied between these regions (refer to Figure 22), including

between the cartridge heaters and their housing as well as between the thermocouples and their inserts (not shown in figure). Adequate amount of pressure was applied between all interfaces sandwiching the module to further reduce contact resistances using threaded bolts and nuts.

Experimental Control

Testing of the thermoelectric modules at various operating conditions required a certain degree of closed loop control. Most manufacturers stipulate the baseline temperatures at which their products were tested. These values also sometimes serve as constraints or limiting factors to which the modules should be operated within. For TEGs the limiting factors include the cold side temperature which the user should maintain in order to achieve desirable performance. As for TECs the limiting factor is the hot side temperature. Furthermore, most testing conducted by the manufacturers are at precise junction temperatures. In order to achieve these temperatures, closed loop control was exercised onto the test stand by manipulating the heat and cold sources (i.e. the heater and chiller) so that the junction temperatures were maintained at desired values.

Figure 23 shows the a connection schematic of the test stand to two power supplies (one controlling the heater and the other supplying power to TECs), thermocouples and an electronic load (when testing for TEGs). The power supplies and thermocouples were connected to a National Instruments data acquisition system (DAQ) that consists of an SCXI-1000 chassis with a SCXI-1303 isothermal terminal block. The thermocouples were attached to the terminal block that had a high-accuracy thermistor

cold-junction temperature sensor allowing for a built-in cold junction reference when taking temperature measurements. The power supplies had remote control capabilities and were connected to the DAQ via a PCI 6063-E analog terminal block. 0 to 5 V scales were used to control the output voltage of the power supplies independently. The DAQ was connected to a computer while the electronic load and recirculating chiller were connected straight to the computer using RS 232 serial communication. The temperature readings had a sampling rate of 1 kHz or 1000 samples per second. The sampling rate was set to 1 Hz or 1 sample per second since transient data was not crucial to this experiment.

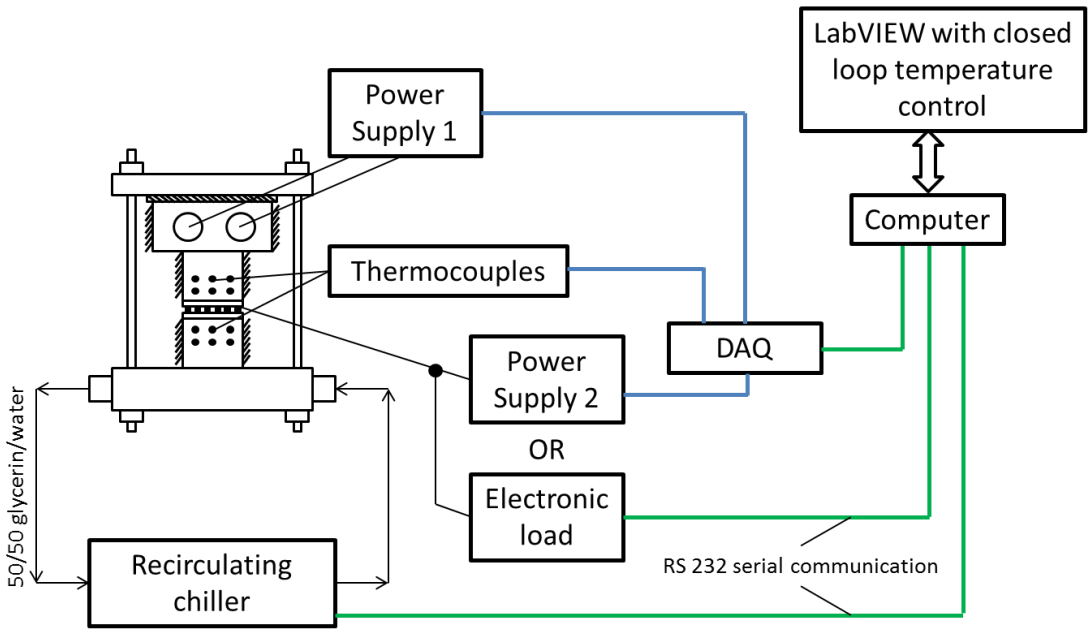

Figure 23. Overview of Experimental Control

All data acquisition and apparatus manipulation were achieved using National Instruments LabVIEW software to control the junction temperatures of the module. A

Virtual Instrument (VI) that integrated the power supplies, chiller and electronic load controls as well as temperature readings from the thermocouples was created in LabVIEW. The junction temperatures were maintained as closely as possible to set values by manipulating the voltage output of the power supply connected to the heater and the temperature set point of the chiller. The control loop was able to maintain the junction temperatures within $\pm 0.1\,^{\circ}\mathrm{C}$ of the desired values. Simple proportional gain (determined through a series of trial and error) was used since the settling time (transient behavior) of the system was not crucial.

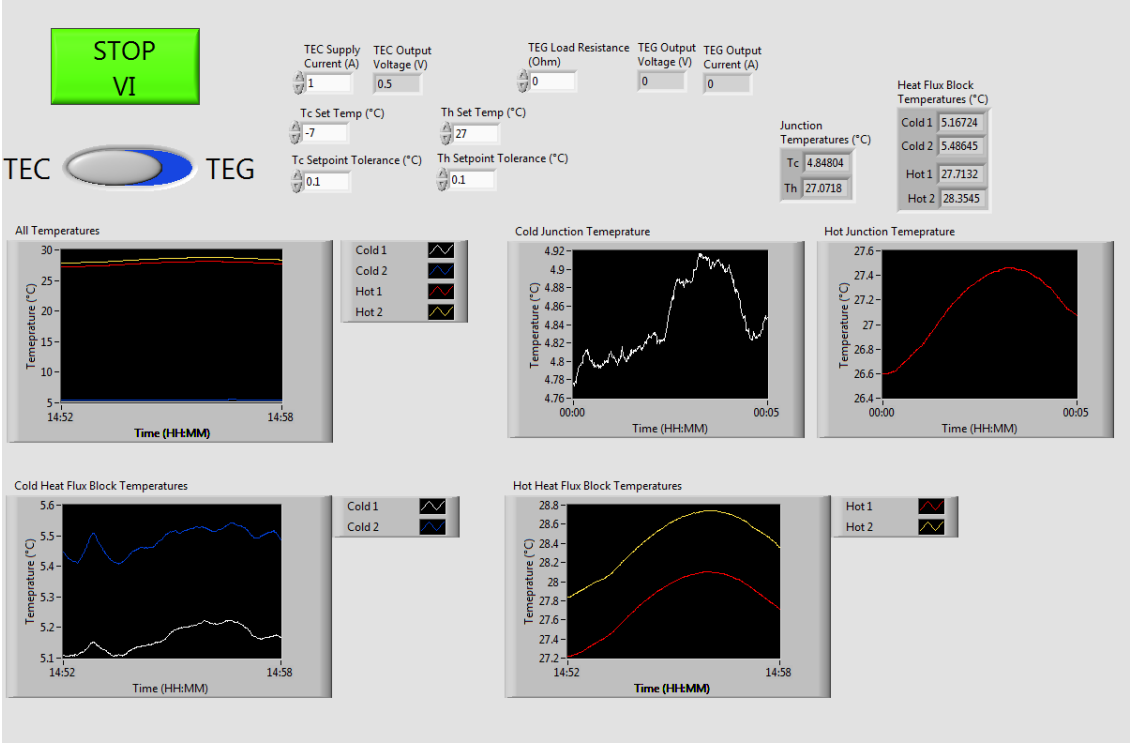

Figure 24. Front Panel of Data Acquisition VI

Figure 24 shows the front panel of the data acquisition VI. There are five waveform charts showing the various thermocouple readings against time. Two of these waveform charts are the junction temperatures of the test subject extrapolated from the thermocouple readings. It should be noted that the VI was captured while the testing was still in transient state.

Experimental Procedure

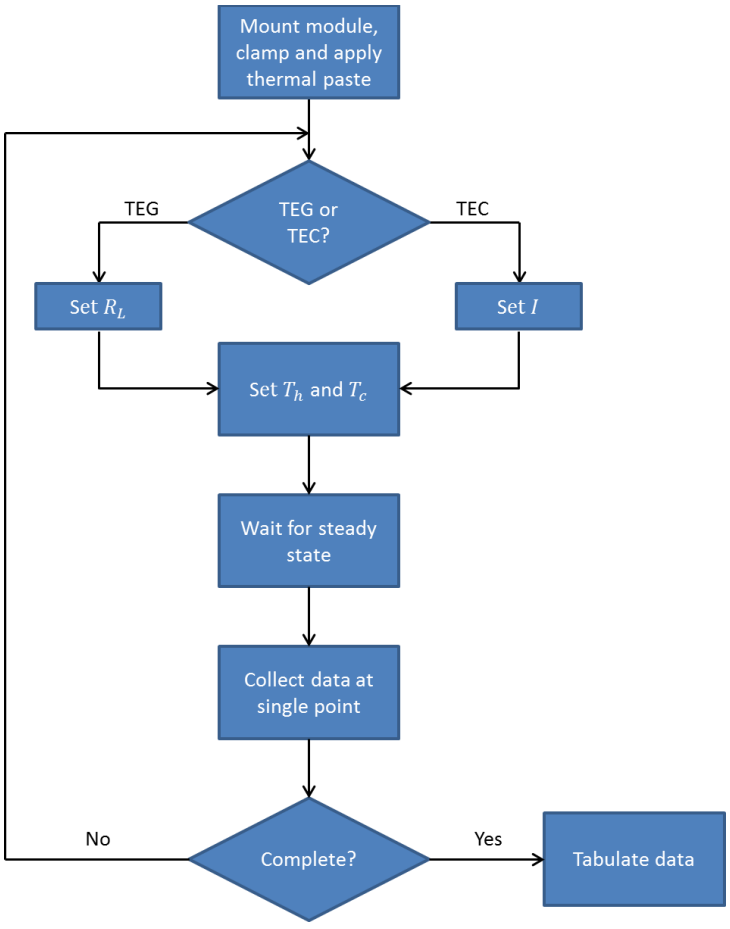

Figure 25. Process Flowchart of Experimental Performance Evaluation

This section outlines the steps involved when obtaining performance data on a module being tested. Figure 25 illustrates the processes to obtaining various data points that would be tabulated or graphed to show the performance of particular module. The first step in the process was to mount the specific test subject between the heat flux blocks (refer to Figure 17). Since the surfaces of the heat flux blocks had micro cracks and surface imperfections highly conductive thermal paste was applied onto such regions to reduce thermal contact resistances. The test stand was then bolted down with using the locking nuts using a torque wrench to ensure that all bolts applied equal pressure.

The VI was executed and the selection of whether the test sample was a TEG or TEC was made. In the TEG testing mode the electronic load was connected to the leads of the module while in TEC testing mode the power supply was connected instead. When TEGs were tested the load resistance was set to a desired value. In this mode the electronic load acted as a variable resistor. Alternatively, the electronic load was capable of operating in steady state modes of constant voltage, constant current and constant power. The electronic load would draw constant voltage, current or power values, respectively, from the TEG in these modes. If TECs were tested then the desired current value was supplied. Alternatively, the desired voltage could have been supplied to the TEC instead.

The subsequent step was to specify the junction temperatures to which the heater and chiller would maintain the test sample while it generated power or produced cooling. The control system required between 20 to 40 minutes to achieve steady state conditions.

It was noticed that larger temperature differences across the module or higher input power values would increase the waiting time. Steady state conditions were approximated by inspecting a waveform chart that shows the temperature readings versus time. When temperature values remained unchanged (within $\pm 0.1°C$) for approximately 2 minutes then steady state conditions were achieved and the VI would begin to write the data out into a spreadsheet file.

Most TEG manufacturers provide their performance curves at matched load resistance values because this value would yield the maximum power output. The initial matched load resistance value was obtained using the analytical approach (using effective material properties). The load resistance was then varied (increased and decreased) about this initial value until the true matched resistance value (one that yielded the maximum power) was identified. Sweeping through a range of resistances to determine the matched load conditions would be excessively time consuming without an initial guess value.

It should be noted here that the AC resistance of the module could not have been measured directly using conventional ohmmeters. Instead, an AC voltage must be used in practice according to [46] and was not conducted in this study. This is because normal DC current would cause a temperature drop across the module, resulting in a build-up of Seebeck voltage that would oppose the applied voltage. This in turn would yield erroneous voltage readings and make the resistance of the device larger than it really is. To counter this effect while still being able to accurate measure the resistance of the device a high a high frequency AC voltage should be applied. This AC voltage would

have a polarity change every half-cycle and would cause the built up Seebeck voltages to effectively cancel each other out.

The data acquisition process was repeated until sufficient data points are available for data tabulation. This data was then compared to the analytical approach and data provided by the manufacturers. These comparisons are shown in CHAPTER IV. The residual thermal paste between the heat flux blocks and module was removed when modules were swapped out by using 91% isopropyl alcohol. Excessive buildup of thermal paste would adversely impair the heat transfer between the interfaces instead of improving it and lead to erroneous temperature readings and heat flux calculations.

CHAPTER IV

RESULTS AND ANALYSIS

One of the goals of this study is to utilize the effective material properties to analytically predict the performance of commercial thermoelectric modules using the effective material properties that were directly derived from the maximum operating parameters provided by the manufacturers of the respective modules. This concept was employed on both TEGs and TECs. A total of four modules (two TEGs and two TECs) were evaluated analytically using the equations aforementioned in CHAPTER III to obtain the effective material properties and later experimentally tested for performance.

The two TEG modules obtained were

- TG12-4-01L by Marlow Industries
- HZ-2 by Hi-Z

The two TEC modules obtained were

- C2-30-1503 by Tellurex
- RC12-04 by Marlow Industries

The material properties were obtained directly when geometrical information regarding the thermoelectric elements were available, i.e. the number of couples n and

geometric ratio G. All thermoelectric couples were physically measured using vernier calipers except HZ-2 since the information was readily available on the manufacturer's website. The process of obtaining these values meant that the modules had to be irreversibly dismantled, rendering them irreparable and non-functional. It should be noted that the effective material properties were obtained for one couple on the assumption of similar materials and geometry between each thermoelectric element. The effective material properties shown here have been divided by two to reflect a single thermoelectric element. Also, all maximum parameters shown by the manufacturer are modular values; they reflect the parameters achieved by one module.

Once geometric information and maximum operating parameters were obtained they were directly employed into the Ideal Equation presented in CHAPTER I to predict the performance of the module. As aforementioned, for either TEGs or TECs, three out of four maximum parameters are required in any case. For TEGs the effective material properties determined from I_{max}, $\dot{W}_{max}$ and η_{mp} are referred henceforth within this study as the I_{max} set while the material properties determined from the alternate set of V_{max}, $\dot{W}_{max}$ and η_{mp} are referred to as the V_{max} set. The maximum efficiency η_{max} is rarely reported by manufacturers but the efficiency at matched load conditions (maximum power) η_{mp} is usually provided and was used throughout this study. Similarly, for TECs, effective material properties derived from ΔT_{max}, I_{max} and $Q_{c,max}$ are referred to as the $Q_{c,max}$ set and effective material properties from ΔT_{max}, I_{max}, and V_{max} are referred to as the V_{max} set.

TEG Results

TG12-4-01L by Marlow Industries

Table 5. Effective Material Properties for TG12-4-01L

Criterion	Symbols (unit)	Set I $T_h = 230$ °C, $T_c = 50$ °C	Set II $T_h = 170$ °C, $T_c = 50$ °C	Set III $T_h = 110$ °C, $T_c = 50$ °C
Provided maximum parameters	$\dot{W}_{max}$ (W)	4.05	2.12	0.61
	V_{max} (V)	9.45	6.50	3.28
	I_{max} (A)	1.71	1.32	0.75
	η_{mp} (%)	4.97	4.08	2.39
	R_M (Ω)	–	–	–
Effective material properties (I_{max} set)	α_I^* (μV K^{-1})	207.2	210.8	213.5
	ρ_I^* (Ω cm^{-1})	1.86×10^{-3}	1.64×10^{-3}	1.46×10^{-3}
	k_I^* (W cm^{-1}K^{-1})	1.56×10^{-2}	1.45×10^{-2}	1.39×10^{-2}
Effective maximum parameters from the I_{max} set	$\dot{W}_{max}$ (W)	4.05	2.12	0.61
	V_{max} (V)	9.47	6.42	3.25
	I_{max} (A)	1.71	1.32	0.75
	η_{mp} (%)	4.97	4.08	2.39
Effective material properties (V_{max} set)	α_V^* (μV K^{-1})	206.7	213.3	215.0
	ρ_V^* (Ω cm^{-1})	1.86×10^{-3}	1.68×10^{-3}	1.48×10^{-3}
	k_V^* (W cm^{-1}K^{-1})	1.55×10^{-2}	1.45×10^{-2}	1.40×10^{-2}
Effective maximum parameters from the V_{max} set	$\dot{W}_{max}$ (W)	4.05	2.12	0.61
	V_{max} (V)	9.45	6.50	3.28
	I_{max} (A)	1.71	1.31	0.74
	η_{mp} (%)	4.97	4.08	2.39
Effective figure of merit	Z^*T_c	0.478	0.611	0.729

Geometric information: number of couples $n = 127$, thermoelectric element cross-sectional area $A = 1.0$ mm^2, thermoelectric element length $L = 1.17$ mm, geometric factor $G = \frac{A}{L} = 0.085$ cm

Table 5 summarizes the effective material properties obtained for the TG12-4-01L TEG module. The manufacturer provided tabular data as well as graphical performance charts. The tabular data was reported at three different hot junction temperatures but with the same base cold side temperature. Since the maximum outputs of a module are dependent on temperature three separate cases of effective material properties were computed based on given maximum parameter information. Both I_{max} and V_{max} sets were employed as well, giving a total of six sets of effective material properties.

Whichever three parameters used in a particular set was exact to the effective maximum parameters (computed using α^*, ρ^* and k^*). As such the recalculated values of $\dot{W}_{max}$ and η_{mp}, from either set, were exact to the originally provided values. Using the I_{max} set to compute V_{max} or vice-versa showed minimal discrepancy. Thus, it was concluded that there was no significant difference in choosing either set to evaluate the effective material properties. The larger discrepancies in effective material properties, however, occur at various temperature ranges. This phenomenon was in agreement with the concept of thermoelectric material properties being dependent on temperature.

Employing the effective material properties into the Ideal Equations the performance of the module was analytically predicted and then compared to the data from the manufacturer. The analytical predictions in Figure 26 were computed using the effective material properties into equation (1.46). Comparing to the commercial data it shows that effective material properties from one set of temperatures could not accurately predict the power output over a large temperature range. Each set did however predict the

results that correspond to its highest temperature fairly well. For example, Set I ($T_h = 230°C$) predicted the power output accurately at higher hot side temperatures but failed to do so at mid to low hot side temperatures. On the other hand Set III ($T_h = 110°C$) accurately predicted the power output at low hot side temperatures where the other two sets failed to accurately do so.

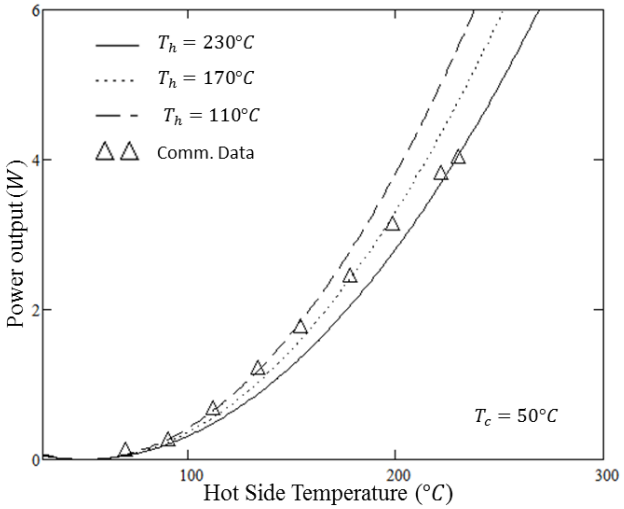

Figure 26. Analytical vs. Commercial Data Power Output (at Matched Load) Comparison for TG12-4-01L

In Figure 27, although all three sets' voltage predictions showed almost no discrepancy between each other, they were unable to accurately predict the output voltage provided by the manufacturer. Upon further inspection it was noticed that the commercial data showed non-linearity. The voltage from the Ideal Equations, equations (1.40) and (1.41), show a linear behavior as long as α and R are independent of temperature. This supported the phenomenon that material properties are temperature dependent over large

operating ranges according to [47]. The analytical plots were generated with equations (1.40) and (1.45) and known effective material properties.

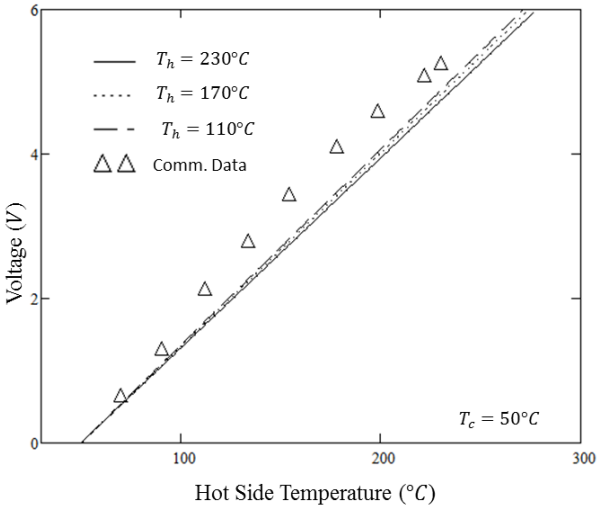

Figure 27. Analytical vs. Commercial Data Voltage (at Matched Load) Comparison for TG12-4-01L

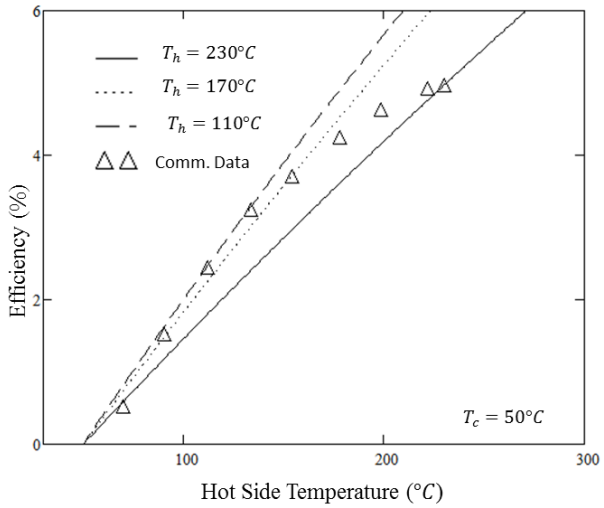

Figure 28. Analytical vs. Commercial Data Efficiency (at Matched Load) Comparison for TG12-4-01L

There were no performance charts provided for the efficiency of the TEG at matched load conditions but the manufacturer did provided the heat input values at corresponding hot side temperatures for the graph of power and voltage output. The efficiency, as defined in equation (1.42), is the ratio of output power to input power (heat transfer rate). The analytical predictions were computed using effective material properties into equation (1.47). Using this provided information the efficiency of the device as a function of temperature was compared to the analytical results in Figure 28. Here, a wide range of analytically predicted efficiencies are seen for each corresponding set. Generally, the commercial values fell between the entire range predicted by the three effective material properties sets. Similar to the comparison of output power in Figure 26 each set of effective material properties predicted the efficiency at its corresponding hot side temperature accurately but failed to do so at other temperature regions. This again showed a strong dependency of material properties towards temperature.

One method to consolidate the three sets of effective material properties was to use a weighted average where the weighting function was the temperature range over which the effective material properties were evaluated. The general statistical formula for weighted average is given as

$$\bar{X} = \frac{X_1 \Delta T_1 + X_2 \Delta T_2 + X_3 \Delta T_3 \ldots + X_n \Delta T_n}{\Delta T_1 + \Delta T_2 + \Delta T_3 \ldots + \Delta T_n} \qquad (4.\ 1)$$

Where $\bar{X}$ is the weighted average and X denotes any effective material property of interest (α, ρ or k), ΔT is the corresponding temperature range and the subscripts refer to the of set at which the corresponding effective material property was derived from.

Applying this to the original three sets the new effective material properties were $\bar{\alpha} = 210.0\ \mu V\ K^{-1}$, $\bar{\rho} = 1.72 \times 10^{-3}\ \Omega\ cm$ and $\bar{k} = 1.49 \times 10^{-2}\ W\ cm^{-1}\ K^{-1}$. It should be noted that the I_{max} set was used arbitrarily because the V_{max} set would have yielded identical results up to two decimal places.

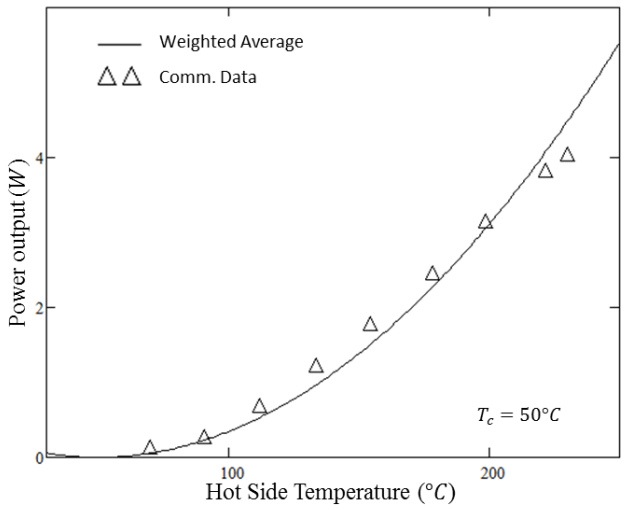

Figure 29. Weighted Average Effective Material Properties Power Output (at Matched Load) Comparison for TG12-4-01L

Figure 29 to Figure 31 show the comparisons using the weighted average effective material properties for power, voltage and efficiency at matched load resistances. The analytical power output showed a better agreement with the commercial data compared to before as well as the efficiency. However, the voltage comparison made no significant difference when either non- or weighted average effective material properties were used. This is because voltage output behaved non-linearly whereas the Ideal Equations that describe voltage were linear. Nonetheless, this method provided

accurate predictions for power output and efficiency performances of this particular TEG module.

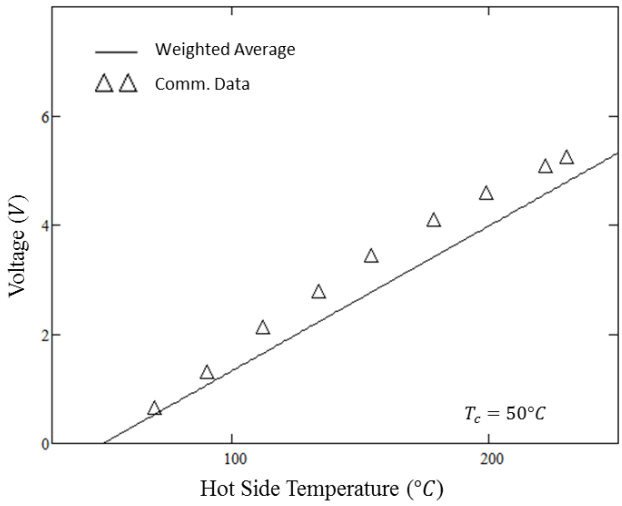

Figure 30. Weighted Average Effective Material Properties Voltage Output (at Matched Load) Comparison for TG12-4-01L

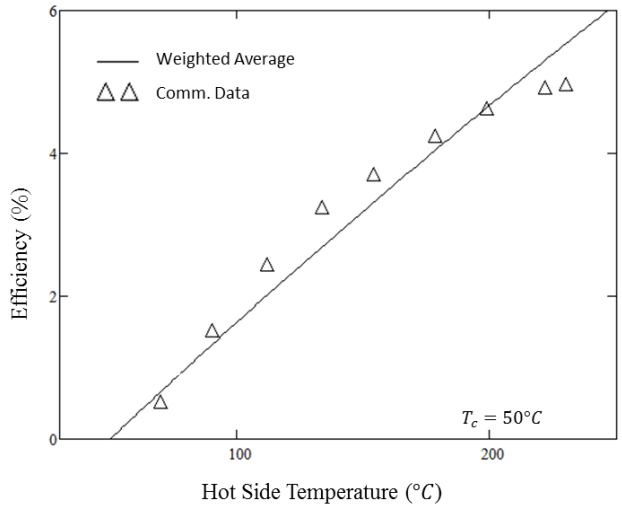

Figure 31. Weighted Average Effective Material Properties Efficiency (at Matched Load) Comparison for TG12-4-01L

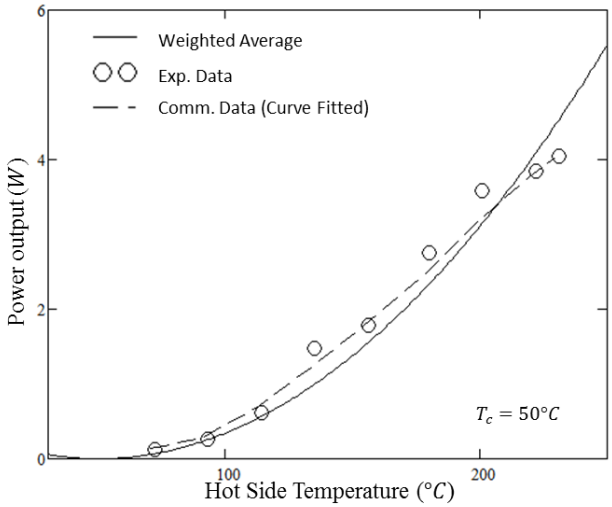

Figure 32. Three-way Power Output (at Matched Load) Comparison for TG12-4-01L

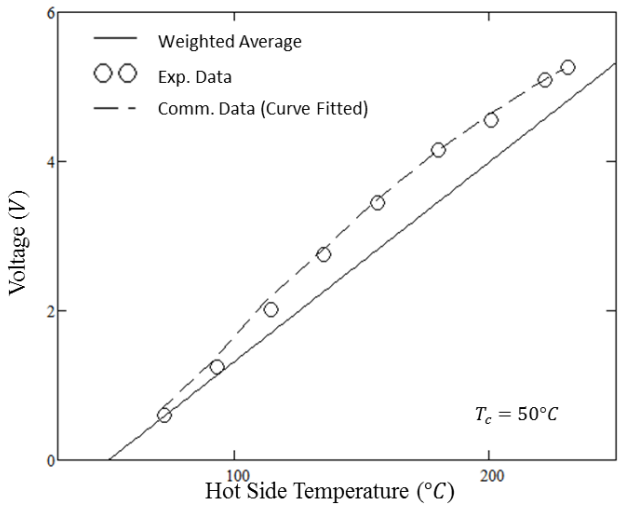

Figure 33. Three-way Voltage (at Matched Load) Comparison for TG12-4-01L

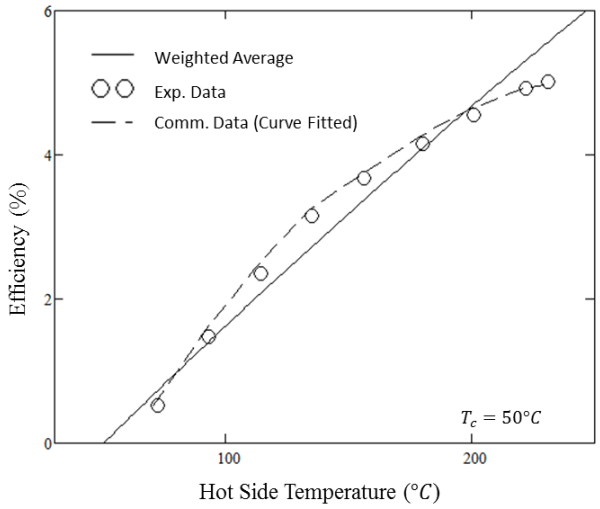

Figure 34. Three-way Efficiency (at Matched Load) Comparison for TG12-4-01L

Figure 32 to Figure 34 provide three-way (analytical, experimental and commercial data) comparisons. The experimental results followed closely to the commercial data provided by the manufacturer, validating that the performance charts were formed on the basis of experimental testing. There were slight discrepancies between the commercially provided values and results obtained in the laboratory through experimental testing.

HZ-2 by Hi-Z

Table 6 summarizes the effective material properties obtained for the HZ-2 TEG module. The maximum parameters were reported only at the recommended operating temperature of $T_h = 230°C$ and $T_c = 30°C$. Similar to the effective material property analysis performed on the TG12-4-01L TEG module either using the I_{max} or V_{max} set showed no significant discrepancies as the recalculated maximum values from either sets

are almost identical. Unlike the data provided by Marlow Industries, Hi-Z only reported the maximum parameters at one set of operating temperatures. The performance charts for power output, voltage and efficiency, all at matched load conditions, were functions of junction temperature differences at various cold side temperatures.

Table 6. Effective Material Properties for HZ-2

Criterion	Symbols (unit)	$T_h = 230$ °C, $T_c = 30$ °C
Provided maximum parameters	$\dot{W}_{max}$ (W)	2.60
	V_{max} (V)	6.53
	I_{max} (A)	1.60
	η_{mp} (%)	4.50
	R_M (Ω)	4.00
Effective material properties (I_{max} set)	α_I^* (μV K^{-1})	167.5
	ρ_I^* (Ω cm^{-1})	1.53×10^{-3}
	k_I^* (W cm^{-1}K^{-1})	1.62×10^{-2}
Effective maximum parameters using (I_{max} set)	$\dot{W}_{max}$ (W)	2.60
	V_{max} (V)	6.50
	I_{max} (A)	1.60
	η_{mp} (%)	4.50
Effective material properties (V_{max} set)	α_V^* (μV K^{-1})	168.3
	ρ_V^* (Ω cm^{-1})	1.55×10^{-3}
	k_V^* (W cm^{-1}K^{-1})	1.62×10^{-2}
Effective maximum parameters using (V_{max} set)	$\dot{W}_{max}$ (W)	2.60
	V_{max} (V)	6.53
	I_{max} (A)	1.59
	η_{mp} (%)	4.50
Effective figure of merit	Z^*T_c	0.343

Geometric information: number of couples $n = 97$, thermoelectric element cross-sectional area $A = 2.1$ mm^2, thermoelectric element length $L = 2.87$ mm, geometric factor $G = \frac{A}{L} = 0.073$ cm

The I_{max} set was arbitrarily used to obtain the effective material properties and predict the performance of the HZ-2 TEG using the Ideal Equations. The comparison results are shown in Figure 35 to Figure 37. The effective material properties and Ideal Equations were accurate in predicting the power output at matched load conditions even without the use of weighted averaging.

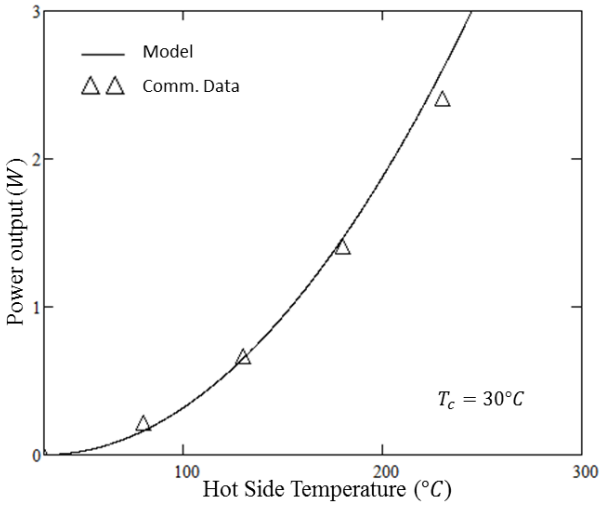

Figure 35. Analytical vs. Commercial Data Power Output (at Matched Load) Comparison for HZ-2

The voltage comparison showed evident discrepancies at regions of non-linearity. This behavior of non-linear voltage output at matched load resistances was seen in both TEGs tested and again, was attributed to the fact that the Ideal Equation only predicts a linear voltage output due to temperature independent material properties being used.

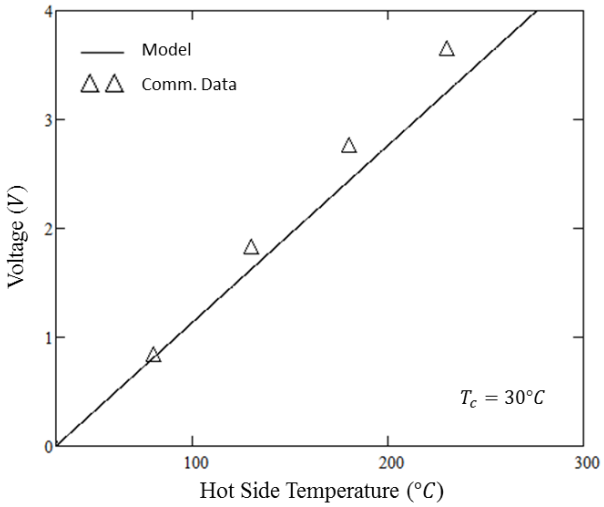

Figure 36. Analytical vs. Commercial Data Voltage (at Matched Load) Comparison for HZ-2

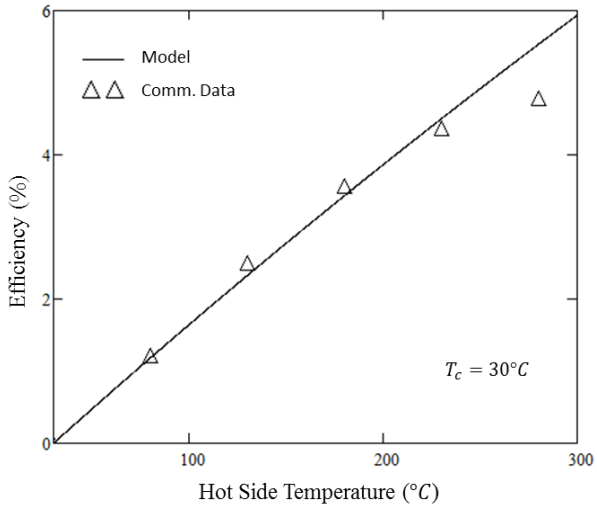

Figure 37. Analytical vs. Commercial Data Efficiency (at Matched Load) Comparison for HZ-2

The efficiency comparison at matched load conditions in Figure 37 shows similar results to the power output comparison in Figure 35; the model predicted accurately up

until the hot side temperature was 230°C at all cold side temperatures. The predictions beyond 230°C were unable to capture the effect of temperature dependent material properties.

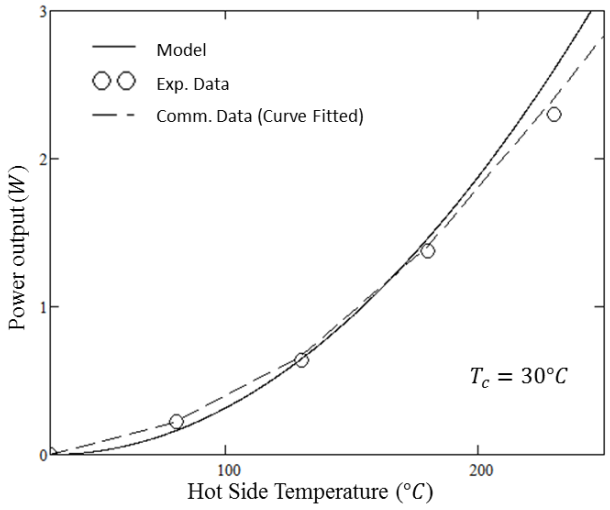

Figure 38. Three-way Power Output (at Matched Load) Comparison for HZ-2

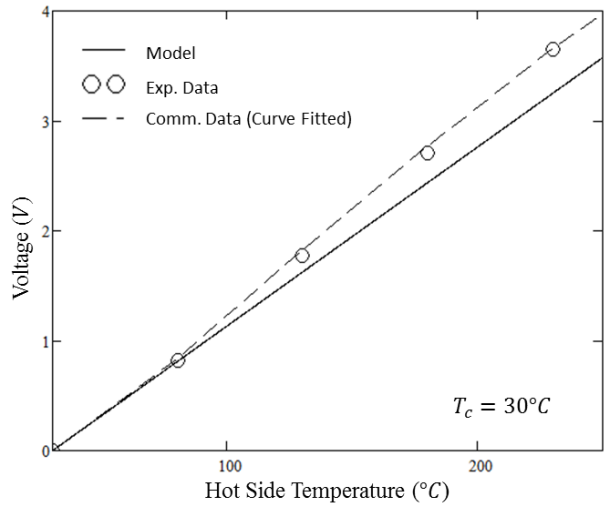

Figure 39. Three-way Voltage (at Matched Load) Comparison for HZ-2

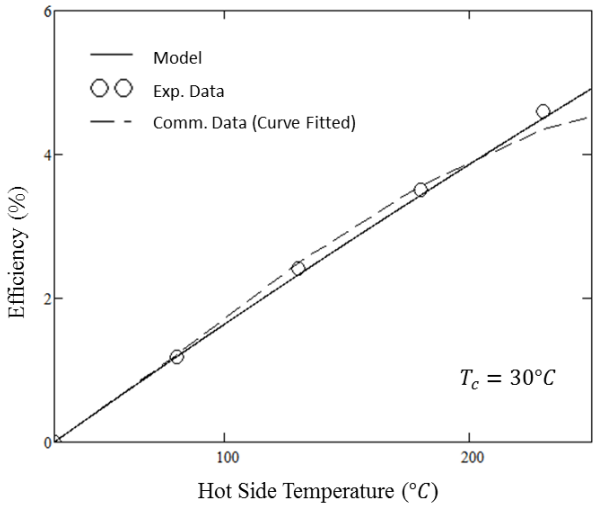

Figure 40. Three-way Efficiency (at Matched Load) Comparison for HZ-2

Experimental data was collected and compared against the analytical results as well as against the data from the manufacturer. The experimental setup only managed to increase the hot side of the module up to about 250°C while the cold side was maintained at 30°C due to the limitations of the cartridge heaters. The experimental results agreed closely to the data provided by the manufacturer. It is of interest to note that the voltage output at matched load conditions exhibited non-linearity in both TEGs, further validating the phenomenon of temperature dependence of the material properties at such high operating temperature ranges.

TEC Results

C2-30-1503 by Tellurex

Table 7. Effective Material Properties for C2-30-1503

Criterion	Symbols (unit)	Value at $T_c = 27$ °C
Provided maximum parameters	$Q_{c,max}$ (W)	34.14
	V_{max} (V)	15.5
	I_{max} (A)	3.5
	ΔT_{max} (K)	68
	R_M (Ω)	3.85
Effective material properties ($Q_{c,max}$ set)	α_Q^* (μV K^{-1})	208.6
	ρ_Q^* (Ω cm^{-1})	1.00×10^{-3}
	k_Q^* (W cm^{-1}K^{-1})	1.71×10^{-2}
Effective maximum parameters using ($Q_{c,max}$ set)	$Q_{c,max}$ (W)	34.14
	V_{max} (V)	15.9
	I_{max} (A)	3.5
	ΔT_{max} (K)	68
Effective material properties (V_{max} set)	α_V^* (μV K^{-1})	203.3
	ρ_V^* (Ω cm^{-1})	1.00×10^{-3}
	k_V^* (W cm^{-1}K^{-1})	1.71×10^{-2}
Effective maximum parameters using (V_{max} set)	$Q_{c,max}$ (W)	32.43
	V_{max} (V)	15.5
	I_{max} (A)	3.41
	ΔT_{max} (K)	68
Effective figure of merit	Z^*T_h	0.757

Geometric information: number of couples $n = 127$, thermoelectric element cross-sectional area $A = 1.21$ mm^2, thermoelectric element length $L = 1.66$ mm, geometric factor $G = \frac{A}{L} = 0.073$ cm

Table 7 summarizes the effective material properties obtained for the C2-30-1503 TEC module using both $Q_{c,max}$ and V_{max} sets. When predicting the maximum effective

parameters the $Q_{c,max}$ set predicted $Q_{c,max}$, I_{max} and ΔT_{max} values exactly while there was a 2.58% error between the predicted V_{max} value and the actual provided one. On the other hand, using the V_{max} set only predicted V_{max} and ΔT_{max} values exactly while a 2.57% error occured when predicting I_{max} and a 5.00% error occured when predicting $Q_{c,max}$. Unlike using either one of two sets in obtaining the effective material properties for TEGs, TECs showed a considerable difference in the two available methods.

Figure 41 and Figure 42 compare the analytically predicted values for cooling power and voltage, respectively, when using effective material properties obtained from either the $Q_{c,max}$ or V_{max} set. Equations (1.67) and (1.72) with known effective material properties were used to generate these plots. There were notable differences between the cooling power predictions but the discrepancies were less significant when predicting the voltages. This is because the Q_{max} set had its errors embedded within the recalculation of V_{max} but the V_{max} set had its errors distributed in both recalculations of $Q_{c,max}$ and I_{max} (refer to Table 7). $Q_{c,max}$ is a more common and crucial parameter to consider in module selection and priority should be given to its prediction accuracy over voltage predictions. Furthermore, Figure 42 shows that by using the $Q_{c,max}$ set the voltage prediction was almost identical to the voltage prediction when using the V_{max} set. Thus, all subsequent TEC predictions henceforth in this study using the effective material properties were derived from the $Q_{c,max}$ set.

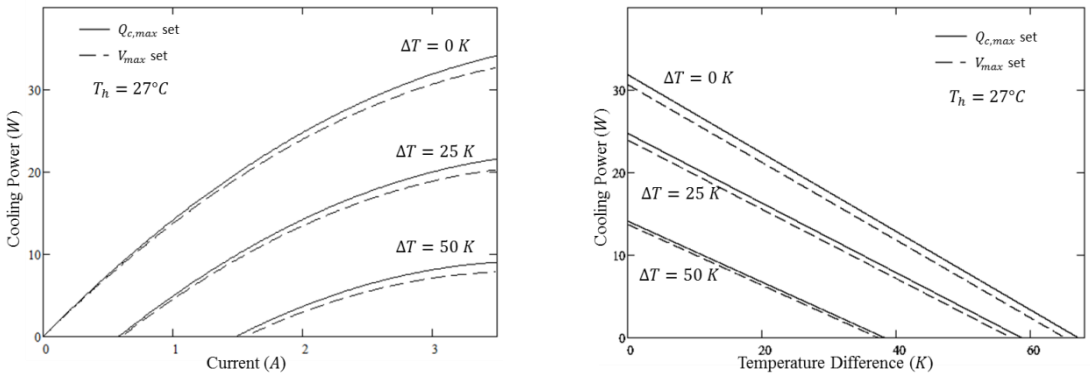

(a) (b)

Figure 41. Analytical Cooling Power Comparison between $Q_{c,max}$ and V_{max} Sets against (a) Current and (b) Temperature Difference for C2-30-1503

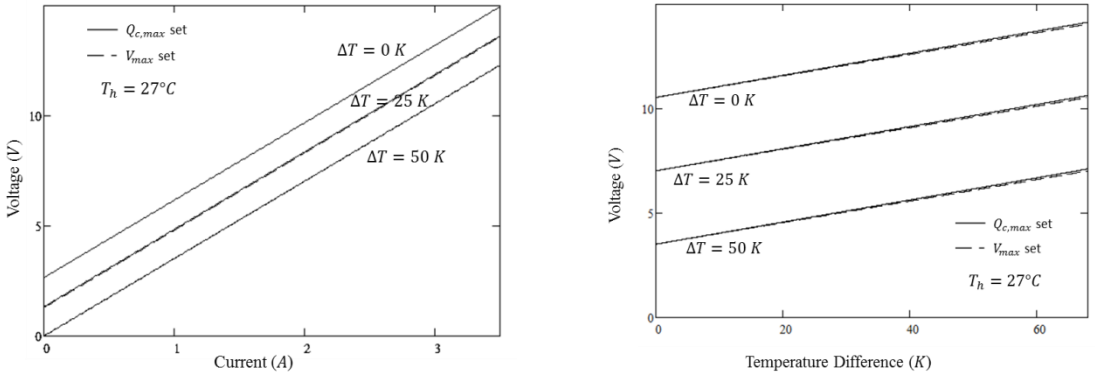

(a) (b)

Figure 42. Analytical Voltage Comparison between $Q_{C,max}$ and V_{max} Sets against (a) Current and (b) Temperature Difference for C2-30-1503

Figure 43, with analytical results computed using equation (1.67) with known effective material properties, compares the predicted cooling power against the data provided by the manufacturer. The prediction was almost identical to the data provided.

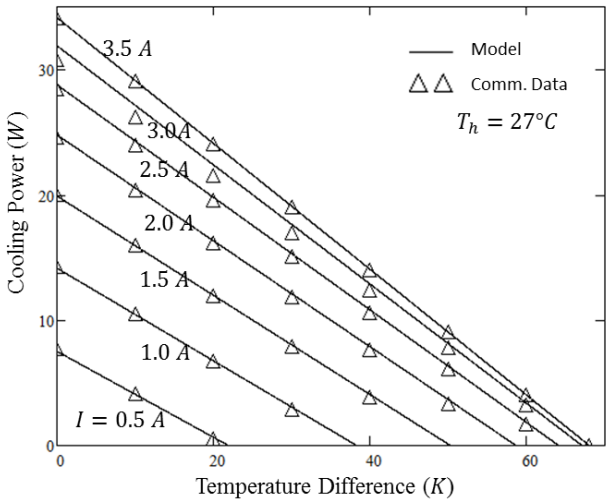

Figure 43. Analytical vs. Commercial Data Cooling Power Comparison for C2-30-1503

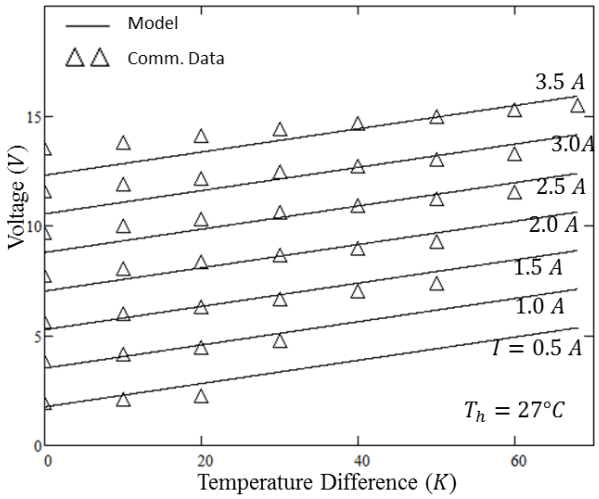

Figure 44. Analytical vs. Commercial Data Voltage Comparison for C2-30-1503

Figure 44, with analytical results computed using equation (1.72) and known effective material properties, compares the predicted voltages against the provided data. It is interesting to note that the error increases with decreasing temperature difference for any of the currents compared to; the analytical results were more accurate at temperature

differences closer to ΔT_{max}, the temperature range at which the effective material properties were derived. This was a very similar trend to the accuracies predicted by the effective material properties for the other two TEG modules. Moreover, using the V_{max} effective material properties set (not shown here) to predict the voltage against temperature difference for various currents showed no improvement in minimizing the discrepancy between the prediction and provided values.

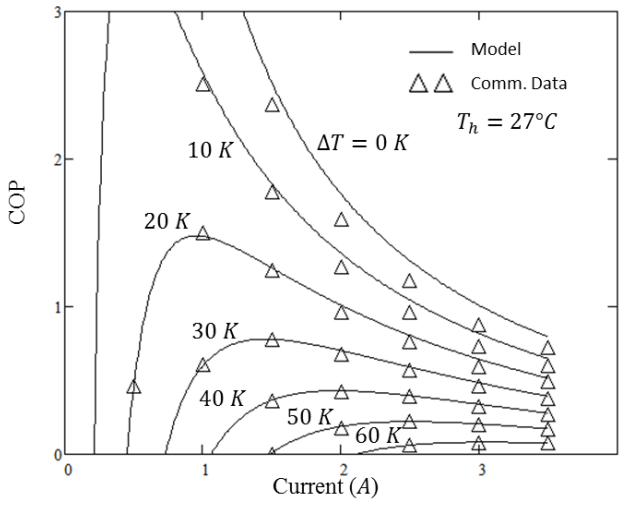

Figure 45. Analytical vs. Commercial Data COP Comparison for C2-30-1503

The manufacturer's charts did not include a COP analysis but it was implicitly obtained since the input power (from voltage against current chart) and cooling power plots for various temperature differences were provided and by using equation (1.73). These were compared in Figure 45 and showed some discrepancy. Albeit the cooling power predictions were accurate the input power had errors associated with it due to the inherent errors from the voltage predictions. Again, the error decreased with increasing

temperature difference for any range of current. This agreed with the concept that the effective material properties have the highest accuracy close to the maximum values, values at which they were derived.

Experimental data was collected and compared against the analytical and commercial data. Figure 46 compares the experimental data with results from the analytical model as a function of current instead of temperature difference on the x-axis. Various temperature differences were plotted nonetheless. The results showed almost no discrepancy between the experimental data and the prediction values, similar when the commercial data was compared to the analytical results.

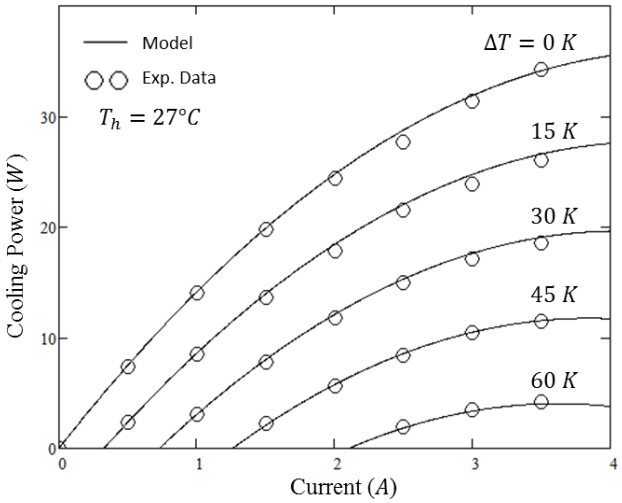

Figure 46. Analytical vs. Experimental Cooling Power Comparison for C2-30-1503

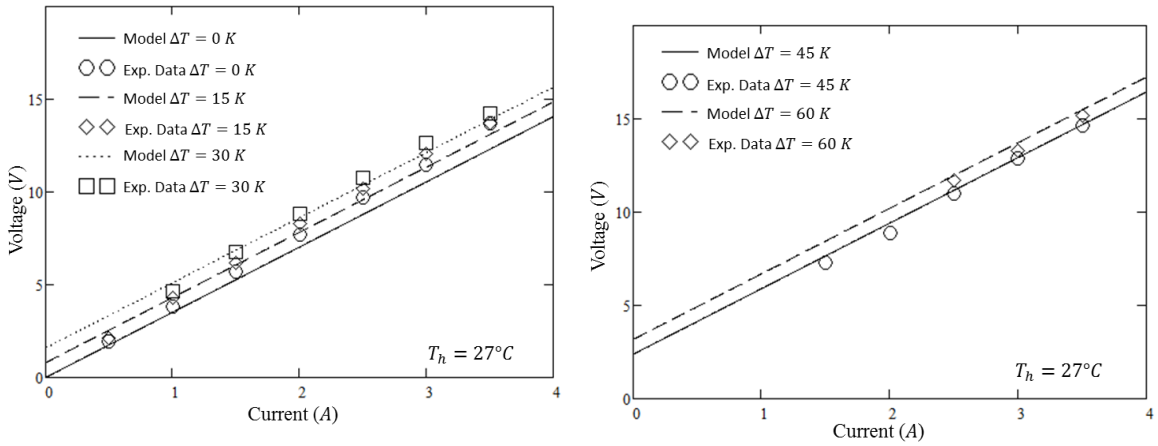

(a) (b)

Figure 47. Analytical vs. Experimental Voltage Comparison for C2-30-1503

Figure 47 compares the experimental voltages to the predicted values and is divided into two separate plots for clearer discernment between the analytical curves and experimental data points. As was expected, there were larger discrepancies at lower temperature differences compared to higher temperature differences. Analytically the voltage could have been predicted for any temperature difference and current but in actuality an input current that was too low would not be able to meet the required temperature difference for a fixed hot side value (27°C in this case). For example, only $2.5\ A$ and above of current could produce a temperature difference of $60\ K$. Thus, only the valid voltages were reported during the experiment.

Figure 48 compares the experimentally obtained COP (based on cooling power and input power from current and voltage readings) against the analytically predicted

values. The accuracy of the analytical predictions were better at larger temperature differences, similar to comparison against the commercial data.

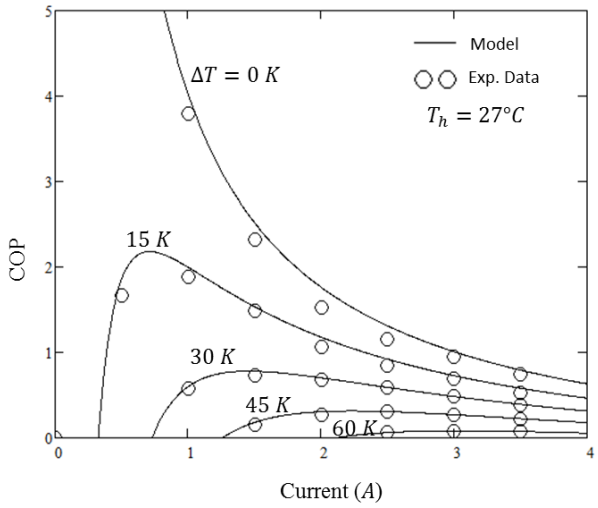

Figure 48. Analytical vs. Experimental COP Comparison for C2-30-1503

Figure 49, Figure 50 and Figure 51 compare the experimental cooling power, voltage and COP to the commercially provided values, respectively. The results indicated almost exact agreements. This validated that the commercial data was indeed experimental results.

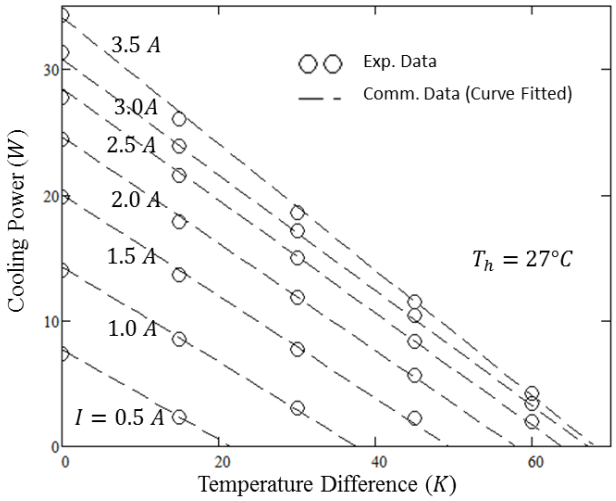

Figure 49. Commercial vs. Experimental Cooling Power Comparison for C2-30-1503

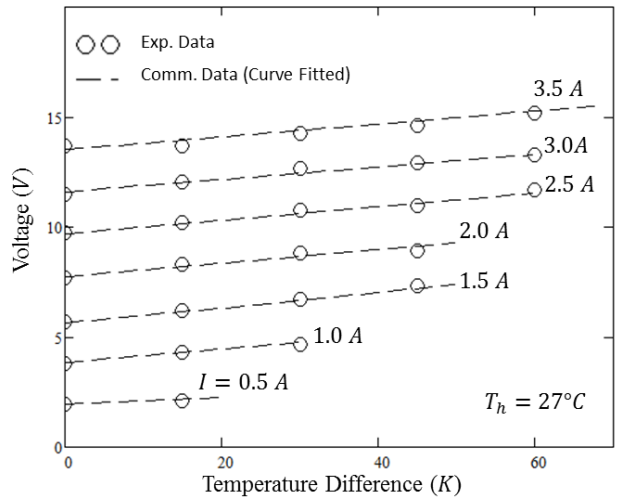

Figure 50. Commercial vs. Experimental Voltage Comparison for C2-30-1503

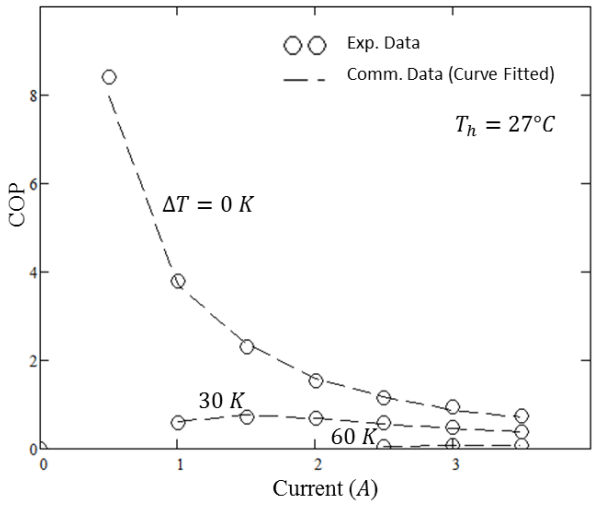

Figure 51. Commercial vs. Experimental COP Comparison for C2-30-1503

RC12-04 by Marlow Industries

Table 8 summarizes the effective material properties obtained for the RC12-04 TEC module using both $Q_{c,max}$ and V_{max} sets. When predicting the maximum effective parameters through recalculation the $Q_{c,max}$ set predicted $Q_{c,max}$, I_{max} and ΔT_{max} values exactly while there was a substantially large error of 9.41% between the predicted V_{max} value and the actual provided one. The V_{max} set only predicted V_{max} and ΔT_{max} values exactly while a 8.6% error occured when predicting I_{max} and a 16.47% error occured when predicting $Q_{c,max}$. Both these errors in recalculating the maximum parameters using the effective material properties were considerably higher compared to the errors obtained for the C2-30-1503 TEC module by Tellurex.

Table 8. Effective Material Properties for RC12-04

Criterion	Symbols (unit)	Value at $T_c = 27$ °C
Provided maximum parameters	$Q_{c,max}$ (W)	36.0
	V_{max} (V)	14.7
	I_{max} (A)	3.7
	ΔT_{max} (K)	63
	R_M (Ω)	3.2
Effective material properties ($Q_{c,max}$ set)	α_Q^* (μV K^{-1})	211.1
	ρ_Q^* (Ω cm^{-1})	1.15×10^{-3}
	k_Q^* (W cm^{-1}K^{-1})	1.70×10^{-2}
Effective maximum parameters using ($Q_{c,max}$ set)	$Q_{c,max}$ (W)	36.0
	V_{max} (V)	16.08
	I_{max} (A)	3.7
	ΔT_{max} (K)	63
Effective material properties (V_{max} set)	α_V^* (μV K^{-1})	192.8
	ρ_V^* (Ω cm^{-1})	1.16×10^{-3}
	k_V^* (W cm^{-1}K^{-1})	1.72×10^{-2}
Effective maximum parameters using (V_{max} set)	$Q_{c,max}$ (W)	30.07
	V_{max} (V)	14.7
	I_{max} (A)	3.38
	ΔT_{max} (K)	63
Effective figure of merit	Z^*T_h	0.672

Geometric information: number of couples $n = 127$, thermoelectric element cross-sectional area $A = 1.00$ mm^2, thermoelectric element length $L = 1.17$ mm, geometric factor $G = \frac{A}{L} = 0.085$ cm

Figure 52 and Figure 53 compares the analytically predicted values for cooling power and voltage, respectively, when using effective material properties obtained from either the $Q_{c,max}$ or V_{max} set. Similar to evaluating the C2-30-1503 TEC module by Tellurex, the RC12-04 module showed a similar trends of discrepancy between the

predicted cooling power and voltages from the $Q_{c,max}$ and V_{max} sets, but with larger variations. This was inherently due to the differences in predicting the maximum parameters using the effective material properties themselves where more significant errors were present for this module. However, using the V_{max} set of effective material properties had more significant errors when predicting the maximum parameters and also had errors in two of the four parameters compared to the $Q_{c,max}$ set that only had errors associated with voltage predictions. Thus, by virtue of least error, the $Q_{c,max}$ set of effective material properties was used to compare against the data from the manufacturer as well as experimental results.

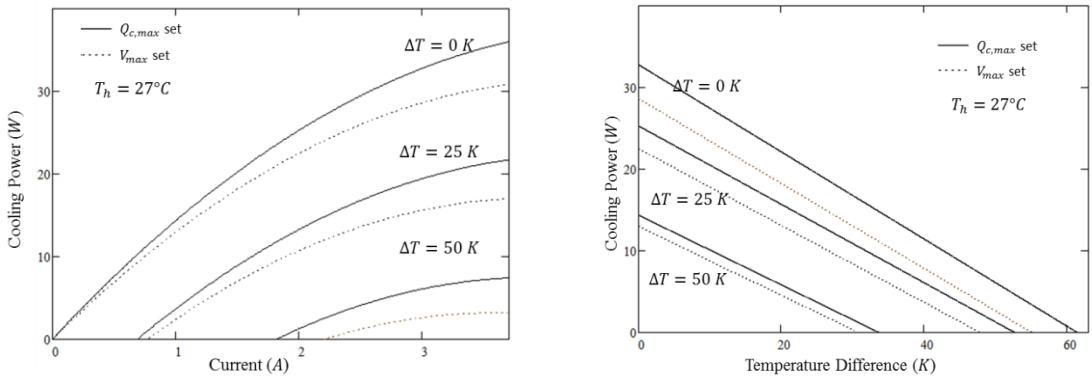

(a) (b)

Figure 52. Analytical Cooling Power Comparison between $Q_{c,max}$ and V_{max} Sets against (a) Current and (b) Temperature Difference for RC12-04

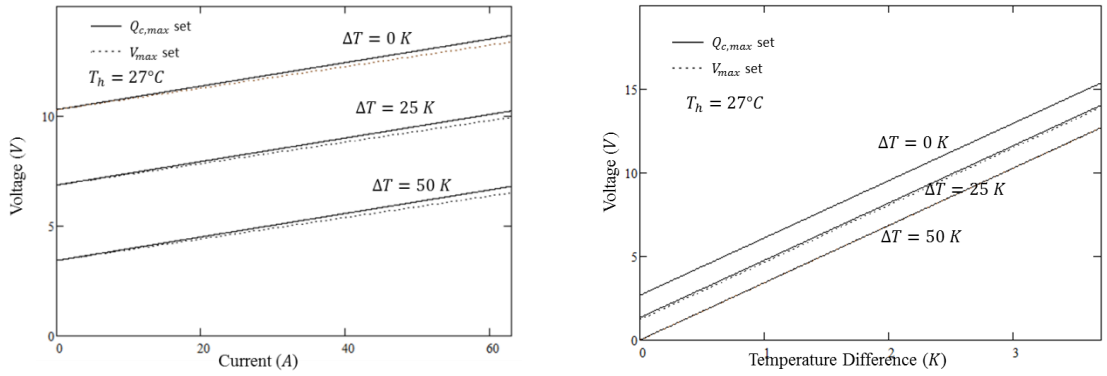

(a) (b)

Figure 53. Analytical Voltage Comparison between $Q_{c,max}$ and V_{max} Sets against (a) Current and (b) Temperature Difference for RC12-04

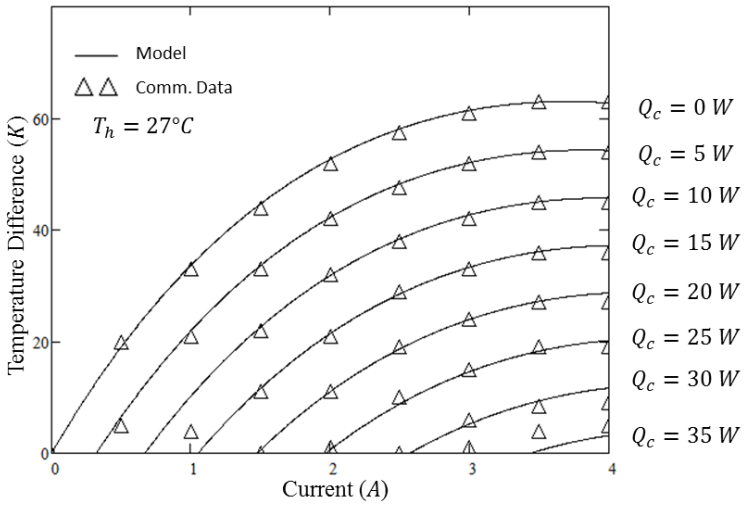

Figure 54. Analytical vs. Commercial Data Temperature Difference (at Various Cooling Powers) Comparison for RC12-04

The cooling power against current at various temperature differences data provided by the manufacturer was in an unorthodox format compared to the data provided by Tellurex. Figure 54 compares the original format of the commercial data

points with the prediction from the model using effective material properties for temperature differences against current at fixed cooling powers. The result was plotted by setting the Q_c to the desired value in equation (1.67) and solving for ΔT at various values of I. The analytical results agreed well with the data provided.

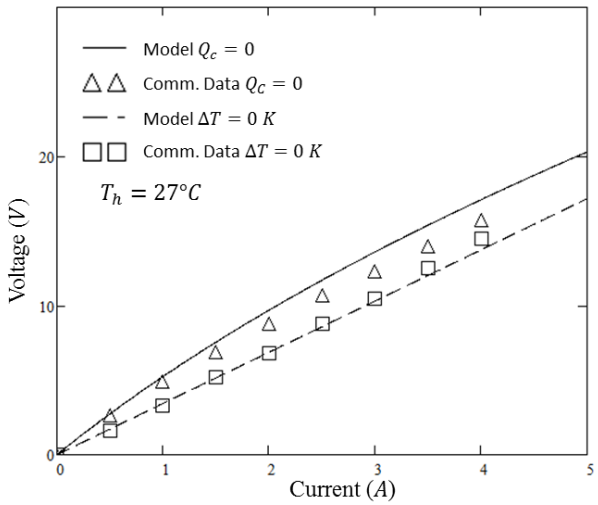

Figure 55. Analytical vs. Commercial Data Voltage Comparison for RC12-04

The manufacturer did not provide comprehensive voltage against current data but only at two particular operating conditions: at $Q_c = 0$ and at $\Delta T = 0$. The analytical results for the $Q_c = 0$ condition was obtained by setting $Q_c = 0$ in equation (1.67) and solving for ΔT at various values of I. ΔT and I were then substituted into equation (1.72) to obtain the voltage as a function of current when the cooling power was zero. The voltages under the second condition of $\Delta T = 0\ K$ were obtained directly from equation (1.72). Figure 55 compares the analytical voltages to the provided values and shows a degree of discrepancy for the $Q_c = 0$ condition at higher current values. It was inconclusive whether the analytical results were more accurate at higher ΔT values, such

as the case of the C2-30-1503 module evaluation, due to an insufficiency of data points to be compared against. It should also be noted that the voltage under the $Q_c = 0$ condition exhibited non-linearity due to the non-linear interaction between ΔT and I in equation (1.67), which was then carried into equation (1.72).

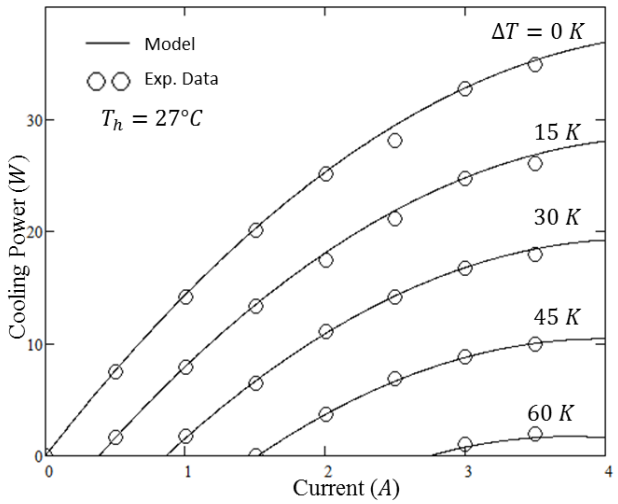

Figure 56. Analytical vs. Experimental Cooling Power Comparison for RC12-04

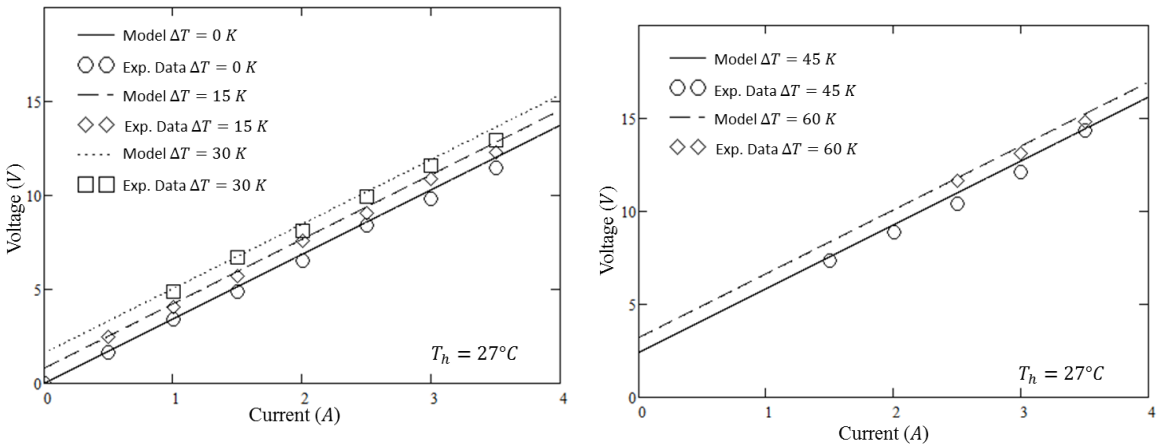

(a) (b)

Figure 57. Analytical vs. Experimental Voltage Comparison for RC12-04

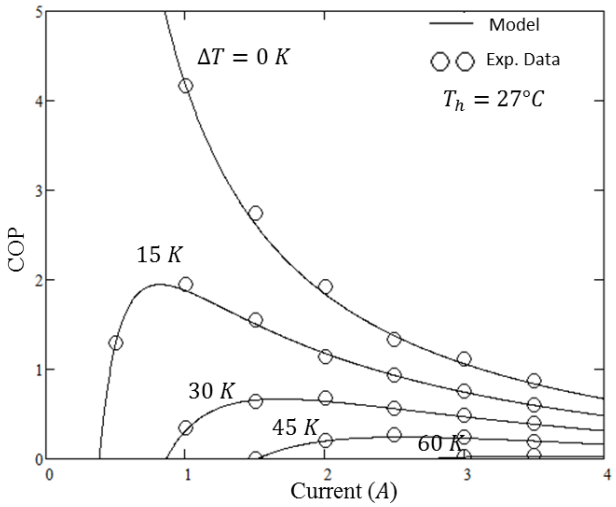

Figure 58. Analytical vs. Experimental Cooling Power Comparison for RC12-04

The analytical to experimental comparison of cooling power against current at various temperature differences (refer to Figure 56) showed only slight errors between the two methods. It was expected that the voltage comparison (refer to Figure 57) would show larger discrepancies at lower temperature differences but instead, the results indicate an unexpectedly decent agreement across all currents and temperature differences. The COP was also evaluated experimentally and then compared to the analytical results in Figure 58. The results indicated a satisfactory degree of accuracy overall with the recurring trend of improved accuracy at higher temperature differences.

The experimental to commercial data comparison was unsuccessful due to the experimental setup being able to control junction temperatures and read heat transfer rates (in the form of heat fluxes), but not the other way around. The control systems were initially programmed to vary the heater input power and chiller set temperatures such that the desired junction temperatures were obtained and the corresponding heat flux was

measured and recorded at steady state. It was only discovered much later that the RC12-04 TEC had its performance charts constructed in a different format of temperature difference against current at various constant cooling powers. As such, no experimental to manufacturer data comparisons were made for the RC12-04 module. Nonetheless, the similar trends occurring from the comparison of analytical-to-commercial data and analytical-to-experimental results would suggest a close agreement of the commercial data to experimental results.

Normalized Charts

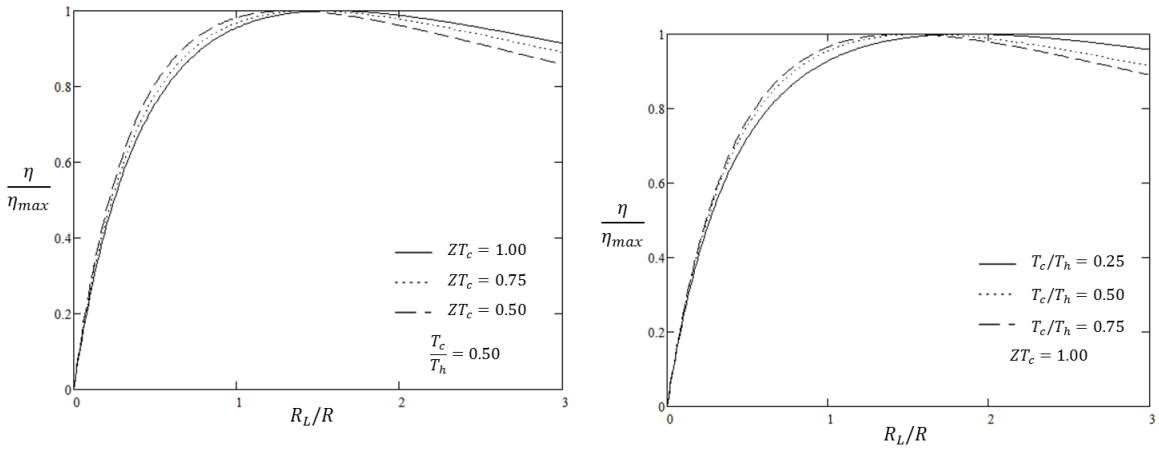

(a) (b)

Figure 59. Normalized Efficiency for TEGs for various (a) ZT_h and (b) T_c/T_h

The concept of normalized charts for universal performance evaluation of modules is revisited in this section. For TEGs the normalized power output, current, voltage and efficiency are given in equations (1.53), (1.55), (1.57) and (1.58), respectively. Upon inspection, only the normalized efficiency is a function of the

dimensionless figure of merit evaluated at the cold side temperature ZT_c and junction temperature ratio T_c/T_h, all other normalized parameters are sole functions of the resistance ratio R_L/R.

The normalized efficiency charts in Figure 59 may be helpful in specific TEG designs where efficiency is paramount to the application. These charts can aid designers in quickly determining the load resistance conditions required for the maximum possible conversion efficiency. However, most TEG manufacturers provide the performance curves at matched load conditions (maximum power output). Regardless of the junction temperature ratios or dimensionless figure of merit the maximum power will always occur at matched load conditions.

As for TECs the normalized parameters of cooling power, COP and voltage, on the basis of T_h are given in equations (1.90), (1.93) and (1.95) respectively. All parameters are functions of normalized current I/I_{max}, normalized temperature difference $\Delta T/\Delta T_{max}$ and the dimensionless figure of merit evaluated at the hot side ZT_h. Figure 60 and Figure 61 show two common forms of normalized performance parameters of TECs. Here, the effect of varying $ZT_h$is seen. It can be seen that the cooling power is a relatively weak function of ZT_h but the voltage and COP are substantially affected by ZT_h. The value of $ZT_h = 0.7$ is a typical value possessed by most TEC modules whereas the hypothetical value of $ZT_h = 0.4$ is a lower value that was used to evoke detrimental performance effects such as electrical and contact resistances. These effects have been

reported to be the primary source of discrepancies between actual experimental results and results from the Ideal Equations [18].

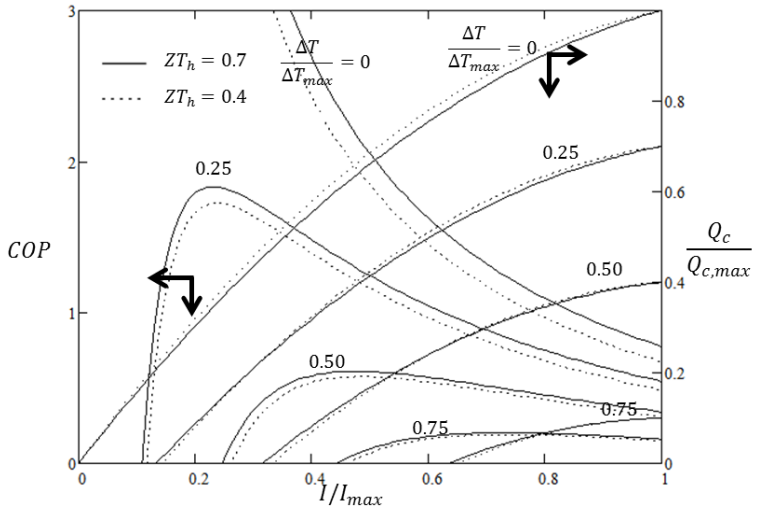

Figure 60. Normalized Cooling Power and COP for TECs against Normalized Current at Various Normalized Temperature Differences

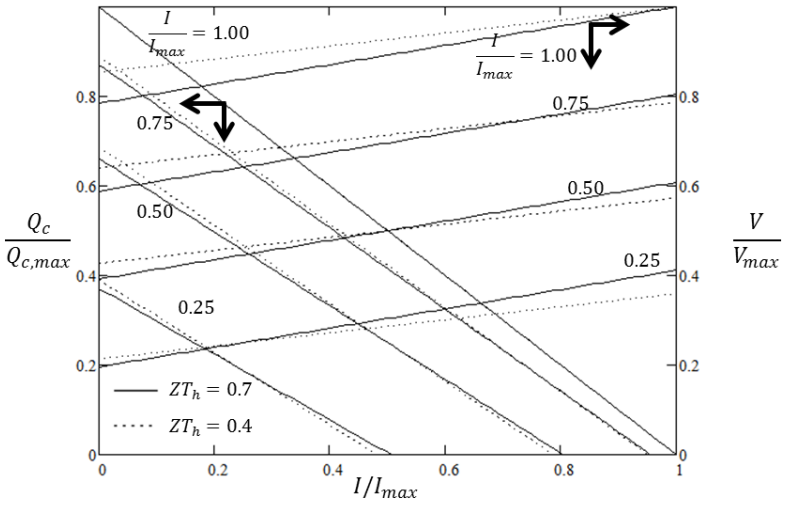

Figure 61. Normalized Cooling Power and COP for TECs against Normalized Temperature Difference at Various Normalized Currents

Summary of Results

Table 9. Summary of TEG Effective Material Properties using the I_{max} Set

Criterion	Symbols (unit)	TG-12-04L	HZ-2
Junction temperatures	T_h (°C)	230	230
	T_c (°C)	50	30
Geometric information	n	127	97
	A (mm^2)	1.0	2.1
	L (mm)	1.17	2.87
	$G = A/L$ (cm)	0.0875	0.073
Provided maximum parameters	$\dot{W}_{max}$ (W)	4.05	2.60
	V_{max} (V)	9.45	6.53
	I_{max} (A)	1.71	1.60
	η_{mp} (%)	4.97	4.50
	R_M (Ω)	−	4.00
Effective material properties	α_I^* (μK V^{-1})	209.4^a	167.5
	ρ_I^* (Ω cm^{-1})	$1.72 \times 10^{-3\,a}$	1.53×10^{-3}
	k_I^* (W cm^{-1}K^{-1})	$1.48 \times 10^{-2\,a}$	1.62×10^{-2}
Effective maximum parameters	$\dot{W}_{max}$ (W)	4.48	2.60
	V_{max} (V)	9.58	6.50
	I_{max} (A)	1.87	1.60
	η_{mp} (%)	5.61	4.50
Effective figure of merit	Z^*T_c	0.564	0.343

a – Weighted average values

It is of interest to note that the recalculated effective material properties for the TG12-04L module (refer to Table 9) showed a high degree of discrepancy compared to the originally provided values. The error associated with $\dot{W}_{max}$ was 10.46%, I_{max} was 9.47%, V_{max} was 1.33% and η_{mp} was 12.90%. These substantially high errors stemmed from the weighted average method that inaccurately predicted the maximum effective

parameters but seemed to provide a more accurate prediction when compared to the provided data over an entire range as opposed to using the effective material properties derived from only one temperature set (refer to Figure 29 to Figure 31). This trade-off must be acknowledged and caution should be exercised when predicting the maximum parameters of a module if the method of weighted averaging is applied.

Table 10. Summary of TEC Effective Material Properties using the $Q_{c,max}$ set

Criterion	Symbols (unit)	C2-30-1503	RC12-04
Junction temperatures	T_c (°C)	27	27
Geometric information	n	127	127
	A (mm^2)	1.12	1.0
	L (mm)	1.66	1.17
	$G = A/L$ (cm)	0.073	0.0875
Provided maximum parameters	$Q_{c,max}$ (W)	34.14	36.0
	V_{max} (V)	15.5	14.7
	I_{max} (A)	3.5	3.7
	ΔT_{max} (K)	68	63
	R_M (Ω)	3.85	3.20
Effective material properties	α_Q^* (μK V^{-1})	208.6	211.1
	ρ_Q^* (Ω cm^{-1})	1.00×10^{-3}	1.15×10^{-3}
	k_Q^* (W $cm^{-1}K^{-1}$)	1.71×10^{-2}	1.70×10^{-2}
Effective maximum parameters	$Q_{c,max}$ (W)	34.14	36.0
	V_{max} (V)	15.9	16.08
	I_{max} (A)	3.5	3.7
	ΔT_{max} (K)	68	63
Effective figure of merit	Z^*T_h	0.757	0.672

Experimentally, the average error of the performance parameters, when compared to the commercial data, had an average percentage error of approximately 4%. Although testing conditions of the manufacturer are unknown most of the discrepancies can be accounted for from the uncertainties of the instruments presented in Table B1 in APPENDIX A. Assuming the mean temperature measurement (between $-20°C$ to $350°C$) to be $185°C$, the contributions of uncertainty from the temperature measuring instruments are $\pm 3.1°C$ or $\pm 1.67\%$ equivalently. The sum of all uncertainties of the remaining instruments is $\pm 6.44\%$. This brings the total uncertainty of measurement up to $\pm 8.11\%$. Since the percentage error of the experimental results against the commercial data fall within the band of the total instrument uncertainties these discrepancies can be accounted for.

CHAPTER V

SUMMARY AND CONCLUSION

One of the main objectives of this study was to provide designers, aiming to implement thermoelectric modules into their designs, a straightforward analytical method of evaluating the performance of a certain thermoelectric module. The motivation behind this objective was the non-uniformity and inconsistency of performance curves and data provided by various thermoelectric manufacturers which would impede the efforts of designers who wanted to compare modules from different manufacturers. Also, some performance charts lacked the conditions at which the consumer may choose to operate a particular module. The forms of commercial data provided CHAPTER IV is evidence that designers would not have a unified basis to compare performances between modules of different manufacturers.

Furthermore, the insufficiency of information provided regarding the material properties of these products by the manufacturers rendered designers incapable of applying direct theoretical means of predicting the performances of these modules. This study has shown that as long as the maximum parameters of the module are specified by the manufacturer one could employ the method of obtaining the effective material properties (or module properties when geometric information is unavailable) to analytically evaluate the performance of a module. Once the effective material properties

have been obtained the performance of any module can easily be predicted using the Ideal Equations in CHAPTER I.

The results of comparing the analytical solutions, using the effective material properties derived directly from information provided by the manufacturers, showed acceptable levels of accuracy. Important performance parameters such as power output (TEGs) and cooling power (TECs) were accurately predicted using such means. Secondary parameters, especially voltage values, had a considerable amount of discrepancy but showed favorable results at higher temperatures and currents. In TEGs the range of operating temperatures were large and the temperature dependence of material properties were evident when both experimental voltage results and commercial voltage data showed non-linearity whereas the Ideal Equations would only predict a linear behavior of voltage with temperature independent material properties. However, these discrepancies reduced closer to the temperature regions at which the effective material properties were derived. In the case of TECs the operating temperature ranges were much smaller compared to TEGs. The effect of temperature dependence of the material properties was not as strong in such cases.

Moreover, the maximum parameters used to derive the effective material properties were directly from the manufacturers. As such, the effective material properties have detrimental effects that reduce the performance of either TEGs or TECs, such as both electrical and thermal contact resistances, material degradation embedded into them. In addition, the Thomson effect, if present, is also captured when employing

this method of reverse computation. Hence, direct utilization of these effective material properties into the Ideal Equations account for a majority of parasitic losses and uncertainties that would otherwise be encountered when only using intrinsic material properties to evaluate the performance of thermoelectric modules. Using intrinsic material properties would then require correction factors to predict realistic values, rendering the procedure rather cumbersome.

The second objective of this study was to experimentally validate the analytical results and commercial data. The experimental results agreed closely with the commercial data signifying experimental method were indeed used by the manufacturers to obtain their data. This validates the integrity of the commercial data provided by the manufacturers. More importantly, the experimental performance evaluation of thermoelectric modules throughout the study proved to be a challenging and time consuming task. Designers without access to such testing capabilities would have to rely on analytical means to evaluate the performance of a certain module. Thus, this is where the effective material properties and Ideal Equations could serve as one of the possible analytical tools to comprehensively and realistically evaluate the performance of thermoelectric modules.

REFERENCES

[1] S. Kim et al., "Thermoelectric power generation system for future hybrid vehicles using hot exhaust gas," *Journal of Electronic Materials*, vol. 40, no. 5, pp. 778-784, 2011.

[2] V. V. Gusev, A. A. Pustovalov, N. N. Rybkin, L. I. Anatychuk. B. N. Demchuk, and I. Y. Ludchak, "Milliwatt-power radioisotope thermoleectric generator (RTG) based on plutonium-238," *Journal of Electronic Materials*, vol. 40, no. 5, pp. 807-811, May 2011.

[3] D. Kraemer et al., "High performance flat-panel solar thermoelectric generators with high thermal concentration," *Nature*, vol. 10, no. 7, pp. 532-537, July 2011.

[4] K. McEnaney, D. Kraemer, and Z. and Chen, G. Ren, "Modeling of concentrating solar theroelectric generators," *Journal of Applied Physics*, 2011.

[5] A. Attar, H. Lee, and S. Weera, "Optimal design of automotive thermoelectric air conditioner (TEAC)," *Journal of Electronic Materials*, vol. 43, no. 2, pp. 1-9, January 2014.

[6] L. B. Ershova and G. G. Gromov, "Optimal thermoelectric cooling in laser diode sub-assemblies," RMT Ltd., Moscow,.

[7] G. J. Snyder, M. Soto, R. Alley, D. Koester, and B. Conner, "Hot spot cooling using embedded thermoelectric coolers," in *Semiconductor Thermal Measurement and Management Symposium*, Dallas, 2006, pp. 135-15.

[8] T. J. Seebeck, *Magnetic polarization of metals and minerals*, Abhandlungen der Königlichen Akademie der Wissenschaften zu Berlin ed. Berlin, Germany, 1822.

[9] G. S. Nolas, J. Sharp, and H. J. Goldsmid, *Thermoelectrics*. Heidelberg, Germany: Springer, 2001.

[10] H. Lee, *Thermal Design: Heat Sinks, Thermoelectrics, Heat Pipes, Compact Heat Exchaners, and Solar Cells*. Hoboken: John Wiley & Sons, Inc., 2010.

[11] G. J. Snyder and E. S. Toberer, "Complex thermoelectric materials," *Nature*, vol. 7, no. 2, pp. 105-114, February 2008.

[12] H. Alam and S. Ramakrishna, "A review on the enhancement of figure of merit from bulk to nano-thermoelectric materials," *Nano Energy*, vol. 2, pp. 190-212, October 2012.

[13] Thermoelectrics California Insitute of Technology. [Online]. http://www.thermoelectrics.caltech.edu/thermoelectrics/index.html

[14] B. Poudel et al., "High-thermoelectric performance of nanostructured bismth antimony telluride bulk alloys," *Science*, vol. 320, no. 5876, pp. 634-638, May 2008.

[15] H. Lee, "The Thomson effect and the ideal equation on thermoelectric coolers," *Energy*, vol. 56, pp. 61-69, 2013.

[16] E. J. Sandoz-Rosado, "Investigation and Development of Advanced Models of Thermoelectric Generators for Power Generation Applications," Rochester Institute of Technology, Rochester, Master Thesis UMI Number: 1469748, 2009.

[17] F. L. Tan and S. C. Fok, "Methodology on sizing and selecting thermoelectric cooler from different TEC manufacturers in cooling system design," *Energy Conversion & Management*, vol. 49, pp. 1715-1723, January 2008.

[18] H. Lee, A. Attar, and S. Weera, "Performance evaluation of commercial thermoelectric modules using effective material properties," in *2014 International Conference on Thermoelectrics*, Nashville, 2014, pp. 1-5.

[19] J. D'Angelo and T. Hogan, "Long term thermoelectric module testing system," *Review of Scientific Instruments*, vol. 80, pp. 1-3, October 2009.

[20] J. Vazquez, R. Palcios, M. A. Sanz-Bobi, and A. Arenas, "Test bench for measuring the electrical properties of commercial thermoelectric modules," in *22nd International Conference on Thermoelectrics*, 2003, pp. 589-593.

[21] L. Rauscher et al., "New approach for highly accurate efficiency determination of thermoelectric generator," in *22nd International Conference on Thermoelectrics*, 2003, pp. 508-511.

[22] L. Rauscher, S. Fujimoto, H. T. Kaibe, and S. Sano, "Efficiency determination and general characterization of thermoelectric generators using an absolute measurement of the heat flow," *Measurement Science and Technology*, vol. 16, pp. 1054-1060, March 2005.

[23] L. I. Anatychukl and M. V. Havrylyuk, "Procedure and equipment for measuring parameters of thermoelectric generator modules," *Journal of Electronic Materials*, vol. 40, no. 5, pp. 1292-1297, March 2011.

[24] H. Takazawa et al., "Efficiency measurement of thermoelectric modules operating in the temperature difference of up to 550K," in *2006 International Conference on Thermoelectrics*, 2006, pp. 189-192.

[25] E. J. Sandoz-Rosado and R. J. Stevens, "Experimental characterization of thermoelectric modules and comparison with theoretical models for power generation," *Journal of Electronic Materials*, vol. 38, no. 7, pp. 1239-1244, 2009.

[26] K. Chen and S. B. Gwilliam, "An analysis of the heat transfer rate and efficienct of TE (thermoelectric) systems," *International Journal of Energy Research*, vol. 20, pp. 399-417, 1996.

[27] B. J. Huang, C. J. Chin, and C. L. Duang, "A design method of thermoelectric cooler," *International Journal of Refrigeration*, vol. 23, pp. 208-218, 2000.

[28] T. Leephakpreeda, "Experimental determination of the thermoelectric-module parameters and modeling for cooling/heating control design," *Experimental Techniques*, vol. 36, pp. 13-20, 2012.

[29] Y. Kraftmakher, "Simple experiments with a thermoelectric module," *European Journal of Physics*, vol. 26, pp. 959-967, 2005.

[30] A. Y. Faraji and A. Akbarzadeh, "Design of a compact, portable test system for thermoelectric power generator modules," *Journal of Electronic Materials*, vol. 42, no. 7, pp. 1535-1541, November 2013.

[31] A. Montecucco, J. Buckle, J. Sivter, and A. R. Knox, "A new test rig for accurate nonparametric measurement and characterization of thermoelectric generators," *Journal of Electronic Materials*, vol. 42, no. 7, pp. 1996-1973, 2013.

[32] F. A. Leavitt, N. B. Elsner, and J. C. Bass, "Use, application and testing of Hi-Z thermoelectric modules," Hi-Z Technology, Inc., San Diego, Product Testing Instructions.

[33] C. Hsu, G. Huang, H. Chu, B. Yu, and D. Yao, "An effective Seebeck coefficient obtained by experimental results of a thermoelectric generator module," *Applied Energy*, vol. 88, pp. 5173-5179, 2011.

[34] D. Mitrani et al., "Methodology for extracting thermoelectric module parameters," *IEEE Transactions on Instrumentation and Measurement*, vol. 54, no. 4, pp. 1548-1552, August 2005.

[35] Y. Tanji, Y. Nakagawa, and M. Yasuoka, "Electric and thermal contact resistances of the new type thermoelectric module," in *18th Internation Conference on Thermoelectrics*, 1999, pp. 260-264.

[36] A. Muto, D. Kraemer,. Hao, Z. F. Ren, and G. Chen, "Thermoelectric properties and efficiency measurements under large temperature differences," *Review of Scientific Instruments*, vol. 80, no. 9, pp. 1-7, September 2009.

[37] T. C. Harman, "Special techniques for measurement of thermoelectric properties," *Journal of Applied Physics*, vol. 29, pp. 1373-1374, June 1958.

[38] S. B. Mahajan, "Design of a compact, portable test system for thermoelectric power generator modules," Rochester Institute of Technology, Rochester, Master Thesis UMI Number: 1543212, 2013.

[39] P. G. Lau, "Convection correction factor determination for use with the transient test method for thermoelectric modules," in *18th International Conference on Thermoelectrics*, 1999, pp. 252-255.

[40] G. Min and D. M. Rowe, "A novel principle allowing rapid and accurate measurement of a dimensionless thermoelectric figure of merit," *Measurement Science and Technology*, vol. 12, pp. 1261-1262, May 2001.

[41] S. Lineykin and S. Ben-Yaakov, "Modeling and analysis of thermoelectric modules," *IEEE Transactions on Indusry Applications*, vol. 43, no. 2, pp. 505-512, March/April 2007.

[42] H. Y. Zhang, "A general approach in evaluating and optimizing thermoelectric coolers," *International Journal of Refrigeration*, vol. 33, pp. 1187-1196, April 2010.

[43] Z. Luo, "A simple method to estimate the physical characteristics of a thermoelectric cooler from vendor datasheets," *Journal of Electronics Cooling and Thermal Control*, pp. 1-14, August 2008.

[44] R. Ahiska, S. Dislitas, and G. Omer, "A new method and computer-controlled system for measuring the time constant of real thermoelectric modules," *Energy Conversion and Management*, vol. 53, pp. 314-321, September 2011.

[45] B. Ciylan and S. Yilmaz, "Design of a thermoelectric module test system using a novel test method," *Internation Journal of Thermal Systems*, vol. 46, pp. 717-725, 2007.

[46] Tellurex. (2011) Tellurex Peltier FAQ. [Online]. http://www.tellurex.com/technology/peltier-faq.php

[47] G. J. and Ursell, T. S. Snyder, "Thermoelectric Efficiency and Compatibility," *Physical Review Letters*, vol. 91, no. 14, p. 148301, October 2003.

[48] Omega. (2014) Wire Color Codes and Limits of Error. [Online]. http://www.omega.com/techref/colorcodes.html

[49] National Instruments, "SCXI -1303 32-Channel Isothermal Insulation Block," National Instruments, Installation Guide 321923-B, 2000.

[50] National Instruments, "NI 6034E/6035E/6036E User Manual," National Instruments, User Manual 322339B-01, 2001.

[51] Lambda EMI, "Instruction Manual for TCR 1 Phase Power Supply," Lambda EMI, Neptune, Instruction Manual 83-470-001 Revision E,.

[52] BK Precision, "8500 Series DC Electronic Loads User Manual," B&K Precision Corp., Yorba Linda, User Manual 060313, 2013.

APPENDIX A

NOMENCLATURE

Variable	Nomenclature	Variable	Nomenclature
A	Cross-sectional area (mm^2)	$\vec{q}$	Heat flux vector (W m^{-2})
COP	Coefficient of performance	$\dot{q}$	Internal heat generation rate (W m^{-3})
c_p	Heat capacitance (J kg^{-1} K^{-1})	Q	Heat transfer rate (W)
$\vec{E}$	Electric field vector (V m^{-1})	R	Internal Electrical resistance (Ω)
G	Geometric factor (cm)	R_L	Load resistance (Ω)
I	Electrical current (A)	T	Temperature (°C)
$\vec{J}$	Electrical current density (A m^{-2})	ΔT	Temperature change (K)
k	Thermal conductivity (W m^{-1} K^{-1})	$\bar{T}$	Average temperature (°C)
K	Thermal conductance (W K^{-1})	V	Electrical voltage (V)
L	Element length (mm)	$\dot{W}$	Electrical power (W)
L_z	Lorenz number (2.44×10^{-8} W Ω K^{-2})	Z	Figure of merit (K^{-1})
n	Number of couples		

Greek Symbol	Nomenclature
α	Seebeck coefficient (μV K^{-1})
η	Efficiency
$\vec{\nabla}$	Grad, $\frac{\partial}{\partial x} + \frac{\partial}{\partial y} + \frac{\partial}{\partial z}$
π	Peltier coefficient (W A^{-1})
ρ	Electrical resistivity (Ω cm)
τ	Thomson coefficient (V K^{-1})

Subscript	Nomenclature
I	Effective material property using the I_{max} set
m	Modular quantity
n	n-type element
p	p-type element
Q	Effective material property using the $Q_{c,max}$ set
V	Effective material property using the V_{max} set (either TEG or TEC)

Superscript	Nomenclature
$*$	Effective quantity

APPENDIX B

EXPERIMENTAL UNCERTAINTY

Despite using high quality instruments to conduct the experiments there are always uncertainties associated with such devices. These uncertainties have to be taken into account to identify the acceptable margin of error when justifying the discrepancies encountered during the comparison of results. Table B1 summarizes the uncertainties for the various aspects of experimental measurement and control.

Table B1. Summary of Measurement Uncertainties

Criterion	Uncertainty
Thermocouple	$\pm 2.2°C$
DAQ Temperature Accuracy	± 0.9°C
Heat flux block (hole center points)	$\pm 4.00\%$
DAQ Current Control	$\pm 1.00\%$
TEC power supply (Voltage)	$\pm 0.1\%$
Electronic load (Resistance)	$\pm 1.3\%$
Electronic load (Voltage)	$\pm 0.04\%$

The thermocouple uncertainties for standard K-type thermocouples (manufactured by Omega Engineering) was prescribed to have an uncertainty of ± 2.2°C or $\pm 0.75\%$,

whichever was greater [48]. Temperature readings beyond $293.33\,℃$ would have the $\pm 0.75\%$ uncertainty applied to them. The SCXI-1303 terminal block (part of the DAQ system) was prescribed in the manual to have a maximum uncertainty of $\pm 0.9℃$ for temperatures beyond $55℃$ [49]. The most conservative value was used.

During the fabrication of the aluminum heat flux blocks there were uncertainties associated with metrology but these values were insignificant compared to the uncertainty of the actual location where the thermocouple probes resided. The thermocouple inserts had a diameter of $2\,\text{mm} \pm 0.05\,\text{mm}$ with a depth of $20\,\text{mm} \pm 0.05\,\text{mm}$. The depth to diameter ratio of the holes was limited to 10 times due to the availability of drill bits. The K-type thermocouples, clad in a stainless steel thermowell had an outside diameter of $1.98\,\text{mm} = 5/64"$. This led to an uncertainty of $\pm 0.02\,\text{mm}$ of space that was filled with thermal paste. It was assumed that the tip of the probe would be centered in its insert with a maximum uncertainty of $\pm 0.1\,\text{mm}$. The heat flux blocks were also fabricated such that $\Delta x_s = \Delta x_{TC}$ (refer to Figure 22). The uncertainty of the distances during extrapolation of the temperatures in equation (3.34) would depend on the uncertainty of the actual thermocouple locations, assuming that the temperatures T_1 and T_2 were accurate. The manufacturing uncertainty of machining these holes were estimated to be $\pm 0.1\,\text{mm}$. Cumulatively, the total uncertainty of $\pm 0.2\,\text{mm}$ over a distance of 5.0 mm would be 4%.

There were uncertainties associated when controlling the current of the power supply attached to the TEC using the PCI 6036-E I/O terminal block. A full scale analog

output of 0 to 5 V was used to control a 30 A power supply remotely. The uncertainty reported for the analog output was ± 0.05 V, translating to $\pm 1.00\%$ of uncertainty when selecting a current value to be supplied to the TEC [50]. The voltage readings from the same power supply were reported to have uncertainties of $\pm 0.1\%$ [51]. The electronic load in constant resistance mode had a reported resistance set point uncertainty of $\pm 1.3\%$ and voltage measurement of $\pm 0.04\%$ [52].

APPENDIX C

TEST STAND DRAWINGS

All units here are shown in mm.

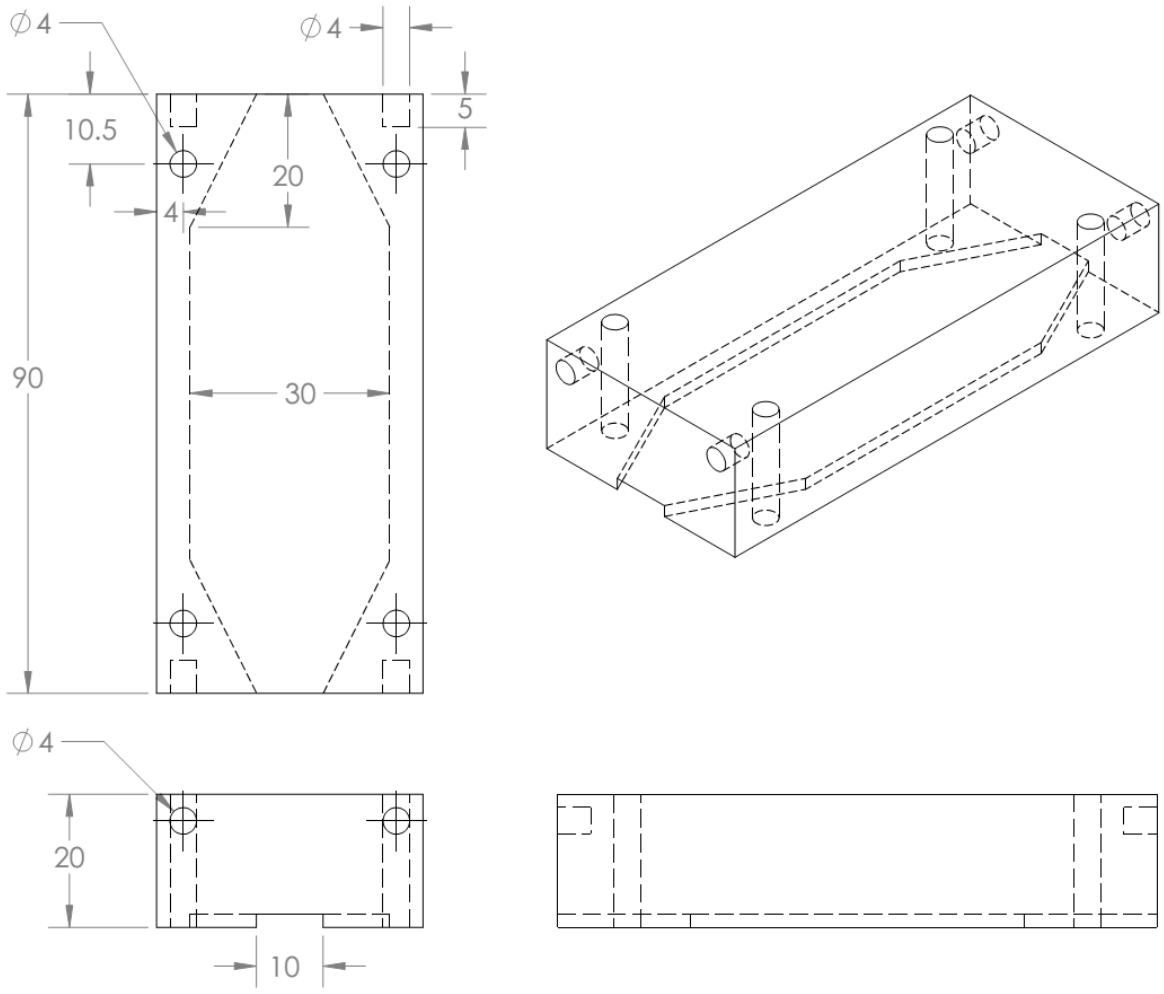

Figure B 1. Cold Heat Exchanger Top and Bottom Plates

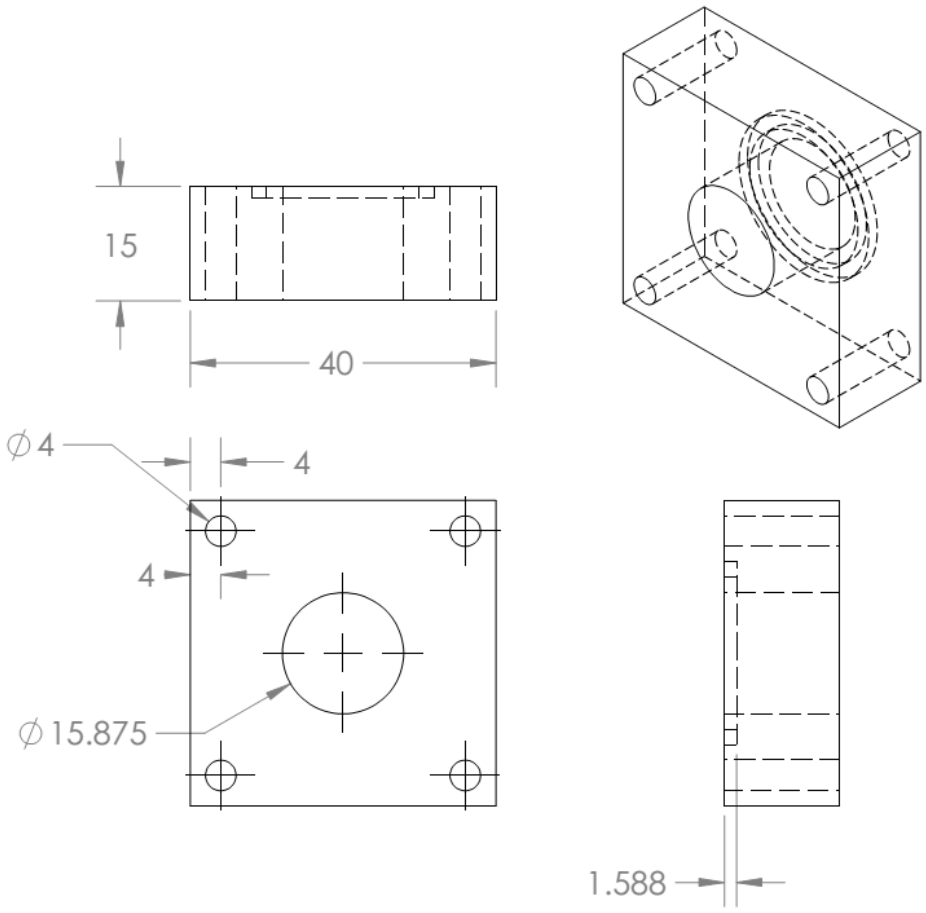

Figure B 2. Cold Heat Exchanger Attachment Plates

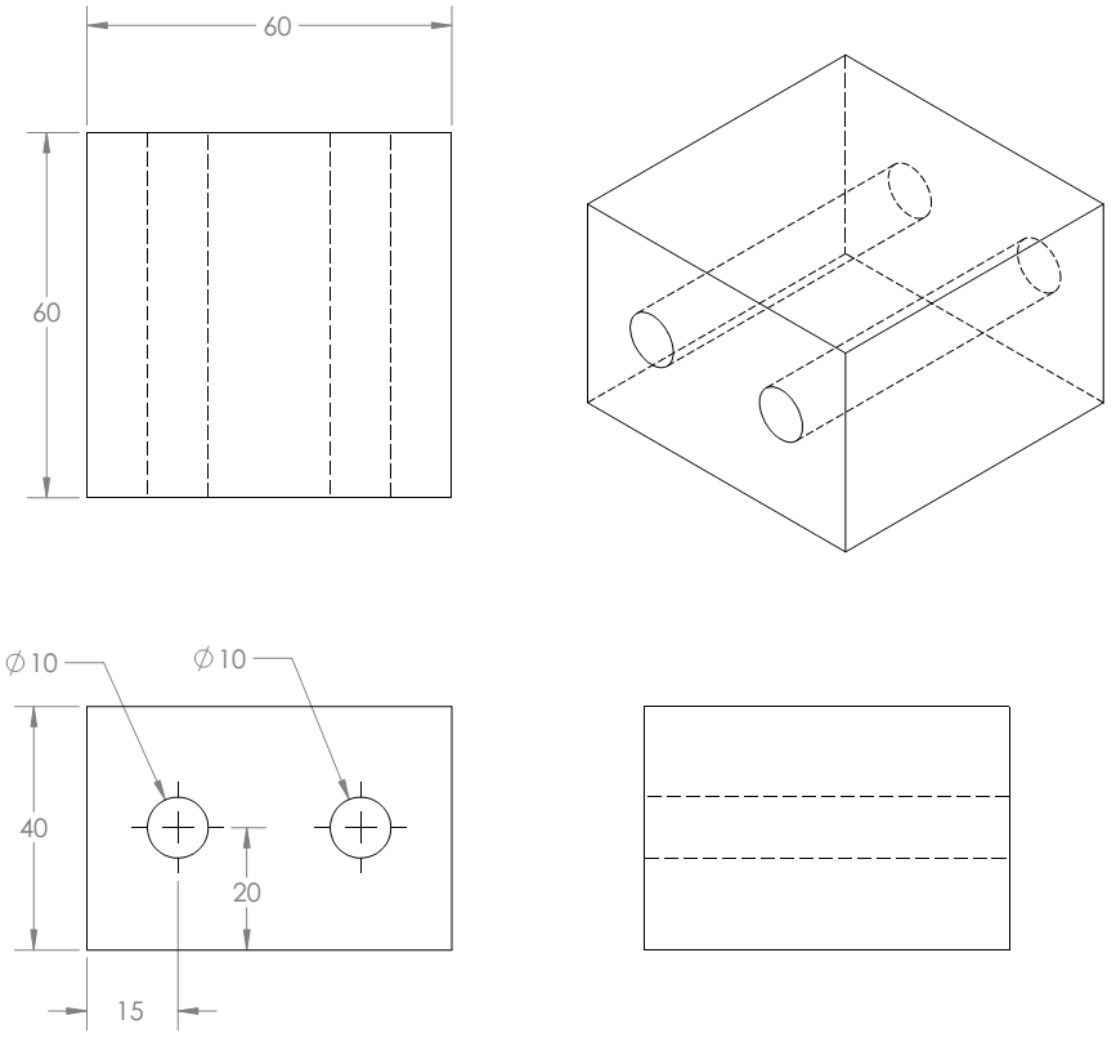

Figure B 3. Cartridge Heater Block

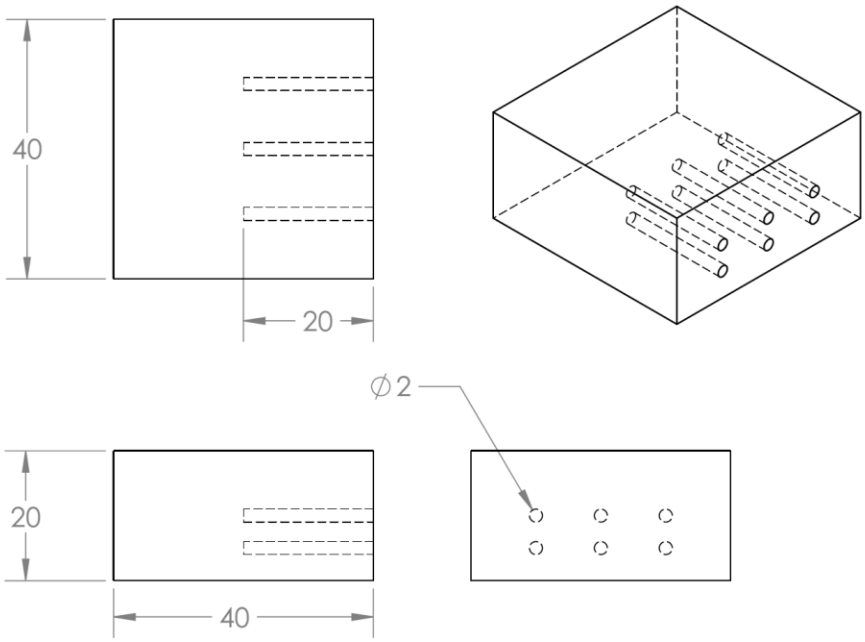

Figure B 4. Heat Flux Block

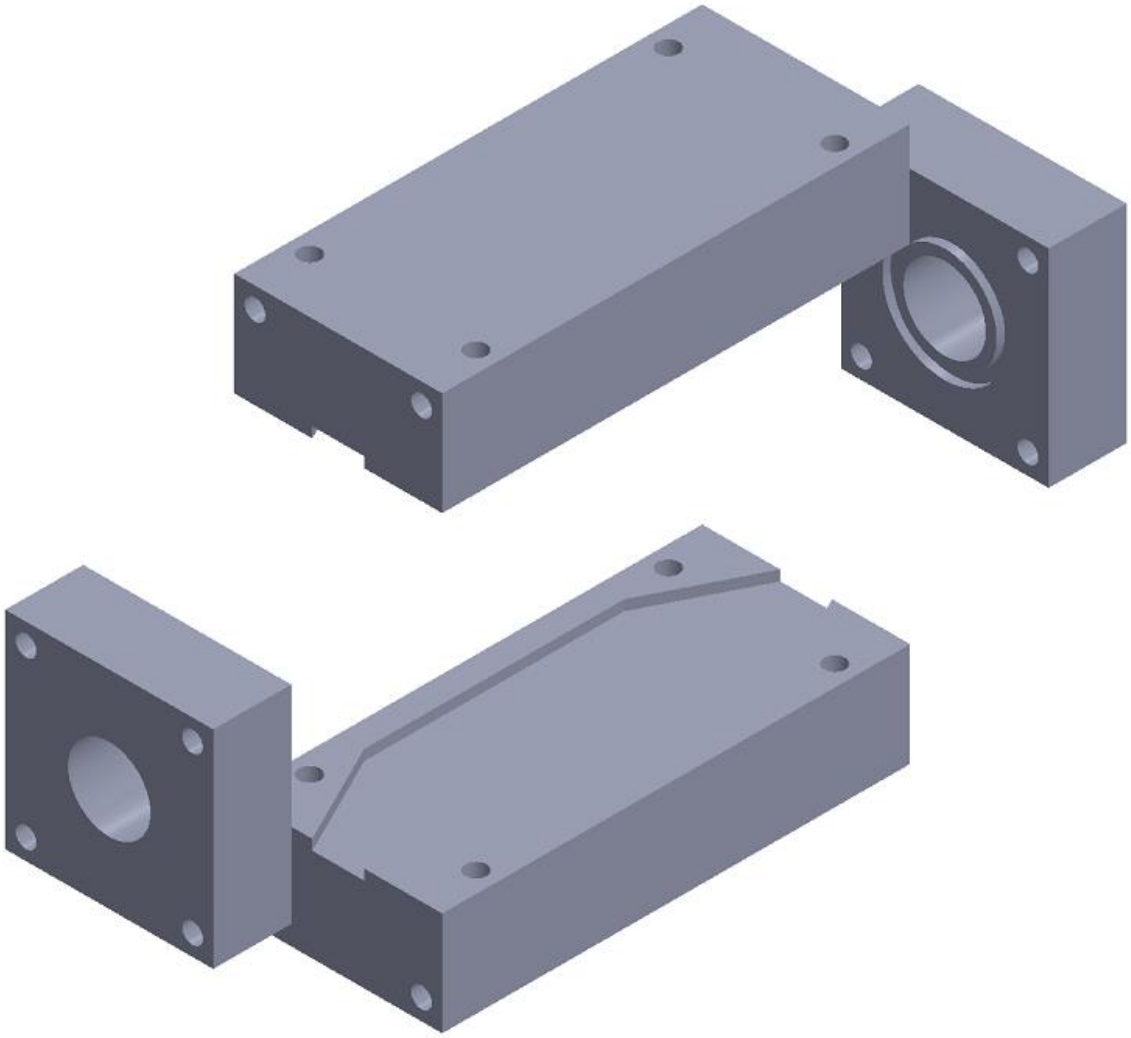

Figure B 5. Cold Heat Exchanger Assembly in an Exploded View